

UHPC Decked I-Beam for Accelerated Bridge Construction

Nebraska Department of Transportation (NDOT)

Project No. FY21-005

Final Report

March 2023



UHPC Decked I-Beam for Accelerated Bridge Construction

A Report on Research Sponsored by

Nebraska Department of Transportation (NDOT)

Principle Investigators

George Morcous, Ph.D., P.E.

Durham School of Architectural Engineering and Construction (DSAEC), University of
Nebraska-Lincoln (UNL)

Maher K. Tadros, Ph.D. PE.

e.Construct.US, Omaha, NE

Research Assistants

Antony Kodsy, Ph.D., PE

Dulitha Fredrick, Soumitra Das, and Mohammed Hedia

Durham School of Architectural Engineering and Construction (DSAEC), College of
Engineering, University of Nebraska-Lincoln (UNL)

March 2023

TECHNICAL REPORT DOCUMENTATION PAGE

1. Report No. FY21-005	2. Government Accession No.	3. Recipient's Catalog No.	
4. Title and Subtitle UHPC Decked I-Beam for Accelerated Bridge Construction		5. Report Date March, 2023	
		6. Performing Organization Code	
7. Author(s) George Morcouc and Maher K. Tadros		8. Performing Organization Report No. No.	
9. Performing Organization Name and Address Durham School of Architecture Engineering and Construction University of Nebraska-Lincoln Omaha, Nebraska 68182-0178		10. Work Unit No.	
		11. Contract FY21-005	
12. Sponsoring Agency Name and Address Nebraska Department of Transportation Research Section 1400 Hwy 2 Lincoln, NE 68502		13. Type of Report and Period Covered Final Report July 2020-November 2022	
		14. Sponsoring Agency Code	
15. Supplementary Notes			
16. Abstract <p>Ultra-High-Performance Concrete (UHPC) is an excellent material for bridge construction due to its exceptional durability and superior mechanical properties. Several Departments of Transportations (DOTs), including NDOT, have limited the use of UHPC in bridge construction to joints and connections between bridge components due to the relatively high materials cost of commercially UHPC products. Recently, NDOT has sponsored a research project to develop a non-proprietary UHPC using local materials to reduce materials cost and ensure its availability to local contractors and precast producers. The project was completed successfully and an economical UHPC mix that satisfied all workability, durability, and strength requirements was developed and tested. Therefore, it is economically feasible to expand the use of UHPC to bridge superstructure components that can have a service life of over 150 years.</p> <p>The objective of this project is to develop a UHPC superstructure system for bridges in Nebraska that is optimized with respect to structural efficiency, constructability, and economy. Several UHPC superstructure systems used in France, Korea, Malaysia, USA, and Canada including pi-girders, bulb-tee girders, tub girders, box girders, decked I-beams, and waffle slabs, were reviewed and evaluated to determine the system(s) that meet NDOT needs. A decked I-beam (DIB) section was selected due to its ease of production, constructability, and structural efficiency. Formwork design, production trials, and material/structural testing were conducted for UHPC DIB specimens with ribbed and solid slabs using pre-tensioning and post-tensioning systems. Design examples of a typical bridge using DIBs were also presented to demonstrate the implementation of the latest UHPC design specifications/guidelines.</p>			
17. Key Words Decked I-beam, accelerated construction, superstructure system, UHPC production, post-tensioning, flexure strength, shear strength.		18. Distribution Statement No restrictions. This document is available through the National Technical Information Service. 5285 Port Royal Road Springfield, VA 22161	
19. Security Classification (of this report) Unclassified	20. Security Classification (of this page) Unclassified	21. No. of Pages 100	22. Price

DISCLAIMER

The contents of this report reflect the views of the authors, who are responsible for the facts and the accuracy of the information presented herein. The contents do not necessarily reflect the official views or policies neither of the Nebraska Department of Transportations nor the University of Nebraska-Lincoln. This report does not constitute a standard, specification, or regulation. Trade or manufacturers' names, which may appear in this report, are cited only because they are considered essential to the objectives of the report.

The United States (U.S.) government and the State of Nebraska do not endorse products or manufacturers. This material is based upon work supported by the Federal Highway Administration under SPR-FY21(005). Any opinions, findings and conclusions or recommendations expressed in this publication are those of the author(s) and do not necessarily reflect the views of the Federal Highway Administration.”

ACKNOWLEDGEMENTS

Funding for this project was provided by the Nebraska Department of Transportation (NDOT) under project number FY21-005 – UHPC Decked I-Beam for Accelerated Bridge Construction. The authors would like to express their gratitude for the support and guidance provided by the NDOT Technical Advisory Committee. Findings and conclusions of this project are of the authors and do not reflect the sponsor agencies and collaborators.

ABSTRACT

Ultra-High-Performance Concrete (UHPC) is an excellent material for bridge construction due to its exceptional durability and superior mechanical properties. Several Departments of Transportations (DOTs), including NDOT, have limited the use of UHPC in bridge construction to joints and connections between bridge components due to the relatively high materials cost of commercially UHPC products. Recently, NDOT has sponsored a research project to develop a non-proprietary UHPC using local materials to reduce materials cost and ensure its availability to local contractors and precast producers. The project was completed successfully and an economical UHPC mix that satisfied all workability, durability, and strength requirements was developed and tested. Therefore, it is economically feasible to expand the use of UHPC to bridge superstructure components that can have a service life of over 150 years.

The objective of this project is to develop a UHPC superstructure system for bridges in Nebraska that is optimized with respect to structural efficiency, constructability, and economy. Several UHPC superstructure systems used in France, Korea, Malaysia, USA, and Canada including pi-girders, bulb-tee girders, tub girders, box girders, decked I-beams, and waffle slabs, were reviewed and evaluated to determine the system(s) that meet NDOT needs. A decked I-beam (DIB) section was selected due to its ease of production, constructability, and structural efficiency. Formwork design, production trials, and material/structural testing were conducted for UHPC DIB specimens with ribbed and solid slabs using pre-tensioning and post-tensioning systems. Design examples of a typical bridge using DIBs were also presented to demonstrate the implementation of the latest UHPC design specifications/guidelines.

Table of Contents

ABSTRACT	6
Table of Contents	7
Chapter 1. Introduction	8
1.1. Background	8
1.2. Objectives	9
1.3. Report Outline	9
Chapter 2 Literature Review	10
2.1. Introduction	10
2.2. Current Practices	11
2.3. Experimental Work	17
Chapter 3. System Development	21
3.1 Conceptual Design	21
3.2 Form Design	22
3.3 Design Method	24
Chapter 4. Production Experience	30
4.1 Introduction	30
4.2 Production of Precast Pretensioned DIB	30
4.3 Production of Precast Post-tensioned DIB	39
Chapter 5. Experimental Investigation	56
5.1 Introduction	56
5.2 Component Testing	56
5.3 Full-Scale Testing	70
Chapter 6. Conclusions	86
6.1 Production Conclusions	86
6.2 Design Conclusions	86
REFERENCES	88
APPENDIX A: UHPC DIB FORMS	90
APPENDIX B: TEST CALCULATIONS	94
APPENDIX C: DESIGN EXAMPLES	130

Chapter 1. Introduction

1.1. Background

Ultra-High-Performance Concrete (UHPC) is an excellent material for bridge construction due to its exceptional durability and superior mechanical properties. Several Departments of Transportations (DOTs), including Nebraska DOT (NDOT), have limited the use of UHPC in bridge construction to cast-in-place (CIP) joints and connections between bridge components due to the relatively high materials cost of commercially UHPC products. Other DOTs expanded the use of UHPC to CIP overlay and repair applications to benefit of the UHPC durability by creating a protective layer around the deteriorating component. Recently, NDOT has completed a research project to develop a non-proprietary UHPC using local materials to reduce materials cost and ensure its availability to local contractors and precast producers. The project was successful and an economical UHPC mix that satisfied all workability, durability, and strength requirements was developed and tested. The cost of the developed mix is about 30% of the cost of pre-bagged commercial UHPC. Therefore, it is economically feasible to expand the use of UHPC to precast bridge components, such as deck panels, girders, and decked systems, to have a service life of over 150 years. Some researchers (Voo and Foster 2010) estimated the theoretical service life of UHPC bridges to be about 340 years. UHPC superstructure components will clearly minimize bridge maintenance costs, traffic disruptions, and life cycle cost. Figure 1 shows the different applications of UHPC in bridge construction and highlights the focus of this project, which is the development of bridge decked I-beam (DIB) systems.

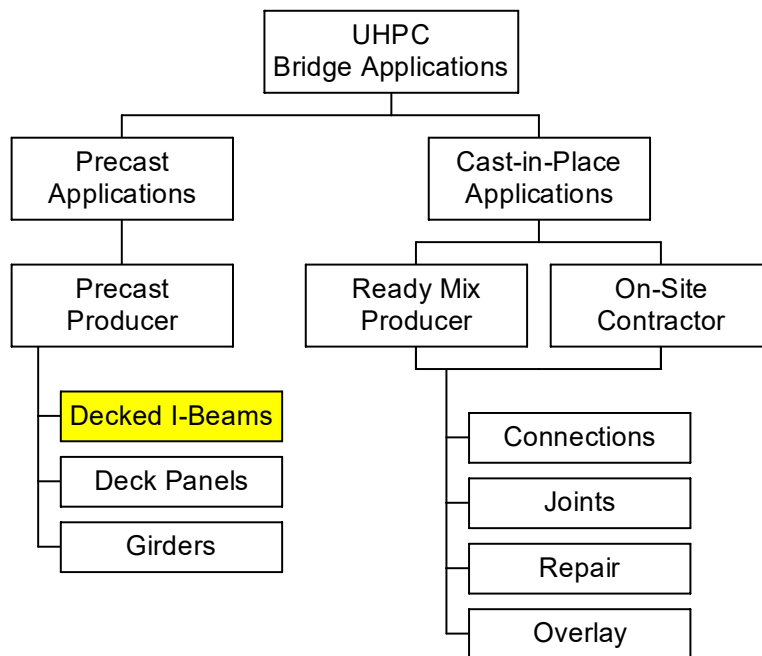


Figure 1.1: UHPC Applications in Bridge Construction

1.2. Objectives

The objective of this project is to develop a UHPC superstructure system for bridges in Nebraska that is optimized with respect to structural efficiency, constructability, and economy. Few highway bridges have already been built using UHPC superstructure in France, Korea, Malaysia, USA, and Canada. These bridges had different superstructure systems including pi-girders, bulb-tee girders, tub girders, box girders, decked I-beams, and waffle slabs. Precast UHPC decked I-beam superstructure system was selected in this study as it saves construction time, enhances superstructure durability, and reduces superstructure weight. The project includes conducting necessary material testing and structural testing; addressing production and forming challenges; and performing design calculations using latest approaches. The work in this project is collaborative effort among research team, NDOT bridge engineers, and local bridge designers, producers and contractors.

1.3. Report Outline

This report is organized as follows:

Chapter 2 Literature Review: It summarizes the current practices of using UHPC in prefabricated superstructure bridge components in the World with emphasis on USA implementation projects as well as experimental investigations conducted on UHPC bridge girders.

Chapter 3 System Development: It discusses the different design alternatives, form design, and the detailed design calculations for an example bridge using different design approaches.

Chapter 4 Production Experience: It presents the production sequences and QA/QC procedures followed by each bridge producer in fabricating the two UHPC specimens for pretensioned and post-tensioned options.

Chapter 5 Experimental Investigation: It presents the testing of the UHPC components and full-scale specimens conducted to evaluate flexure strength, shear strength, punching shear, transverse load distribution, and anchorage zone.

Chapter 6 Conclusions: It summarizes the outcomes of this project and highlights the lessons learned from the production challenges experienced during the fabrication of test specimens as well as the design recommendations resulted from structural testing.

Chapter 2 Literature Review

2.1. Introduction

According to FHWA UHPC interactive map (FHWA, 2023), the use of UHPC in bridge construction in the United States is increasing exponentially in the recent years. Table 2.1 lists the different uses/applications of UHPC in bridge construction, which includes connections, components, and repair applications. By reviewing the number of projects in each of these uses, it was found that the majority of projects benefit from UHPC in connections, link slabs, and deck overlays, with the connections being the most dominant application as shown in Figure 2.1. This figure also shows that the use of UHPC in precast/prestressed bridge girders is very limited, which is the main focus of this project. The authors believe that the reason is that using UHPC with traditional girder sections is neither efficient nor economical and new girder sections are needed to optimize the use of UHPC and maximize the benefits of its unique properties.

Table 2.1: Different uses of UHPC in bridge construction in US (FHWA, 2023)

Abbreviation	Definition
CPBE	connections between prefabricated elements
BDO	bridge deck overlay
BER	beam end repair
EJP	expansion joint header
ECPBE	repair of connections between existing prefabricated elements
LS	link slab
PCG	precast, pretensioned UHPC girder
PCP	precast, pretensioned UHPC pile
PCD	precast deck
PR	minor preservation or repair application

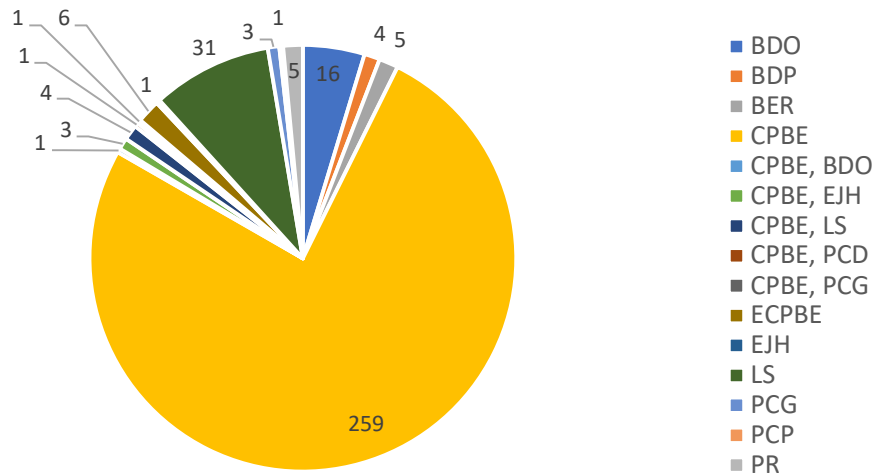


Figure 2.1: Distribution of UHPC uses in US (FHWA, 2023)

2.2. Current Practices

The world's first UHPC highway bridge was built on the Bourg-les-Valence bypass in France in 2002 (Hajar et al., 2003). The bridge has two spans of 72 ft each and a total width of 42 ft 8 in. The superstructure system consisted of five pi-girders that are 2 ft 11 in. deep and connected longitudinally using a cast-in-place UHPC and conventional reinforcement as shown in Figure 2.1. Each pi-girder has 26-0.6 in. diameter Grade 270 low-relaxation bottom strands and 4 top stands. The two spans were made continuous using cast-in-place UHPC over the intermediate pier. No conventional reinforcement was used in the girders except at the joints. The bridge was recently inspected and is performing satisfactorily after 18 years of service with no signs of cracking or deterioration.

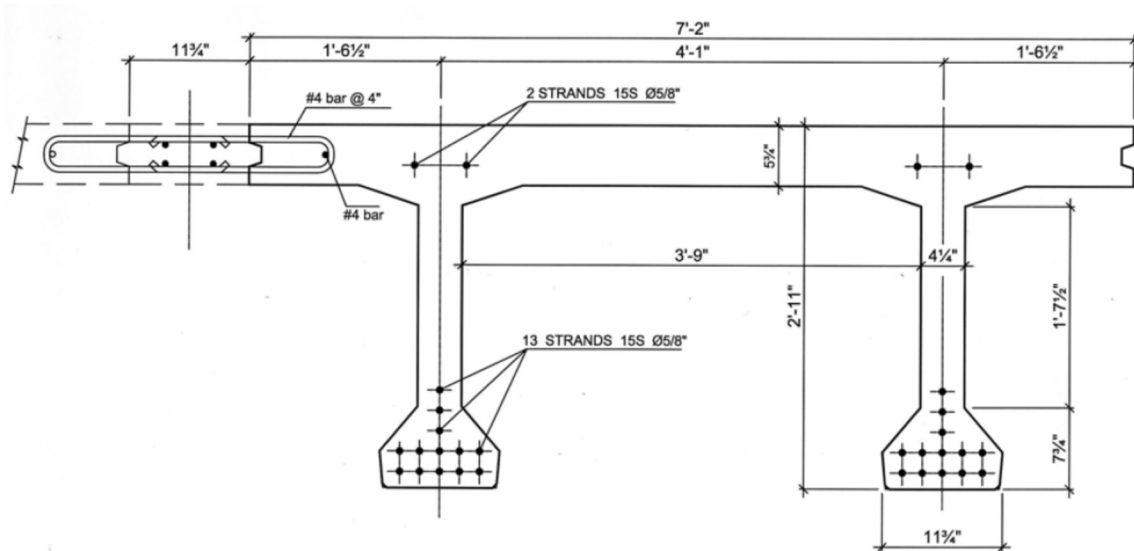


Figure 2.1: Cross Section of the UHPC Girder of Bourg-les Valence Bridge (Hajar et al., 2003)

The construction of an experimental UHPC highway bridge was conducted by the Korea Institute of Construction Technology in 2012 (Park et al., 2013). The bridge has a single simple span of about 37 ft and a total width of 16.6 ft. It consisted of three pi-girders that are 2 ft deep connected longitudinally using cast-in-place UHPC as shown in Figure 2.2. The girders were longitudinally post-tensioned using 7-0.6 in. diameter Grade 270 low relaxation strands in each stem, and transversally post-tensioned using a high strength rod at the intermediate cross beam. No conventional reinforcement was used in this bridge.

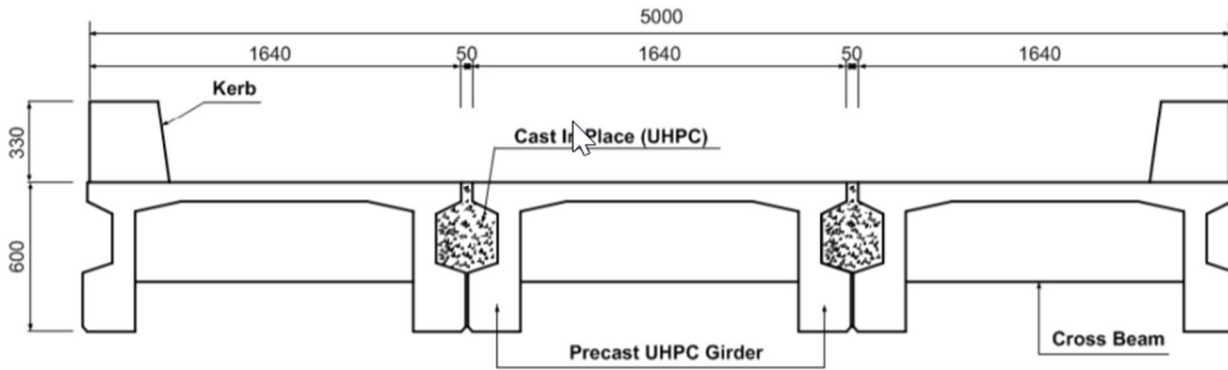


Figure 2.2: Cross Section of the UHPC trial Bridge in Korea (Park et al., 2013)

The first UHPC bridge in US is the Mars Hill Bridge built in Wapello County, IA in 2006 (Bierwagen, et al., 2010). The bridge has a single simple span of 111 ft and total width of 27 ft 2 in. It consists of three modified Iowa bulb-tee girders that are 3.5 ft deep and spaced at 9 ft 7 in. as shown in Figure 2.3. Each girder has a 4.5 in. thick unreinforced web and prestressed using a total 49-0.6 in. diameter Grade 270 low relaxation strands: 2 top strands, 5 draped strands, and 42 straight bottom strands (16 strands were debonded). The bridge has 8 in. thick cast-in-place conventional concrete deck connected to the UHPC girders using conventional steel hairpin bars embedded in the top flange.

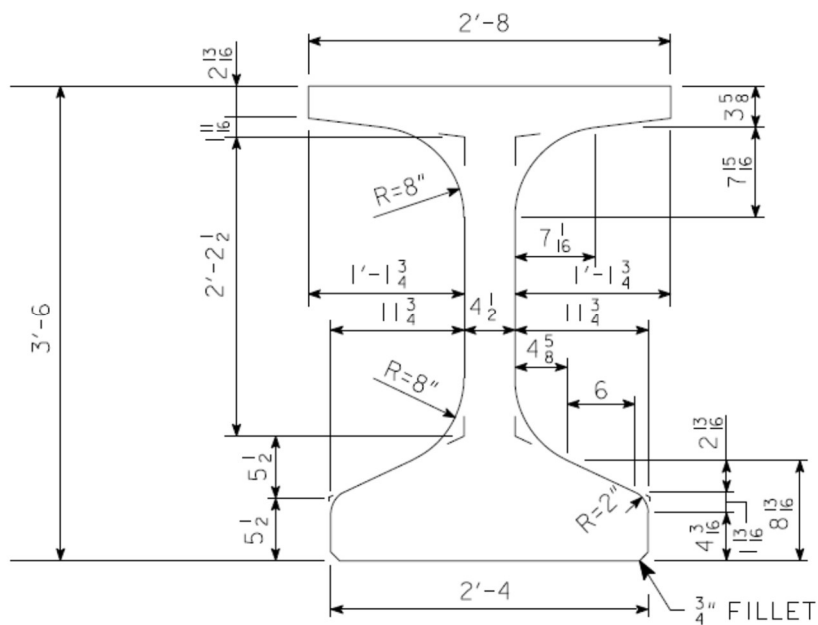


Figure 2.3: Cross Section of Mars Hill Bridge UHPC Girder (Bierwagen, et al., 2010)

The second UHPC bridge in US is the Virginia Department of Transportation (VDOT) bridge on Route 624 over Cat Point Creek completed in 2008. The bridge has 10 spans of 81.5 ft long each. One of the spans

used five UHPC bulb-tee girders that are 45 in. deep. The UHPC had the same cross section of the other bulb-tee girders in the bridge. The only difference was eliminating conventional shear reinforcement and using only confinement reinforcement at the beam ends and interface shear reinforcement in the top flange (Ozyildirim, 2011).

Another UHPC bridge was built in Buchanan County, IA and completed late in 2008 (Bierwagen, et al., 2010). This bridge uses the pi-girder section that was optimized based on finite element analysis and laboratory testing of its first and second generations as shown in Figure 2.4. The Jackway Park bridge has a roadway width of 24 ft 9 in. and total length of 115 ft comprising three spans. Only the center span of 51 ft 2 in. was built using three UHPC pi-girders. Each girder is pretensioned using 18-0.6 in. diameter Grade 270 low relaxation strands and uses conventional reinforcement only at the top flange and connection between adjacent girders.

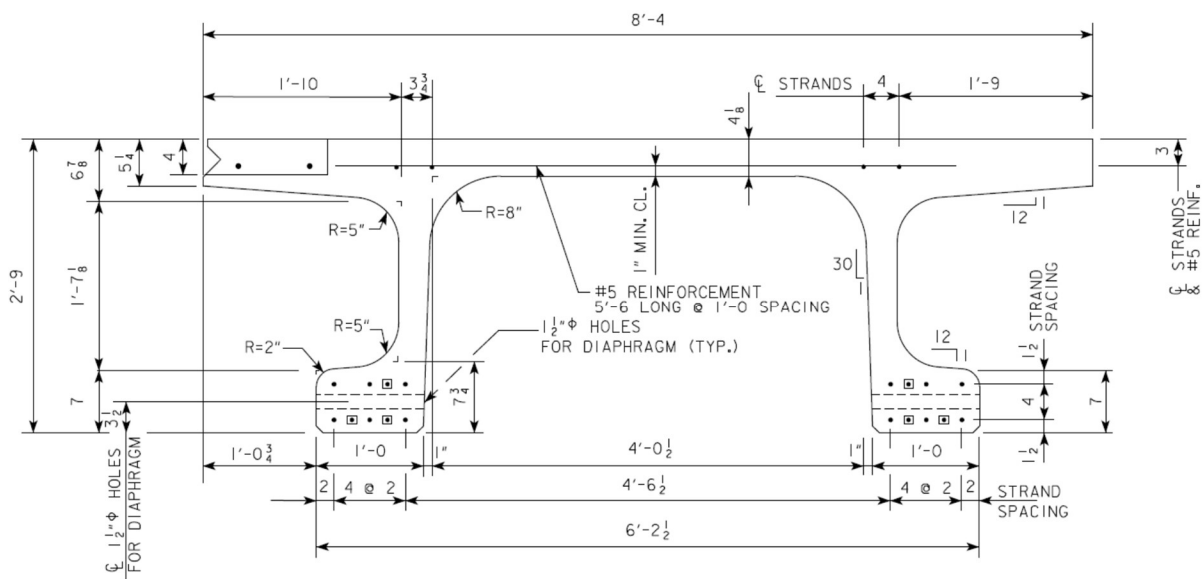


Figure 2.4: Cross Section of Jackway Park Bridge UHPC Girder (Bierwagen, et al., 2010)

In Malaysia, four types of UHPC bridges that are commonly constructed: i) stitched/segmental T-girder come with integral beam-deck system; (ii) segmental U-girders with composite in-situ deck; (iii) UHPC monolithic pretension beam (come with any shape) with composite in-situ deck and (iv) segmental UHPC box-girder construction (Voo, et al. 2014). Figure 2.5 shows the cross section of the three-span Sungai Nerok Bridge built in 2013. Each span is 100 ft long and consists of 10 post-tensioned segmental UHPC T-

girders with integral beam-deck system that are 52 in. deep and spaced at 5 ft. Each girder was fabricated by splicing two segments that are 50 ft long each using one PT tendon. Cast-in-place UHPC is used to connect the T-girders longitudinally by filling the conventionally reinforced joints that are 12 in wide and 5 in. deep. Figure 2.6 shows the cross section of the 172 ft single span Rantau-Siliau Bridge built in 2013. The bridge consists of five U-girders that are 69 in. deep and spaced at 12 ft 4 in. and topped with 8 in. thick cast-in-place concrete deck. Each girder consisted of 7 segments that are spliced and post-tensioned to reduce segment weight in handling and transportation. Conventional reinforcement was only used as interface shear reinforcement and bursting reinforcement at anchorage zones.

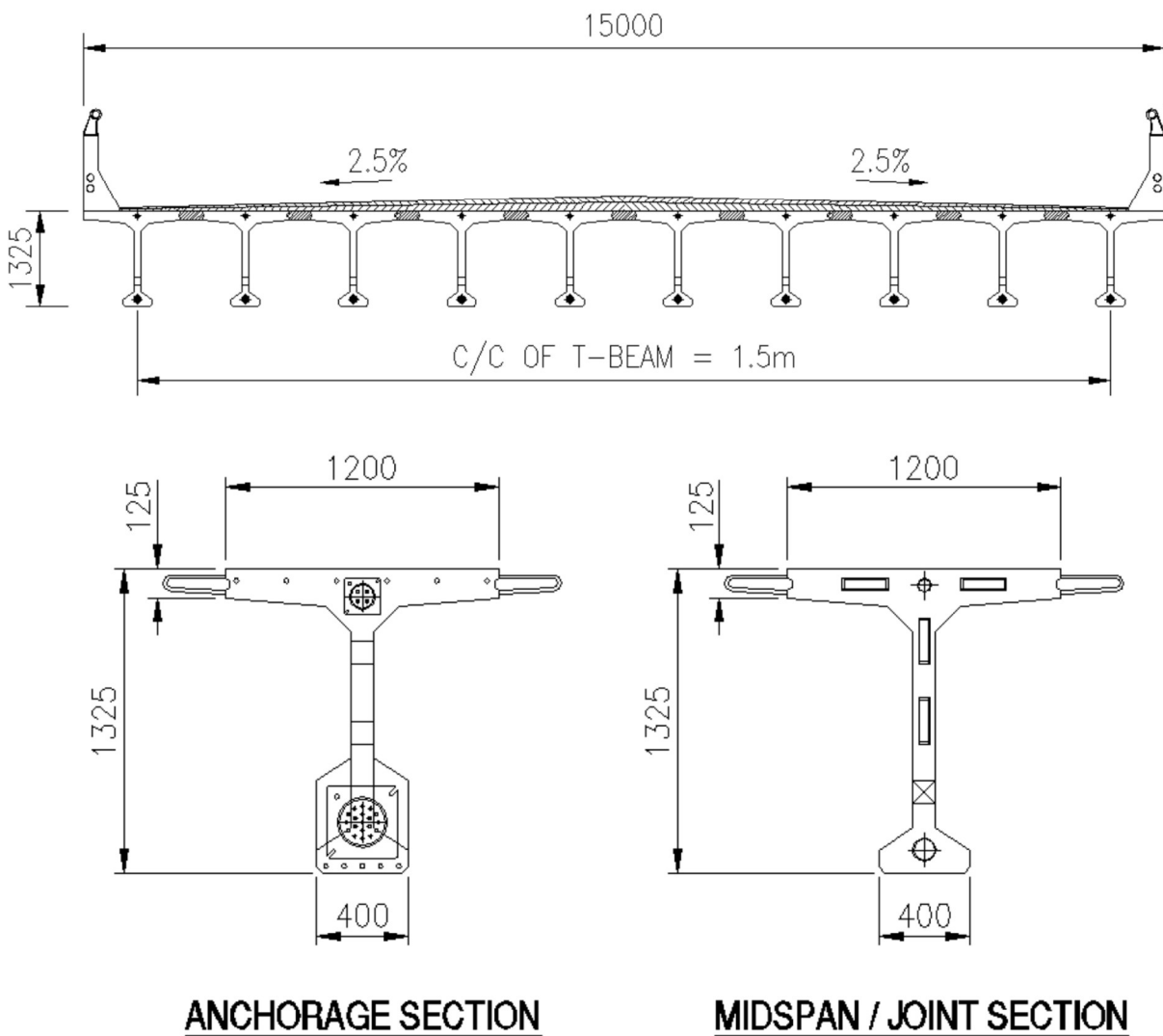


Figure 2.5: Cross Section of UHPC T-Beams of Sungai Nerok Bridge (Voo, et al. 2014)

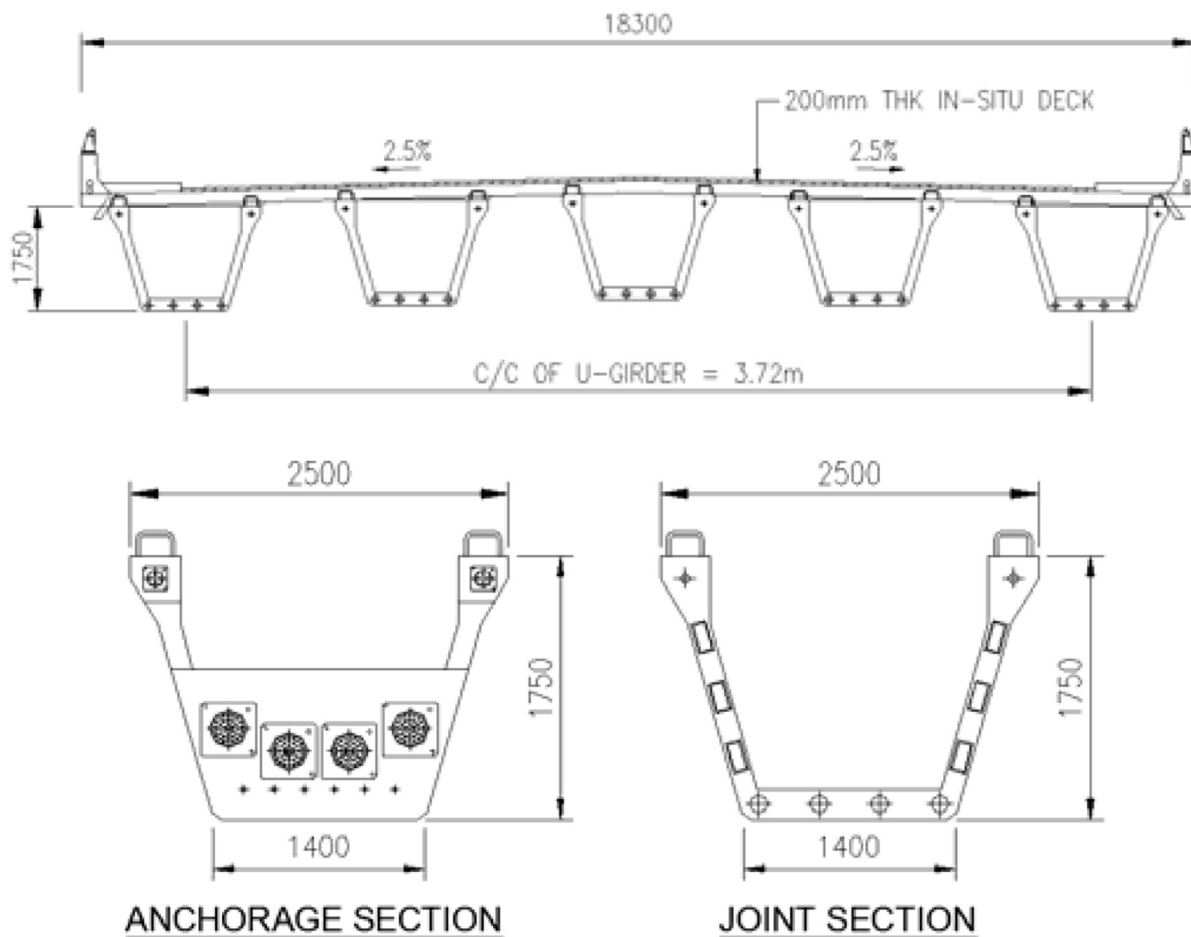


Figure 2.6: Cross Section of UHPC U-Beams of Rantau-Siliau Bridge (Voo, et al. 2014)

A different UHPC superstructure system was developed and implemented in Wapello County, IA using precast UHPC waffle slab panels over conventional concrete girders as shown in Figure 2.7. Each panel has a total thickness of 8 in., skin thickness of 2.5 in., web spacing of 1 ft 9 in., and discrete shear pockets over each girder line at 2 ft spacing. Each web is conventionally reinforced using #7 at the bottom mat and #6 at the top mat in both directions. All joints and connections were filled using cast-in-place UHPC. A total of 14 panels were used to build the deck of the Little Cedar Creek Bridge that was completed in 2010 (Bierwagen, et al., 2010). Coreslab Structures of Omaha, NE was the precaster produced the waffle slab deck panels of this project.

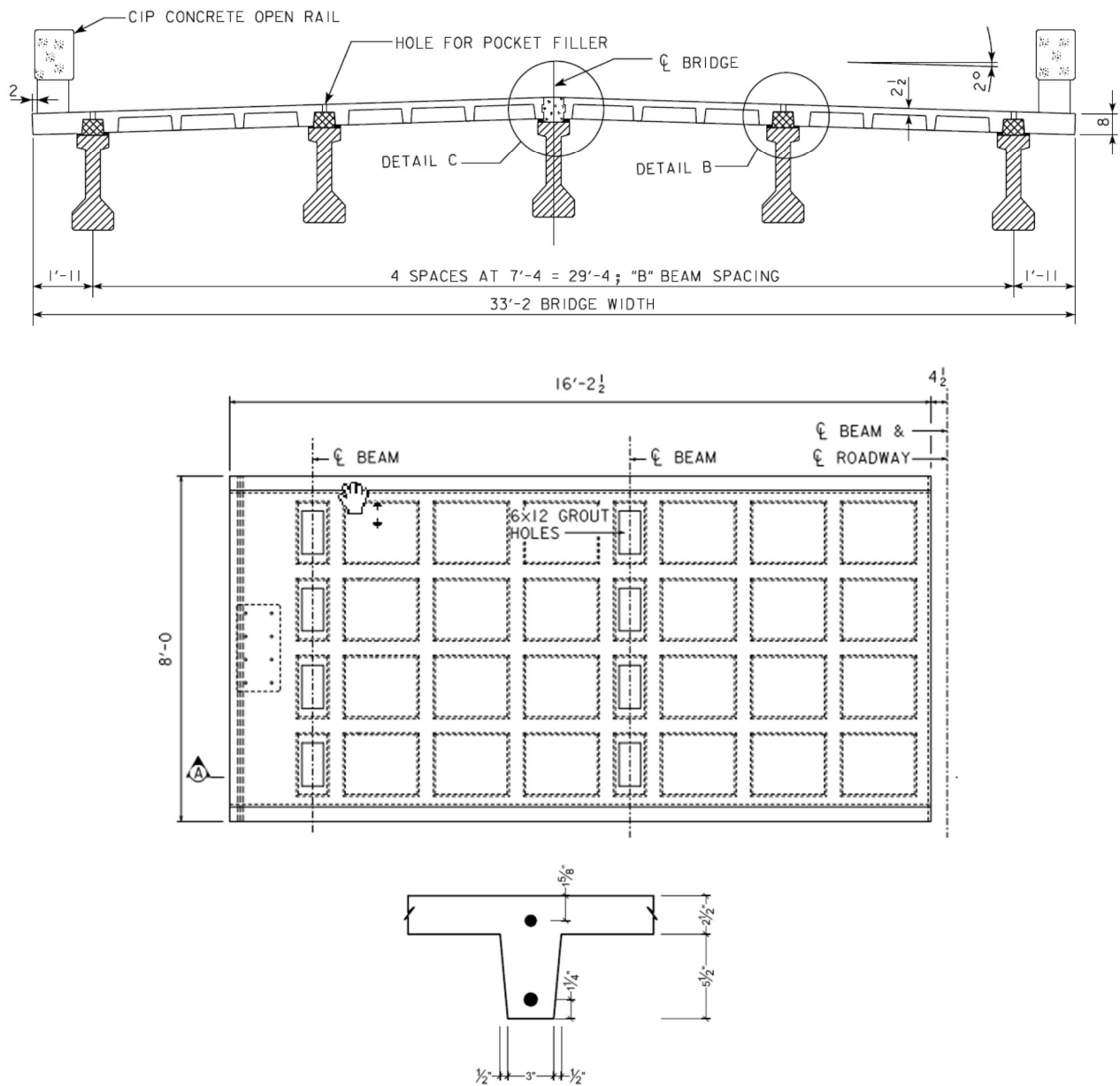


Figure 2.7: Views of UHPC waffle slab of Little Cedar Creek Bridge (Bierwagen, et al., 2010)

Recently e.Construct.US has developed the UHPC decked I-beam section shown in Figure 2.8 for the contractor FACCA Inc. of Ontario, Canada. The beam has been used for the design of the Hitch House Bridge in Ontario completed in early 2020 (Tadros, et al., 2020). The section integrates ribbed slab and I-beam to be precast in one section, which eliminates the need for two-stage casting and reduce the number of precast components in transportation and handling. In addition, this system provides a reduced weight

advantage compared to typical beam and slab construction, which could increase the load carrying capacity of existing bridges. This system combines the advantages of T-beams shown in Figure 2.5 and ribbed slabs shown in Figure 2.7. Connections between adjacent decked I-beams, between decked I-beam and rail, and continuity connection between adjacent spans yet to be developed and tested to ensure their constructability and structural adequacy.

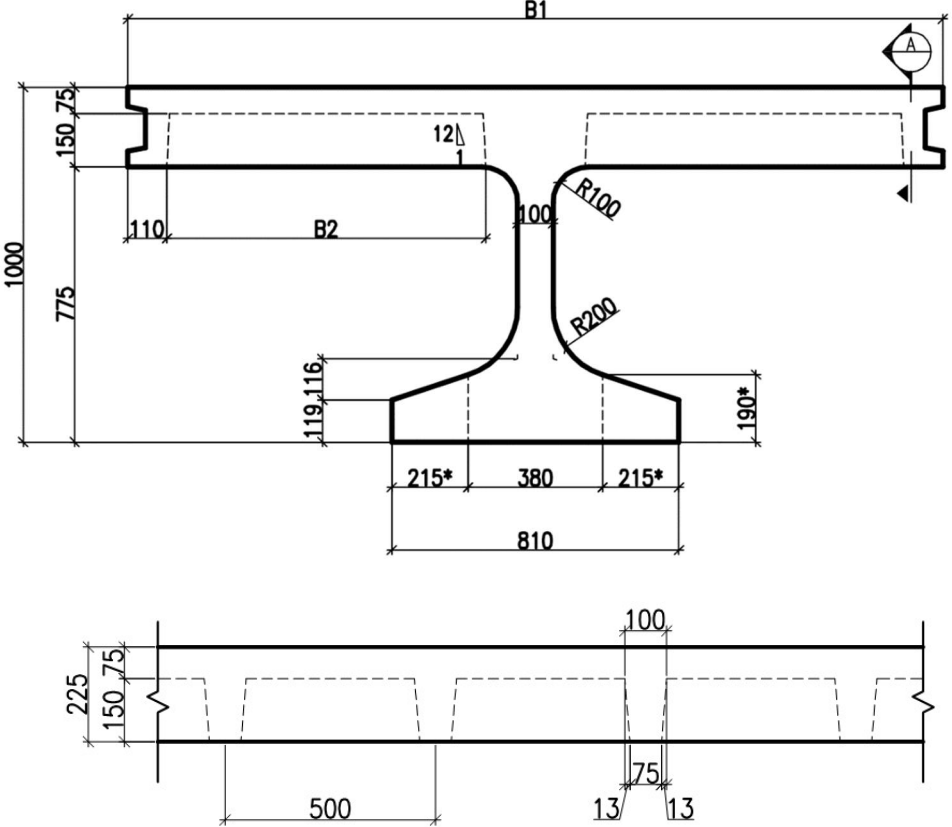


Figure 2.8: Cross Section of UHPC Decked I-Beam Fabricated in Ontario, Canada

2.3. Experimental Work

Several experimental investigations were conducted to evaluate the flexural and shear strength of various precast/prestressed UHPC beams for bridge superstructures. Figure 2.9 shows the five full-scale bridge sections that were tested in flexure: box beam, decked I-beam, AASHTO type II beam, pi-girder, and bulb tee girder. Table 2.2 shows the spans of tested specimens as well as measured versus predicted cracking and peak capacities using the existing design approaches. This table indicates that both cracking and peak flexure capacities of UHPC beams can be accurately and conservatively predicted using existing design approaches as evident in the measured-to-predicted ratios.

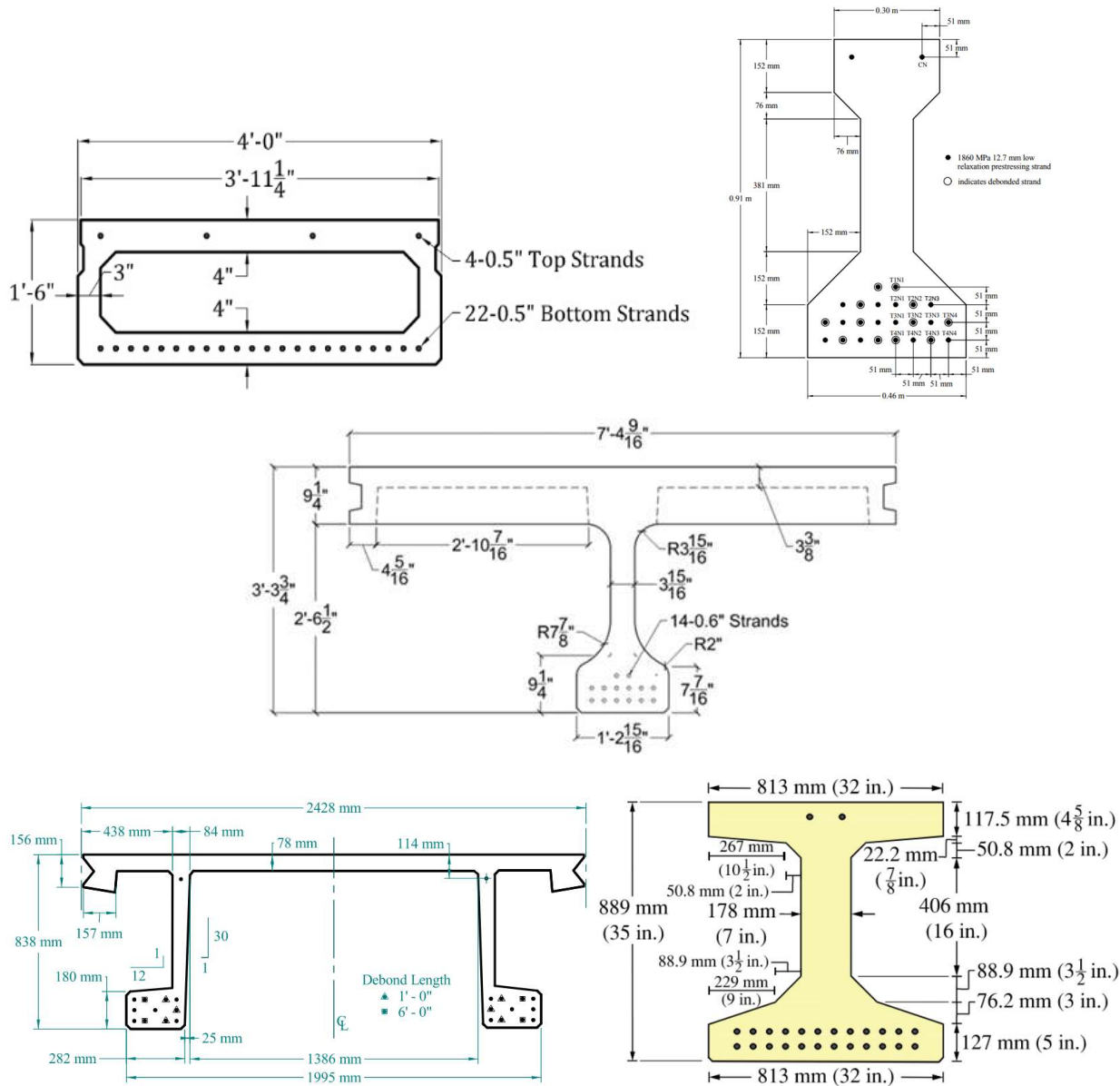


Figure 2.9: Various precast/prestressed bridge superstructure sections tested in flexure

Table 2.2: Summary of flexure tests of UHPC bridge superstructure sections

Reference	Beam Section Type	Specimen Length (ft)	Observed Cracking Moment M_{obs} (kip.ft)	Predicted Cracking Moment M_{cr} (kip.ft)	Ratio M_{obs}/M_{cr}	Measured Flexure Capacity M_{exp} (kip.ft)	Predicted Peak Capacity M_n (kip.ft)	Ratio M_{exp}/M_n
Tadros, et al. (2022) 4.10.2	Bridge Box Beam (BX)	47	869	750	1.16	1454	1208	1.20
Tadros, et al. (2022) 7.7.6	Bridge Decked I-Beam (DIB)	49.25	1803	1709	1.06	3071	2564	1.20
Graybeal, 2006	AASHTO Type II Girder	80	1626	1291	1.26	3522	2457	1.43
Graybeal, 2009	Pi-Girder (1st Generation)	70	1808	1511	1.20	3005	2290	1.31
El-Helou and Graybeal, 2022	NJDOT Bulb-Tee Girder	60	3040	2721	1.12	5734	4748	1.21

Average **1.11** **Average** **1.27**
Std. Dev. **0.08** **Std. Dev.** **0.10**
COV **0.07** **COV** **0.08**

The use of UHPC in bridge girders allows the elimination of traditional shear reinforcement due to the presence of random steel fibers that enhances the girder resistance to diagonal tension. Several experiments were conducted to evaluate the shear strength of precast/prestressed UHPC beams with different configurations to evaluate their impacts on the shear strength. Figure 2.10 shows the parameters considered in the investigation to evaluate their effect on the shear strength and the labels of specimens for each parameter (Tadros, et al. 2022). Figure 2.11 shows the cross section of the reference specimen, which had a height of 34 in., span of 14 ft, and shear span of 7 ft, longitudinal reinforcement of 26-0.6” strands, and no shear reinforcement. Table 2.3 and Figure 2.12 show the results of testing 15 shear specimens (I-beams, DIB, and box beams) as well as the predicted shear strength using the existing design approach. These table and figure indicate that shear capacities of UHPC beams can be conservatively predicted using existing design approaches as evident in the high average of experimental-to-predicted capacity ratio of 1.9 and relatively low coefficient of variation of 0.15.

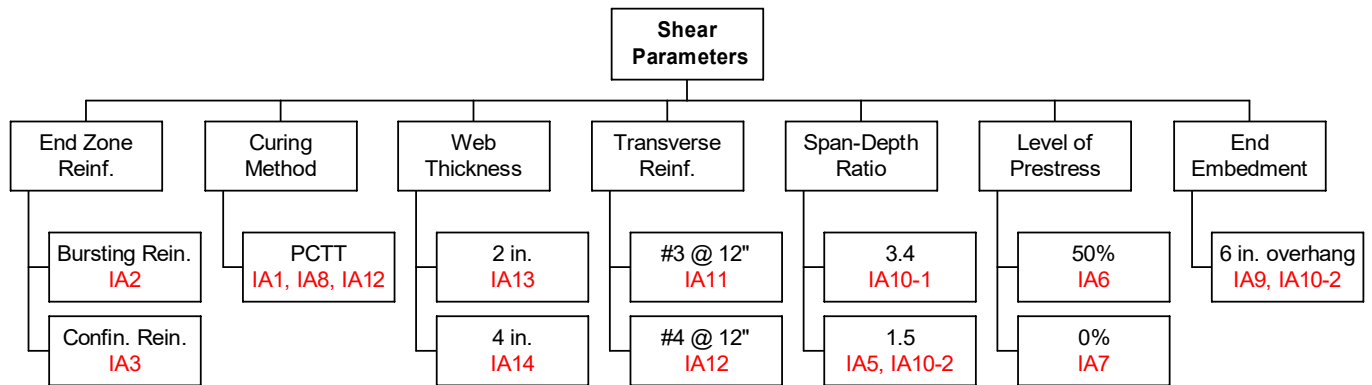


Figure 2.10: UHPC shear test parameters

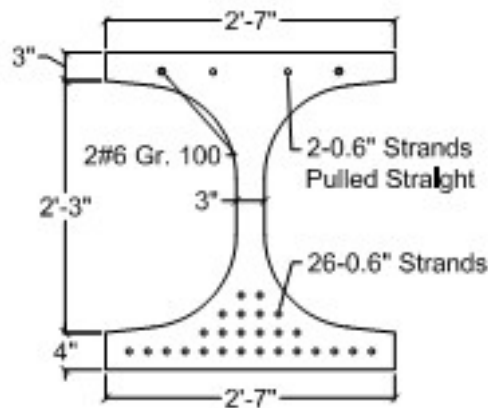


Figure 2.11: Cross section of the reference shear test specimen

Table 2.3: Summary of shear tests of UHPC specimens

Specimen	Section Type	Test Specimens		
		Experimental Capacity	Predicted Capacity	V_{exp}/V_n
		V_{exp} (kip)	V_n (kip)	
IA1	I-Beam	364	162	2.25
IA2	I-Beam	311	162	1.92
IA3	I-Beam	308	162	1.90
IA6	I-Beam	340	155	2.19
IA7	I-Beam	289	142	2.04
IA8	I-Beam	354	162	2.19
IA9	I-Beam	324	162	2.00
IA10-1	I-Beam	318	162	1.96
IA11	I-Beam	391	211	1.85
IA12	I-Beam	406	252	1.61
IA13	I-Beam	236	107	2.21
IA14	I-Beam	410	218	1.88
DIB-1	Decked I-Beam	355	264	1.34
BX-1	Box Slab	273	174	1.57
BX-2	Box Slab	256	174	1.47
Average		329.0	177.9	1.89
Standard Deviation		52.5	41.4	0.28
Coff. Of Variation		0.16	0.23	0.15

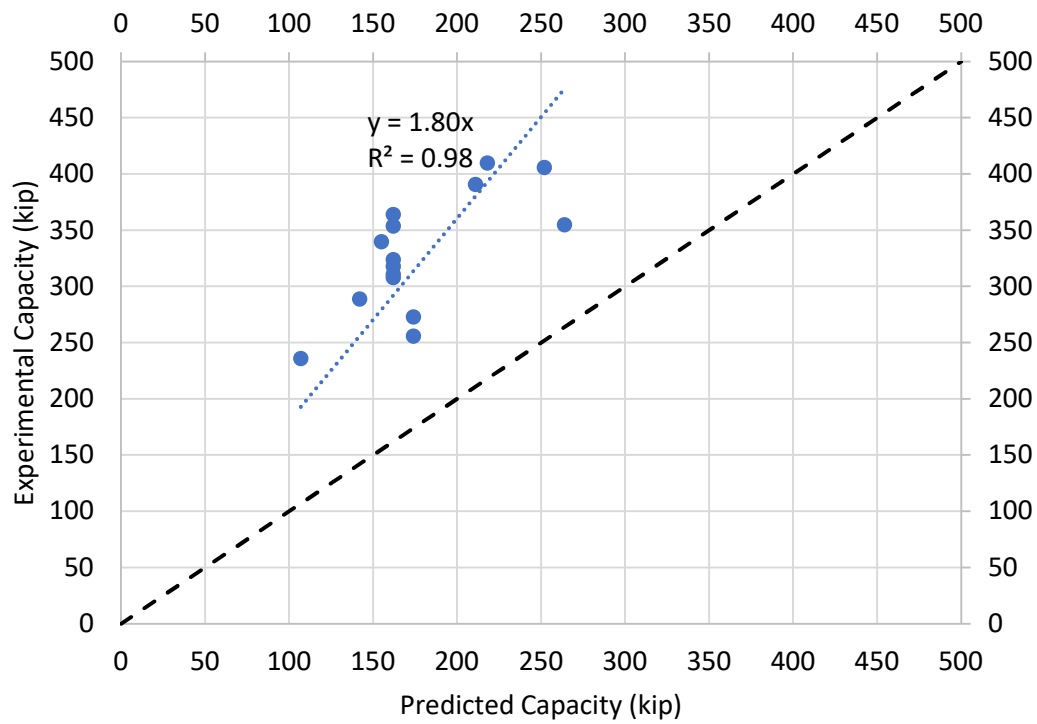


Figure 2.12: Plot of predicted versus experimental shear capacity.

Chapter 3. System Development

3.1 Conceptual Design

At the initial phase of this project, several conceptual design alternatives were considered for a UHPC superstructure system for accelerated bridge construction in the state of Nebraska. The main criterion in all these alternatives is to have a UHPC deck to address the common problem of deteriorating concrete bridge decks that leads to shorter service life, high maintenance cost, and frequent road closures. Figure 3.1 shows the five alternatives considered initially by the research team based on the literature review, which include UHPC DIB with solid slab, UHPC DIB with ribbed slab with and without edge rib, conventional concrete I-beam made composite with UHPC ribbed slab, and UHPC I-beam made composite with UHPC ribbed slab. These alternatives were discussed with NDOT bridge engineers and precast bridge producers and were evaluated with respect to weight, ease of production, and speed of construction. It was decided to eliminate the two alternatives with multiple components that need to be made composite as this could slow down the construction and may require further testing of the shear connectors. For the remaining alternatives, UHPC DIB with ribbed slab is the best alternative with respect to weight, while UHPC DIB with solid slab is the best alternative with respect to ease of production. These two alternatives are considered in this study due to the unique advantage of each alternative. The use of edge rib has the advantage of simplifying beam production and forming the cast-in-place longitudinal joints in the field, but it requires different sets of forms for different widths of the top flange. On the other hand, the elimination of edge rib has the advantage of simplifying form stripping and accommodating variable width of the top flange, but it requires additional forms for casting the longitudinal joints in the field. Therefore, this alternative is not considered in this study as it depends on the bridge contractor preference and will require further discussion with respect to duration and cost of construction.

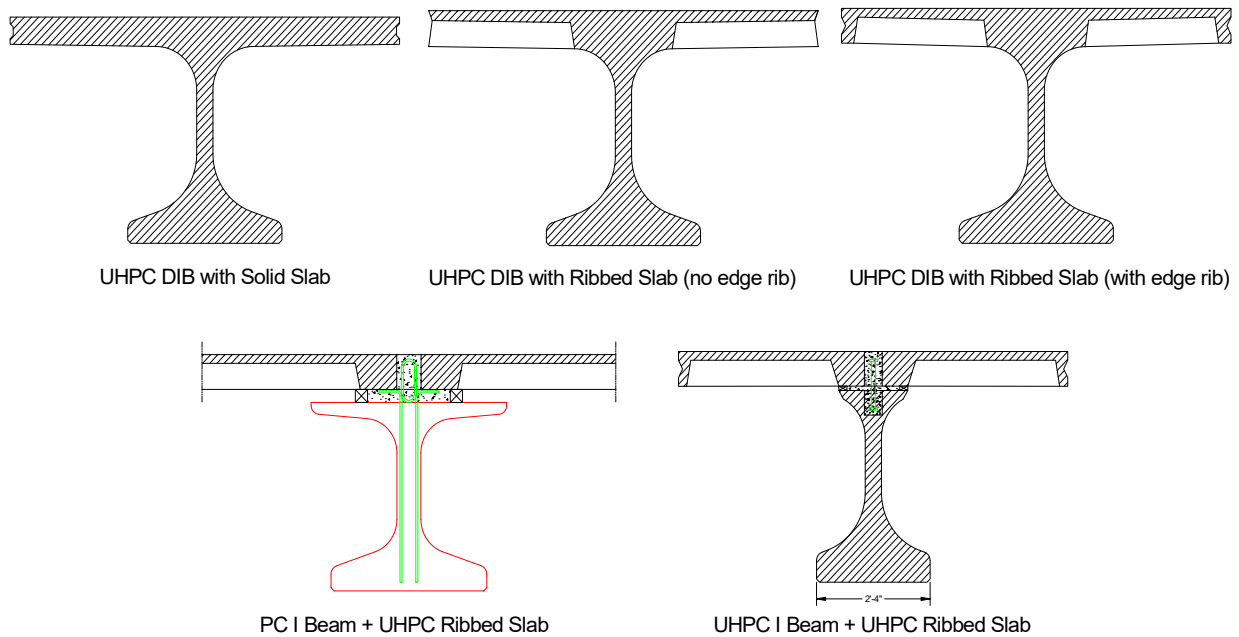
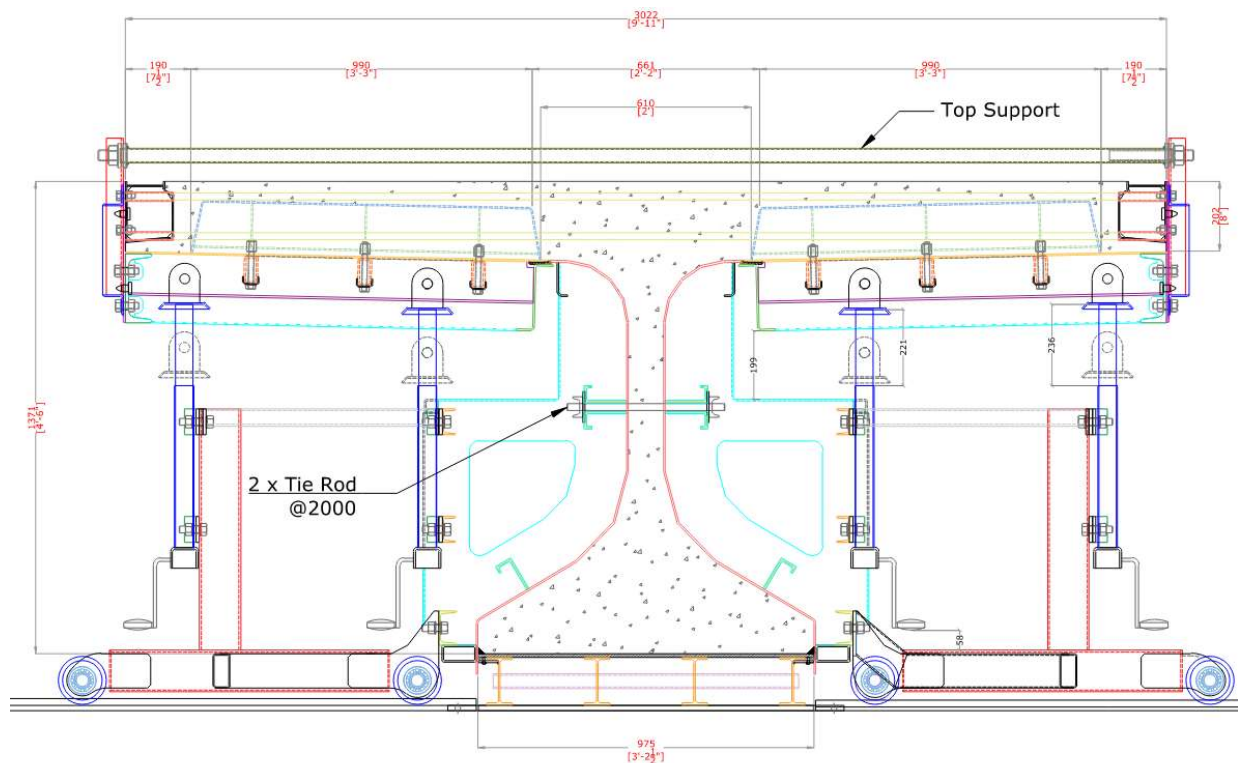


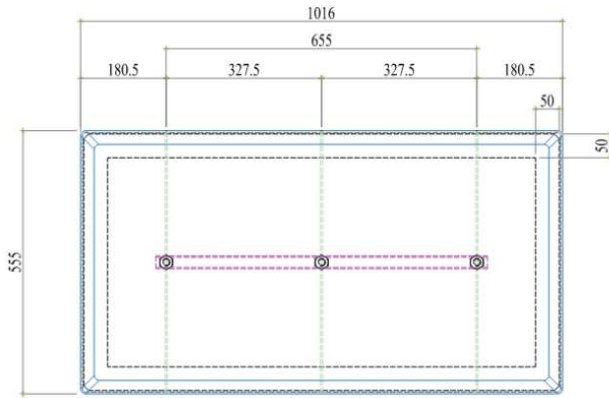
Figure 3.1: Conceptual design alternatives for UHPC bridge superstructure system

For the selected UHPC DIB design alternative, two production options are proposed: 1) pretensioned full length DIB; and 2) post-tensioned DIB segments. Although the pretensioned option is preferred due to its simplicity, speed of production, and economy, it imposes a great challenge for precast bridge producers as their current production facilities are not equipped to produce the large quantity of UHPC needed for a full-length UHPC DIB in a continuous and efficient manner. Therefore, the post-tensioned option is considered as a possible solution that allows the production of short-length UHPC DIB segments that can be match cast and spliced using post-tensioning. Shear keyed exposed joints are expected between the segments (Voo, et al., 2015).

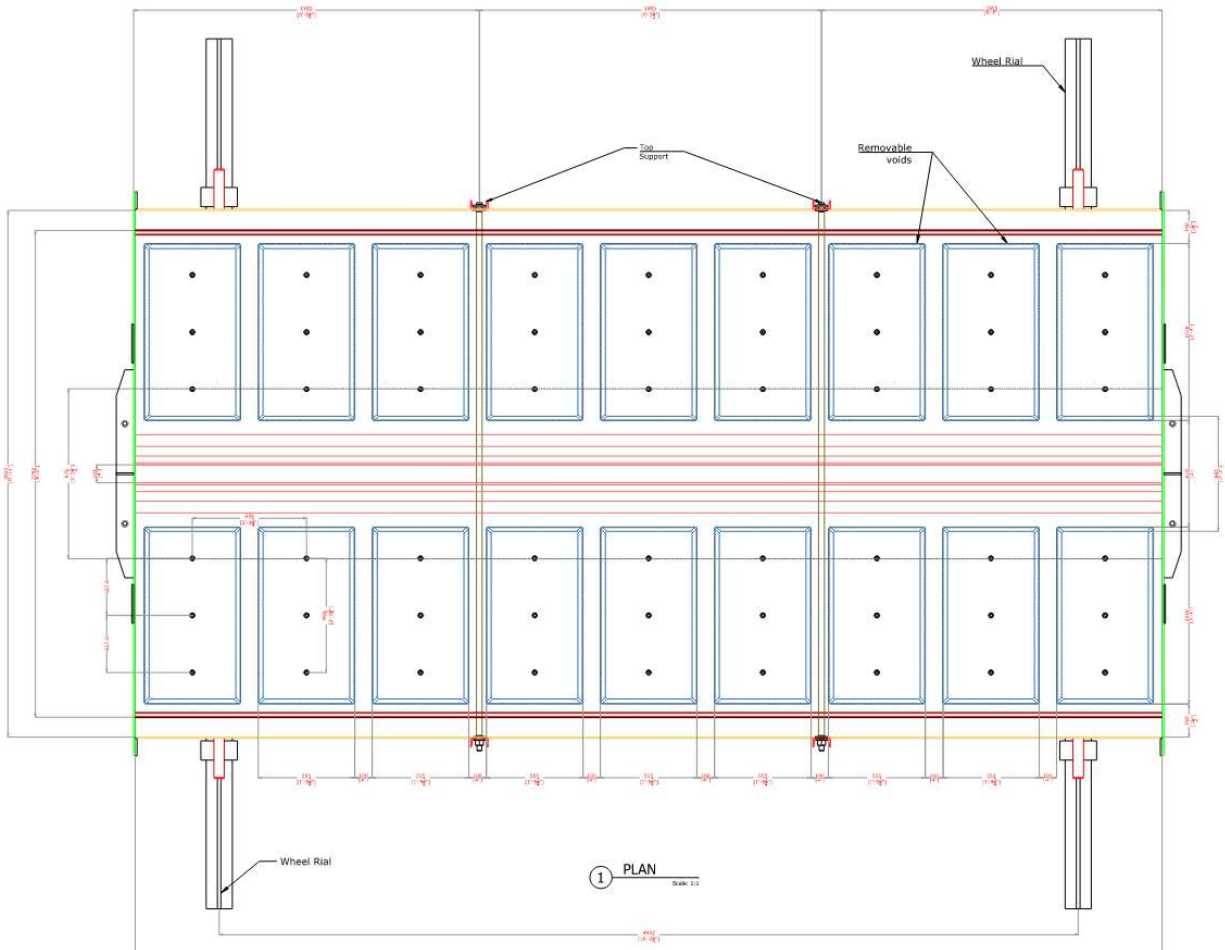
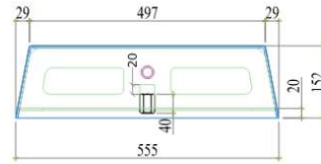
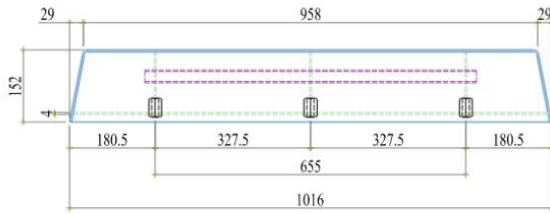
3.2 Form Design

The decked I-beam (DIB) form was designed to allow for the different design alternatives mentioned earlier by using removable rib forms (i.e. pans) to allow for the solid slab alternative, and removable edge forms to allow for using different edge forms or eliminating them all together. DIB form was designed in consultation with KESSAB STEEL LLC (Form Manufacturer in United Arab of Emirates) in several iterations to optimize the DIB section and simplify erection and strip of forms. The manufacturer suggested the use of manually operated cranking system to allow for the vertical movement of the soffit forms. This was designed to help stripping the forms by lowering the soffit first, then moving the side forms outward on wheels and wheel rails. Each pan is anchored from the bottom using three bolts that can be easily removed in case the pans are stuck and cranking system was unable to lower the soffit form. Figure 3.2 shows the DIB cross section and the sectional, plan, and elevation views of the forms for a 19 ft 4 in. long, 9 ft 11 in. wide, and 4 ft 4 in. high DIB. The figure also shows the dimension of the pans used to create the ribbed slab. Figure 3.3 shows a 3D view of the forms and the way of erecting and stripping them. For more photos of the form pieces during manufacturing, refer to Appendix A.





Removable Void Detail



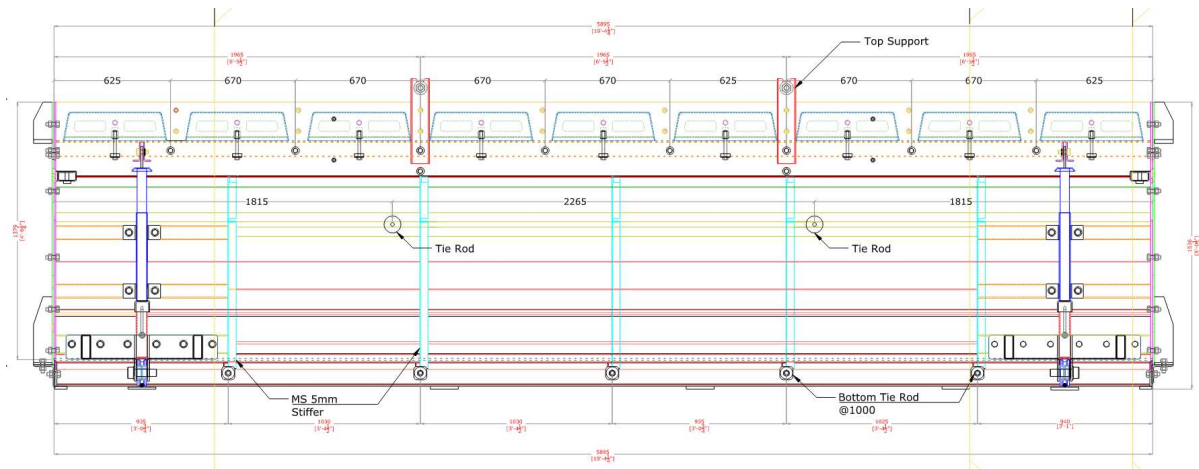


Figure 3.2: Sectional, plan, and elevation views of the DIB forms

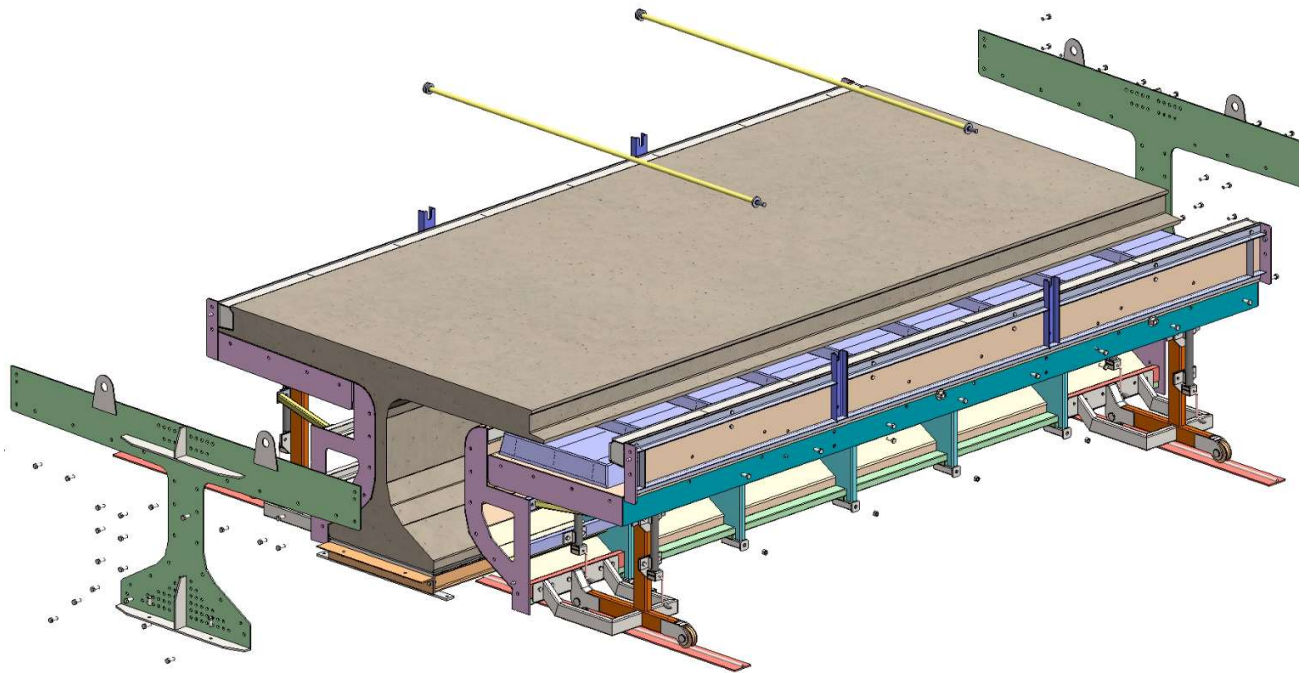


Figure 3.2: 3D view of the DIB forms and its stripping process

3.3 Design Method

To demonstrate the detailed design of the UHPC DIB system, an example of 100 ft long simply supported bridge is used. The bridge will have four DIBs at 10 ft spacing and clear roadway width of 36.5 ft. More information about the design example is shown in Appendix C. In this example, calculations for the pretensioned system with ribbed slab and solid slab options are presented. An alternate system with segmental post-tensioning could be used to alleviate the challenges of producing large batches of UHPC. In this case, design changes will be limited to the allowable tension limit under service loads and the end-zone reinforcement at the post-tensioning anchorages.

Currently, there are two sources for the structural design of precast/prestressed UHPC bridge components: a) PCI Phase II Report v2.0 (Tadros, et al., 2022); and b) AASHTO LRFD Guide Specifications for Structural Design with Ultra-High-Performance Concrete. The latter is still a draft under review and ballot by AASHTO Committee T10 and State DOTs at the time of writing this report. The PCI design approach specifies specific mechanical properties of UHPC that meets minimum material requirements of the specimens prepared and tested according to the general requirements of ASTM C1856, which are: 1) compressive strength = 17.4 ksi, according to ASTM C39, tested using 3 in. by 6 in. cylinders; 2) tensile properties, according to ASTM C1609, 4 in. by 4 in. by 14 in. prisms: (a) cracking strength = 1.5 ksi, (b) peak strength = 2.0 ksi, (c) peak-to-cracking ratio ≥ 1.25 and (d) residual stress at span/150 to cracking ratio ≥ 0.75 . The AASHTO LRFD design approach allows for designing a wider range of UHPC materials with mechanical properties determined using ASTM C1856 for compressive strength and AASHTO T397 for tensile properties.

The PCI Phase II Report v2.0 (Tadros, et al., 2022) and AASHTO LRFD Guide Specifications (draft) have different approaches for characterizing UHPC material, flexure design, shear design, and transfer and development length predictions as presented in side-by-side comparisons in Tables 3.1, 3.2, 3.3, and 3.4. For the purpose of simplification, only PCI UHPC material properties are used in the design example while calculations using both approaches for flexure design and shear design are presented. Calculations have shown that there are no significant differences in the level of prestressing or shear reinforcement required by the two design approaches.

Table 3.1: Comparing UHPC Material Properties

Property	Test Method	PCI Phase II Report*	AASHTO Draft Guide Specs.**
Modulus of Elasticity	ASTM C1856	6500 ksi	6500 - 9400 ksi
Compressive Strength	ASTM C1856	17.4 ksi	18 - 36 ksi
Ultimate Compressive Strain	ASTM C1856	0.003	0.003 - 0.005
Effective Cracking Strength	AASHTO T397 / ASTM C1856	0.75 ksi	0.75 - 1.80 ksi
Crack Localization Strength	AASHTO T397 / ASTM C1856	0.75 ksi	0.75 - 1.80 ksi
Crack Localization Strain	AASHTO T397 / ASTM C1856	0.005	0.0025 - 0.008

* Values are constant for UHPC that meets PCI-UHPC Target Minimum Properties

** Values are determined based on test results

Table 3.2a: Comparing Flexure Design Approaches (Summary)

Item	PCI Phase II Report	AASHTO Draft Guide Specs.
Compression Model	Bilinear with ultimate strain of 0.003	Bilinear with ultimate strain of 0.0035
Tension Model	Elastic Perfectly Plastic Model with maximum stress of 0.75 ksi and ultimate strain of 0.005	Either Elastic Perfectly Plastic or Bilinear Model Based on Direct Tension Test Results
Flexural Strength	The larger of 1st peak (localization) and ultimate values	The one with lesser curvature among localization, ultimate, and rupture
Resistance Factor	AASHTO LRFD Strain-based (0.75 - 0.9 or 1.0)	Using Curvature Ductility Ratio (0.75 - 0.9)
Minimum Reinforcement	AASHTO LRFD with $f_r = 1 \text{ ksi}$	AASHTO LRFD with $f_r = f_{t,cr}$

Table 3.2b: Comparing Flexure Design Approaches (Detailed)

Item	PCI Phase II Report	AASHTO Draft Guide Spec.
Compression and Tension Models		<p>Figure 1.4.2.4.3-1—Idealized compressive stress-strain model for UHPC</p>
		<p>Figure 1.4.2.5.4-1—Idealized tensile stress-strain model for UHPC</p>
		<p>Figure 1.4.2.5.4-2—Idealized tensile stress-strain model for UHPC with $f_{t,loc} \geq 1.20 f_{t,cr}$</p>

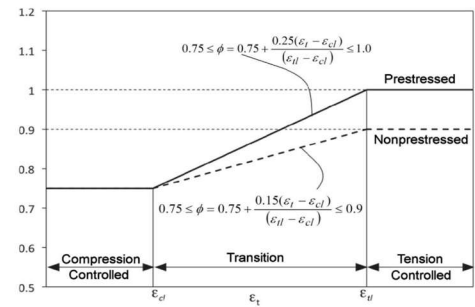
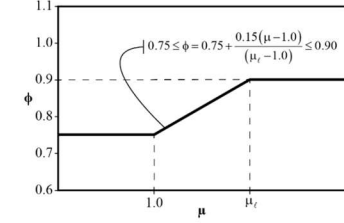
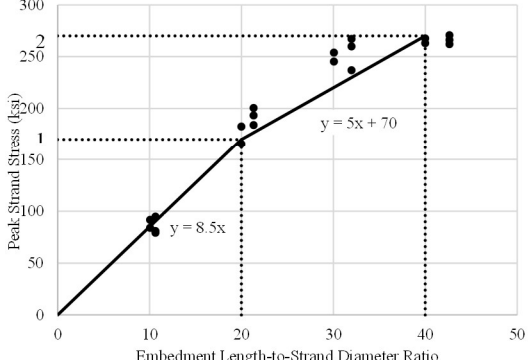
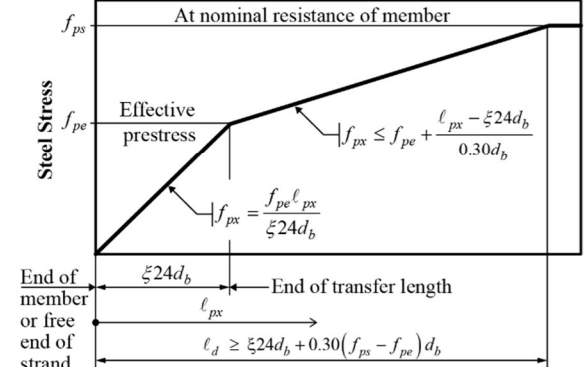
<p style="text-align: center;">Flexure Strength</p>	<p>4.8.2.3.1 Flexural Strength For concrete mixtures meeting the minimum PCI-UHPC properties, flexural strength is to be calculated as the larger of two values, as shown in the following two options:</p> <p>(1) Use the tension and compression stress-strain diagrams construction of the full moment-curvature diagram for given cross section dimensions and reinforcement. Establish the peak values of moment on the curve and the corresponding resistance reduction factors. The value of the moment in this option may need to be modified if the designer wishes to impose an upper limit on the strand strain of 3.5% per ASTM A416. It will be shown that this modification results in accuracy improvement that is not significant in practice, especially in light of the fact that the final recommendation by the authors for prestressed concrete section analysis is to ignore the fibers and to avoid creation of the moment-curvature diagram.</p> <p>(2) Use the conventional equivalent rectangular stress block on the compression side of the neutral axis with the extreme compression strain of 0.003 and the tension model adopted in option (1). Establish the nominal resistance that satisfies equilibrium and strain compatibility as conventional concrete.</p>	<p style="text-align: center;"><i>1.6.3.2.2—Nominal Flexural Resistance</i></p> <p>The nominal flexural resistance shall be obtained from a strain compatibility analysis according to Article 1.6.3.1 and shall be taken as the moment corresponding to the lesser of the sectional curvature values calculated when:</p> <ul style="list-style-type: none"> • The compressive strain at the extreme compression fiber of the UHPC section is equal to the compression strain limit, ϵ_{cu}, • The net tensile strain at extreme tension fiber of the UHPC section is equal to the UHPC tensile strain limit, $\epsilon_{t,loc}$, and • The strain in the extreme tension steel is equal to the minimum total elongation strain of reinforcing steel.
<p style="text-align: center;">Resistance Factor</p>	 <p>The graph shows the resistance factor ϕ on the y-axis (ranging from 0.5 to 1.2) against strain ϵ on the x-axis. It is divided into three regions: Compression Controlled (from ϵ_{cl} to ϵ_t), Transition (from ϵ_t to ϵ_{tl}), and Tension Controlled (from ϵ_{tl} onwards). For the Prestressed region, the equation is $0.75 \leq \phi = 0.75 + \frac{0.25(\epsilon_t - \epsilon_{cl})}{(\epsilon_{tl} - \epsilon_{cl})} \leq 1.0$. For the Nonprestressed region, the equation is $0.75 \leq \phi = 0.75 + \frac{0.15(\epsilon_t - \epsilon_{cl})}{(\epsilon_{tl} - \epsilon_{cl})} \leq 0.9$.</p>	 <p>The graph shows the resistance factor ϕ on the y-axis (ranging from 0.6 to 1.1) against the sectional curvature ductility ratio μ on the x-axis. The curve is constant at $\phi = 0.75$ for $\mu \leq 1.0$. For $\mu > 1.0$, the equation is $0.75 \leq \phi = 0.75 + \frac{0.15(\mu - 1.0)}{(\mu_t - 1.0)} \leq 0.90$.</p> <p style="text-align: center;">Figure C1.5.4.2-1—Variation of the flexural resistance factor, ϕ, with the sectional curvature ductility ratio, μ, for UHPC sections reinforced with prestressed steel, nonprestressed steel, or both.</p>

Table 3.3: Comparing Shear Design Approaches

Item	PCI Phase II Report (E.7.3)	AASHTO Draft Guide Spec. (1.7.3)
Approach	Sectional Design Model and derived from MCFT	Sectional Design Model and based on the principles of MCFT with modifications to material models
Nominal Shear Resistance	$V_n := V_{cf} + V_s + V_p$	$V_n := V_{UHPC} + V_s + V_p$
Upper Limit	$V_{nmax} := 0.25 f'_c \cdot b_v \cdot d_v + V_p$	$V_{nmax} := 0.25 f'_c \cdot b_v \cdot d_v + V_p$
Resistance Factor	$\phi_v := 0.9$	$\phi_v := 0.9$
UHPC Contribution	$V_{cf} := f_t \cdot b_v \cdot d_v \cdot \cot(\theta)$ $f_t := 1 \text{ ksi}$	$V_{UHPC} := \gamma_u \cdot f_{t.loc} \cdot b_v \cdot d_v \cdot \cot(\theta)$ $\gamma_u := 0.85 \quad f_{t.loc} := 1.2 \text{ ksi}$
Transverse Reinforcement	$V_s := \frac{A_v \cdot f_y \cdot d_v \cdot (\cot(\theta) + \cot(\alpha)) \cdot \sin(\alpha)}{s}$	$V_s := \frac{A_v \cdot f_v \cdot d_v \cdot (\cot(\theta) + \cot(\alpha)) \cdot \sin(\alpha)}{s}$
For Vertical Stirrups	$V_s := \frac{A_v \cdot f_y \cdot d_v \cdot \cot(\theta)}{s}$	$V_s := \frac{A_v \cdot f_v \cdot d_v \cdot \cot(\theta)}{s}$
Notes	Stirrups use in PCI-UHPC is highly discouraged as it defeats the simplicity of PCI-UHPC design and production and creates a disturbance to the random flow of fibers down the web.	In composite sections made with UHPC beams and conventional concrete decks, the effective shear depth, d_v , in Eq. 1.7.3.3-2 through 1.7.3.3-4, shall not exceed the portion of d_v within the UHPC section.
Crack Angle	$\theta := (29 + 3500 \cdot \varepsilon_s) \cdot \text{deg}$	<p>General Approach (iterative to find Θ and ε_v)</p> $\varepsilon_{t.loc} = \frac{\varepsilon_s}{2} \cdot (1 + (\cot(\theta))^2) + \frac{2 \cdot f_{t.loc}}{E_c} \cdot (\cot(\theta))^4 \downarrow$ $+ \frac{2 \cdot \rho_v \cdot \min(E_s \cdot \varepsilon_v, f_y)}{E_c} \cdot \sin(\alpha) \cdot (\cot(\theta))^2 \cdot (1 + (\cot(\theta))^2 + \cot(\alpha) \cdot (\tan(\theta) + \cot(\theta)))$ $\varepsilon_v - \varepsilon_{t.loc} + 0.5 \cdot \varepsilon_s = \frac{-2 \cdot f_{t.loc}}{E_c} \cdot (\cot(\theta))^2 \downarrow$ $- \frac{2 \cdot \rho_v \cdot \min(E_s \cdot \varepsilon_v, f_y)}{E_c} \cdot \sin(\alpha) \cdot (1 + (\cot(\theta))^2 + \cot(\alpha) \cdot (\tan(\theta) + \cot(\theta)))$ <p>Simplified Approach (Tables)</p>
Tensile Strain	$\varepsilon_s := \min \left(\frac{\left(\frac{ M_u }{d_v} + 0.5 N_u + V_u - V_p - A_{ps} \cdot f_{po} \right)}{E_p \cdot A_{ps} + E_s \cdot A_s}, 0.006 \right)$ $\varepsilon_s := \text{if} \left(\varepsilon_s < 0, \max \left(\frac{\left(\frac{ M_u }{d_v} + 0.5 N_u + V_u - V_p - A_{ps} \cdot f_{po} \right)}{E_p \cdot A_{ps} + E_s \cdot A_s + E_c \cdot A_{ct}}, -0.0004 \right), \varepsilon_s \right)$	$\varepsilon_s := \min \left(\frac{\left(\frac{ M_u }{d_v} + 0.5 N_u + V_u - V_p - A_{ps} \cdot f_{po} - \gamma_u \cdot f_{t.cr} \cdot A_{ct} \right)}{E_s \cdot A_s + E_p \cdot A_{ps}}, \varepsilon_{t.loc} \right)$ $\varepsilon_s := \text{if} \left(\varepsilon_s < \varepsilon_{t.cr}, \frac{\left(\frac{ M_u }{d_v} + 0.5 N_u + V_u - V_p - A_{ps} \cdot f_{po} \right)}{E_p \cdot A_{ps} + E_s \cdot A_s + E_c \cdot A_{ct}}, \varepsilon_s \right)$
Longitudinal Reinforcement	$A_{ps} \cdot f_{ps} + A_s \cdot f_y \geq \frac{ M_u }{d_v \cdot \phi_f} + 0.5 \frac{N_u}{\phi_c} + \left(\frac{ V_u - V_p }{\phi_v} - 0.5 V_s \right) \cdot \cot(\theta)$	$A_{ps} \cdot f_{ps} + A_s \cdot E_s \cdot \varepsilon_{t.loc} \downarrow \geq \frac{ M_u }{d_v \cdot \phi_f} + 0.5 \frac{N_u}{\phi_c} + \left(\frac{ V_u - V_p }{\phi_v} - 0.5 V_s \right) \cdot \cot(\theta) + A_{ct} \cdot \gamma_u \cdot f_{t.cr}$

Table 3.4: Comparing Transfer and Development Length Predictions

Item	PCI Phase II Report (E.9.3.2)	AASHTO Draft Guide Specs. (1.9.4.3)
Transfer Length	$l_t \geq 20d_b$ d_b = nominal strand diameter (in.)	$l_t = \xi 24d_b$ (1.9.4.3.1-1) where: ξ = 0.75 or less when shorter transfer length results in more severe stress states within the section ξ = 1.0 or more when longer transfer length results in more severe stress states within the section d_b = nominal strand diameter (in.)
Development Length	$l_d \geq 20d_b + 0.2(f_{ps} - f_{pe})d_b$ Eq. E.9.3.2.2-2 where: f_{ps} = average stress in prestressing steel at the time for which the nominal resistance of the member is required (ksi) f_{pe} = effective stress in the prestressing steel after losses (ksi)	$l_d \geq l_t + 0.30(f_{ps} - f_{pe})d_b$ (1.9.4.3.2-1) where: f_{ps} = average stress in prestressing steel at the time for which the nominal resistance of the member is required (ksi) f_{pe} = effective stress in the prestressing steel after losses (ksi)
Relationship		
Example of 0.6 in. strand	$l_t = 12$ in. $l_d = 24$ in.	$l_t = 10.8$ in. – 14.4 in. $l_d = 32.4$ in.

Chapter 4. Production Experience

4.1 Introduction

One of the main goals of this project is to get the precast/prestressed concrete bridge producers in Nebraska to experiment with the production of UHPC bridge girders and gain experience in all production stages including, batching, mixing, forming, casting, curing, and stripping. Therefore, two full-scale DIB specimens were designed to be produced by the two bridge producers that are members of Precast Concrete Association of Nebraska (PCAN). The pretensioned DIB specimen was produced by Coreslab Structure Inc. (Omaha) and the post-tensioned DIB specimen was produced by Concrete Industries Inc. (Lincoln). The two specimens were produced using the same non-proprietary UHPC mixture developed and qualified by UNL and NDOT in an earlier research project (Mendonca, et al. 2020). The following subsections summarize the procedures followed by each precast producer, production challenges, and material testing conducted to meet QA/QC requirements.

4.2 Production of Precast Pretensioned DIB

This specimen was produced by Coreslab Structure Inc. (Omaha) on Friday March 18, 2022. The total quantity required for producing the pretensioned DIB specimen with ribbed slab as estimated at 5.6 cy. The producer decided to make two batches, each batch is 3.2 cy for a total quantity of 6.4 cy using the twin shaft mixers used in everyday production of conventional concrete. Due to the limitations of the available equipment and silos, silica fume, steel fibers, and chemical admixtures were manually added, while sand, cement, slag, and water were added automatically using the batching control system. To control the temperature of the mixture to be between 50°F and 85°F, either cold water is used or a percentage of water quantity is replaced with ice. In this case, cold water is used as the ambient temperature was 42°F. Table 4.1 shows the UHPC mix proportions per cubic yard and for the batched quantity of 3.2 cy. Specifications on these materials are available in (Mendonca, et al. 2020).

Table 4.1: UHPC mixture proportions for pretensioned DIB specimen

Ingredient	Type	Specific Gravity	Absorption, %	Moisture Content, %	Quantity, lb/cy	Absolute Volume ft ³	Moisture Corrected Quantity, lb	Quantity per yd ³	3.20 yd ³
Cement	Ash Grove Type I/II	3.15	0%	0%	1,206.0	6.14	1,206.0	1,206.0	
Silica Fume	Force 10,000 D	2.2	0%	0%	161.1	1.17	161.1	161.1	20.6 bags
Slag	Central Plains GGBFS	2.9	0%	0%	585.9	3.24	585.9	585.9	
Fine Sand	No.10	2.7	0.0%	5.1%	1,640.0	9.73	1,723.6	1,723.6	
Water	cold water	1	0%	0%	325.3	5.21	241.6	241.6	92.7 gal.
Air	Entrapped	0	0%	0%	-	0.41	-	-	
Workability Retaining Admixture (WRA)	Chyso Optima 100	1.06	0%	0%	11.0	0.17	11.0	11.0	35.2 lbs
High Range Water Reducer (HRWR)	Chyso Premia 150	1.06	0%	0%	26.5	0.40	26.5	26.5	84.9 lbs
Fibers	13 mm Steel	7.85	0%	0%	263.0	0.54	263.0	263.0	16.8 bags
TOTAL					27.00	4,218.8	4,219		

It should be noted that moisture sensors indicated that the sand has a moisture content of 5.1%, which was used to adjust the quantity of free water added. Also, to avoid excessive flowability and segregation of steel

fibers, a fraction of water and chemical admixtures was held to be added later on as needed basis. Table 4.2 shows the steps followed in making the first and second batches as well as the time of each step.

Table 4.2: UHPC batching and mixing sequence for pretensioned DIB specimen

Batch	Time (am)	Step
#1	7:50	Discharge sand, add silica fume bags, and mix
	7:55	Discharge cement and slag, and mix
	8:00	Discharge water and add admixtures (57 gal water, 75% Premia, 100% Optima)
	8:10	Added 30 gal. water and remaining Premia
	8:15	Added fibers as it became flowable
	8:25	Stop mixer and take a sample for flow test (too dry)
	8:30	Add 15 pounds of Premia and mix
	8:35	Stop mixer and take a sample for flow test (9.5 in. spread)
	8:40	Discharge UHPC into truck mixer
#2	8:50	Discharge sand, add silica fume bags, and mix
	8:55	Discharge cement and slag, and mix
	9:00	Discharge water and add all admixtures (water was 90 gal)
	9:10	Added fibers as it became flowable
	9:20	Stop mixer and take a sample for flow test (10 in. spread)
	9:25	Discharge UHPC into truck mixer

After the first batch was fully mixed using the twin shaft mixer, it was placed in the truck mixer to remain agitated until the second batch is ready. The two batches were mixed together in the truck mixer, transported to the specimen form at the prestressing bed, and tested for workability before being placed in the form. Figure 4.1 shows the results of the flow test according to ASTM C 1856 of each batch at the mixer, which indicated acceptable flowability (8 – 10 in.). Flow test had to be done again at the form within 5 minutes of the casting, which indicated low flowability. Additional dosage of HRWRA was added and another test was conducted to confirm that the flowability is acceptable.



Figure 4.1: UHPC flow diameter of batch #1 (left) and batch #2 (right)

Figure 4.2 shows the plan, elevation, and section views of the UHPC DIB pretensioned specimen. This specimen is formed using the custom forms presented earlier in Chapter 3 with the flange pans installed to create ribbed slab voids as shown in Figure 4.3. These figures indicate that the specimen does not have transverse reinforcement in the web and does not have longitudinal reinforcement in the ribbed slab, which simplifies production. The only mild reinforcement used is the top and bottom transverse reinforcement in the ribs (2#5 per rib) and end zone bursting reinforcement at one girder end (2#6). This was made by design to evaluate the cracking at girder ends at release with and without bursting reinforcement. The specimen was pretensioned using 16-0.6 in. Grade 270 low relaxation straight bottom strands tensioned to 75% the ultimate strength with no debonding. Two 0.6 in. straight strands were added to the top and were tensioned to 5 kips to support transverse reinforcement and control camber. Figure 4.1 also shows the location of the lifting loops and foam block outs in the flange to allow bracing chains to go through and stabilize the specimen during transportation. The form was sprayed by form oil to allow easy stripping of forms after casting. It should be noted that the edge forms shown earlier in chapter 3 to create a lip for longitudinal joints were not used in this specimen as the stripping of these edge forms was expected to be very difficult due to the presence of transverse reinforcement. Instead, a wooden form without a lip and with shear key formed using Styrofoam was used as shown in Figure 4.4.

Casting UHPC into the forms was done directly from the truck using the chute as shown in Figure 4.5. UHPC continued to lose workability by time, which required the addition of multiple dosages of HRWRA at different times to maintain workability. Slow placement rate of UHPC due to the height of the form and use of chute contributed to loss of workability. Raising the truck to higher elevation relative to the form or using large concrete bucket would allow faster discharge of UHPC and shorten the placement duration. The top surface of UHPC was finished using a concrete screed and with minimal surface vibration to help in leveling the top surface. Plastic sheets were placed over the top surface immediately after finishing as shown in Figure 4.6 to prevent moisture loss and formation of elephant skin and shrinkage cracking.

To minimize the negative effect of UHPC early-age plastic shrinkage on form stripping, it was planned to strip the forms the next day at 24 hours from casting UHPC. Earlier stripping was not recommended due to the long setting time of UHPC (PCI, 2022) and the length of ribbed slab overhangs that could result in top flange cracking. The revised edge forms were easy to strip, however, the flange pans used to create flange ribs were very difficult to strip. This was attributed to the early-age plastic shrinkage of UHPC, inadequate tapering of the pans, large suction force preventing the pans from popping out when lowering the bottom forms. The precast producer had to unscrew all the bolts holding the pans to the form, lower the slightly, and use the bolts again to pull the pans out after wedging the form against the specimen. This process was tedious, long, and labor intensive as pans had to be removed individually and resulted in some minor damage to the forms. Possible solution to alleviate this problem is to add shrinkage reducing admixture to the UHPC mix to reduce early-age plastic shrinkage. Also, using highly tapered pans or plastic-covered pans to reduce friction with UHPC while stripping.

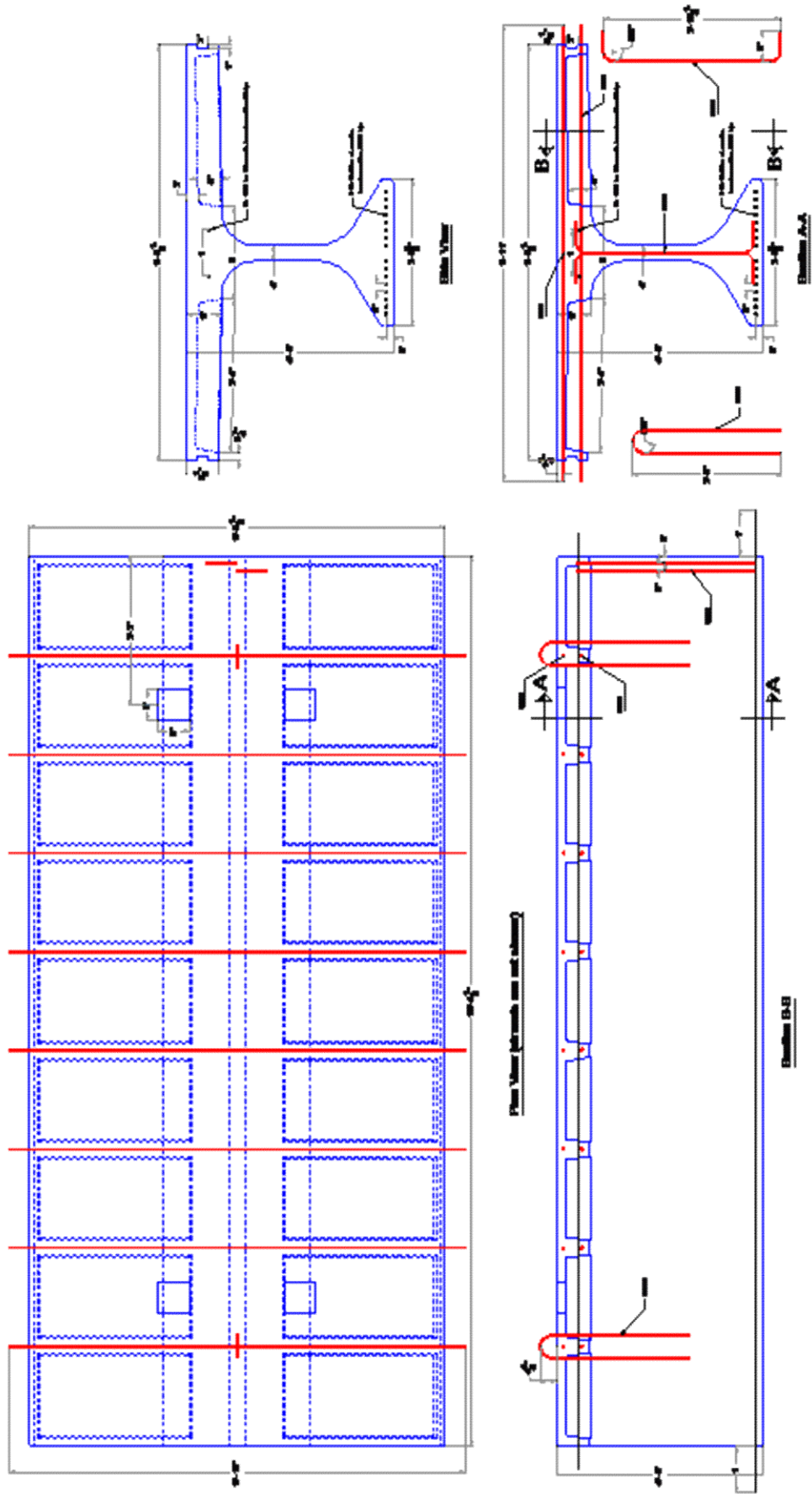


Figure 4.2: UHPC pretensioned specimen drawing



Figure 4.3: Forms and reinforcement of UHPC pretensioned specimen

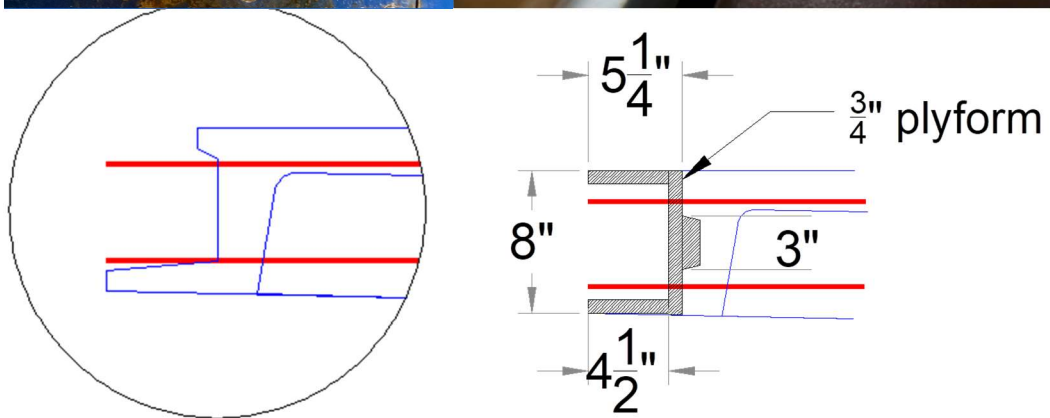


Figure 4.4: Original edge form (left) and revised edge form (right)

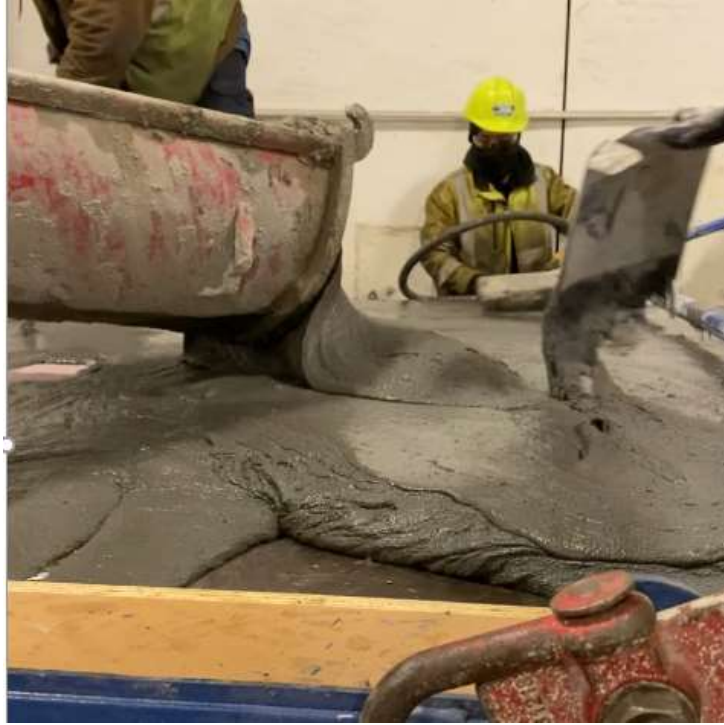


Figure 4.5: Placement of UHPC into the form using truck chute



Figure 4.6: Finishing UHPC top surface and covering with plastic sheets

Table 4.3 shows the compressive strength test results of 3 x 6 in. cylinders taken from the combined batches and tested at 1, 3, 5, 14 and 26 days. Specimen tested at Coreslab Structures were cured by the DIB specimen, while the specimens tested by UNL were moist cured. These results indicate that UHPC compressive strength exceeded the minimum requirement of 17.4 ksi at 28 days and had 10 ksi at release. Figure 4.7 plots the flexural strength of three 3x3x14 in. prisms tested at 28 days, while Table 4.4 summarizes the cracking, peak, and residual strengths, which significantly exceed all the minimum criteria.

Table 4.3: UHPC compressive strength test results

Cast Date	Test Date	Sample #	Age (Days)	Compressive Strength (ksi)	Average Strength (ksi)	Tested By
3/18/2022	3/19/2022	1	1	12.68	12.68	Coreslab Structures
	3/21/2022	1	3	14.67	14.67	
	3/23/2022	1	5	13.49	14.36	UNL
		2		13.39		
		3		16.2		
	4/1/2022	1	14	16.27	16.39	
		2		17.57		
		3		15.33		
	4/13/2022	1	26	18.96	19.35	
		2		19.17		
		3		19.92		

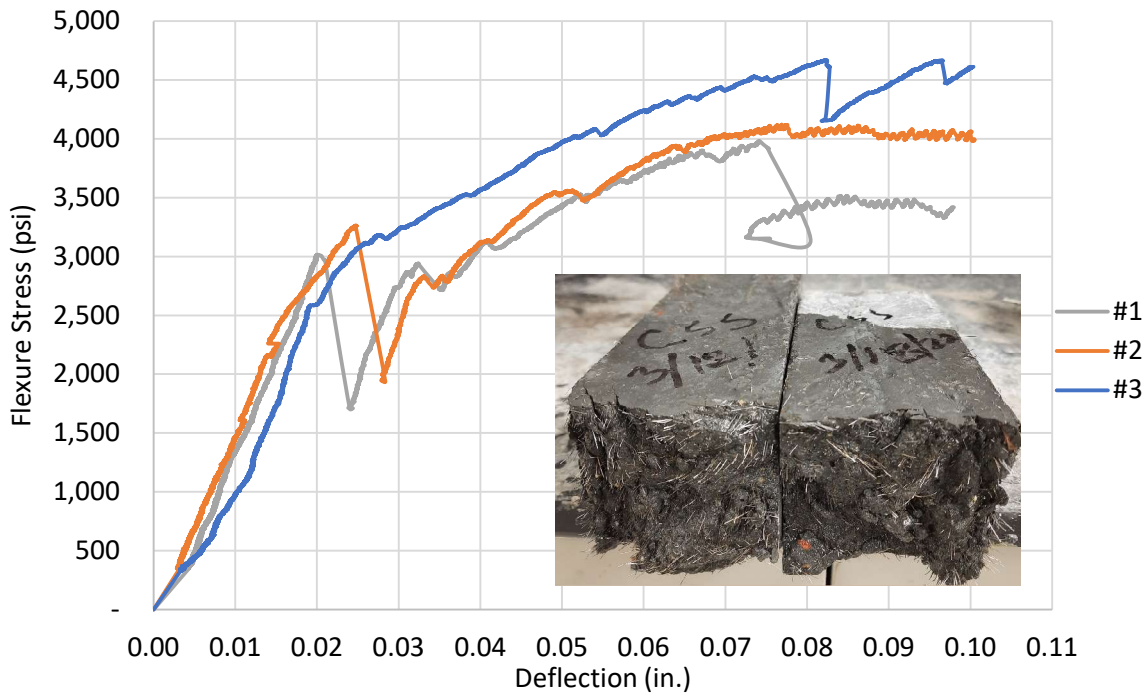


Figure 4.7: Flexure stress versus deflection of three UHPC test prisms at 28 days

Table 4.4: UHPC flexural strength test results and criteria

Cast Date	Specimen No.	28-Day Flexural Strength (ksi)				
		Cracking	Peak	Peak/Cracking	Residual	Residual/Cracking
3/18/2022	1	3,016	3,982	132%	3,403	113%
	2	3,263	4,122	126%	4,059	124%
	3	2,600	4,670	180%	4,621	178%
	Average	2,808	4,326	154%	4,012	143%
<i>Minimum Requirement</i>		<i>1500</i>	<i>2000</i>	<i>125%</i>	<i>N/A</i>	<i>75%</i>

The visual inspection of the DIB specimen indicated that UHPC had good consolidation and the specimen has good surface quality at the shear key, top surface, web surface, and around prestressing strands as shown in Figures 4.7 and 4.8. The presence of fibers at the top surface is an indication of excellent fiber stability. Also, figure 4.9 shows the specimen support system used during transportation and storage at UNL. Some bug holes were detected in the web at few locations, which were shallow and acceptable.



Figure 4.7: Specimen after stripping showing shear key (left) and fibers in the top surface (right)



Figure 4.8: Specimen after stripping and prestress release showing girder end (left) and web (right)



Figure 4.9: Specimen bracing during transportation (top) and storage at the structural lab (bottom)

4.3 Production of Precast Post-tensioned DIB

First Trial (03/09/2022)

This specimen was produced by Concrete Industries Inc. (Lincoln) on Wednesday March 9, 2022. The total quantity required for producing the post-tensioned DIB specimen with ribbed slab as estimated at 5.7 cy. The producer decided to make three batches, each batch is 2.2 cy for a total quantity of 6.6 cy using the twin shaft mixers used in everyday production of conventional concrete. Due to the limitations of the available equipment and silos, silica fume, steel fibers, ice, and chemical admixtures were manually added, while sand, cement, slag, and water were added automatically using the batching control system. To control the temperature of the mixture to be between 50°F and 85°F, 30% of water quantity was replaced with ice. Ambient temperature was 30°F at the time of batching. Table 4.5 shows the UHPC mix proportions per cubic yard and for the batched quantity of 2.2 cy. Table 4.6 lists the steps of mixing the first batch along with the duration of each step. It should be noted an additional 5 gal. of water was added by mistake, which resulted in a highly flowable mix that had fiber segregation. To address this problem, the second and third batches were mixed using the same sequence shown in Table 4.6 but without adding more water. In addition, a 25% reduction of HRWRA was applied to the second and third batches, which were mixed with the first batch in the truck mixer before casting the specimen. Although these changes improved the UHPC stability, it still had more than 10 in. flow at the forms and the low viscosity led to fiber bundles as shown in Figure 4.10. Shortly after, the UHPC was placed in the forms using concrete bucket, was resulted in a very high placement rate.

Table 4.5: UHPC mixture proportions for post-tensioned DIB specimen

Ingredient	Type	Specific Gravity	Absorption, %	Moisture Content, %	Quantity, lb/cy	Absolute Volume ft ³	Moisture Corrected Quantity, lb	Quantity per X ft ³	2.20 yd ³
Cement	Ash Grove Type I/II	3.15	0%	0%	1,206.0	6.14	1,206.0	1,206.0	
Silica Fume	Force 10,000 D	2.2	0%	0%	161.1	1.17	161.1	161.1	14.2 bags
Slag	Central Plains GGBFS	2.9	0%	0%	585.9	3.24	585.9	585.9	
Fine Sand	No. 10	2.7	0.0%	0.0%	1,621.0	9.62	1,621.0	1,621.0	
Water	30% Ice	1	0%	0%	321.4	5.15	321.4	321.4	84.8 gal.
Air	Entrapped	0	0%	0%	-	0.41	-	-	
Workability Retaining Admixture (WRA)	Chryso Optima 100	1.06	0%	0%	14.2	0.22	14.2	14.2	31.3 lbs
High Range Water Reducer (HRWR)	Chryso Premia 150	1.06	0%	0%	34.4	0.52	34.4	34.4	75.7 lbs
Fibers	13 mm Steel	7.85	0%	0%	263.0	0.54	263.0	263.0	11.6 bags
TOTAL						27.00	4,207.0	4,207	

Table 4.6: Sequence of making the first UHPC batch

Batch	Step	Duration
#1	Discharge sand, add silica fume bags manually, and mix	4
	Discharge cement and slag, and mix	3
	Discharge water and add ice manually (5 gal. water extra)	3
	Add all admixtures and mix	3
	Add fiber bags manually through a vibrating screen	6
	Discharge UHPC into truck and test flow	4
TOTAL		23



Table 4.10: UHPC flow with fiber segregation

Figure 4.11 shows the plan, elevation, and section views of the UHPC DIB post-tensioned specimen. The specimen was formed using the same custom forms presented earlier in Chapter 3, which was used for the pretensioned specimen. Figure 4.12 shows the form with the pans installed to create ribbed slab voids. The specimen does not have either transverse reinforcement in the web or longitudinal reinforcement in the ribbed slab, which simplifies production. The only mild reinforcement used is the top and bottom transverse reinforcement in the ribs (2#5 per rib) and end zone reinforcement at both girder end (8#6). This reinforcement had an L-shape to reinforce around the post-tensioning anchorage as the conventional spiral reinforcement was eliminated due to limited space. The specimen has a 4.25 in. diameter bottom plastic duct to host 19-0.6 in. bottom strands and 3 in. diameter top plastic duct to host 7-0.6 in. top strands as shown in Figure 4.13. Figure 4.11 also shows the location of the lifting loops and foam block outs in the flange to allow bracing chains to go through and stabilize the specimen during transportation. The form was sprayed with form oil to allow easy stripping after casting. The original edge form with a lip for longitudinal joints was used in this specimen as shown in Figure 4.14.

Casting UHPC into the forms was done using a concrete bucket filled by the truck chute and placed over the form using a crane as shown in Figure 4.15. UHPC remained high flowable during placement, which resulted in high placement rate and having self-leveling UHPC that did not need finishing as shown in Figure 4.16. Plastic sheets were placed over the top surface immediately to prevent moisture loss and early-age cracking. Form stripping started in two days after reaching an early strength of 16.5 ksi. Edge forms with lips were very difficult to strip due to the early-age plastic shrinkage of UHPC and having transverse reinforcement through the edge forms directly over the lips, which made it very hard to remove. It took the precast producer almost two days to remove all edge forms and pans individually as the manually operated cranking system did not work. Therefore, it was recommended to replace the original edge forms with a simpler edge form with a shear key similar to the one used in the pretensioned specimens. Also, it was recommended to eliminate the pans used to form ribbed slab voids to simplify the fabrication and stripping.

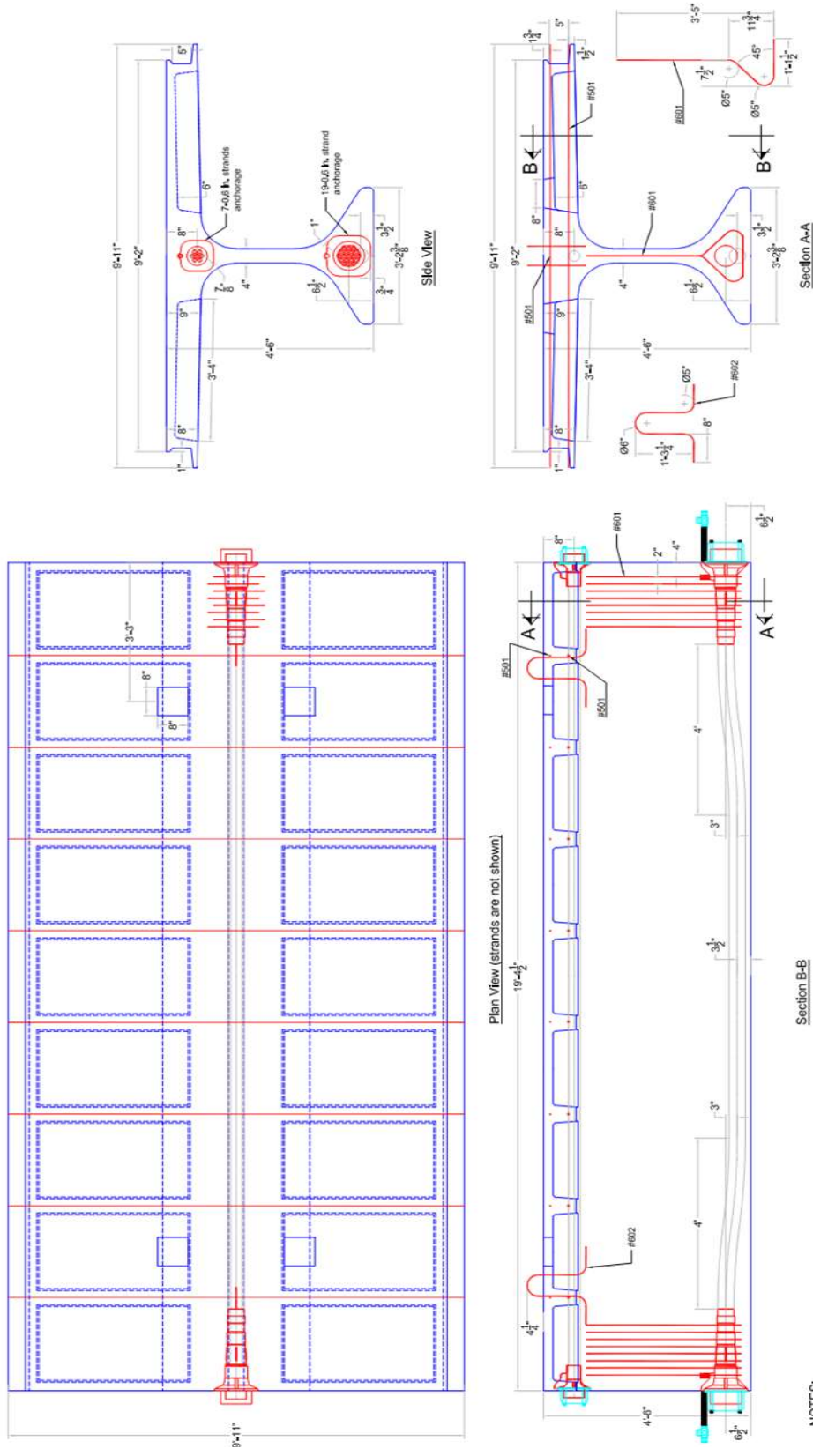


Figure 4.11: UHPC post-tensioned specimen drawing



Figure 4.12: Ribbed slab forms and top PT duct

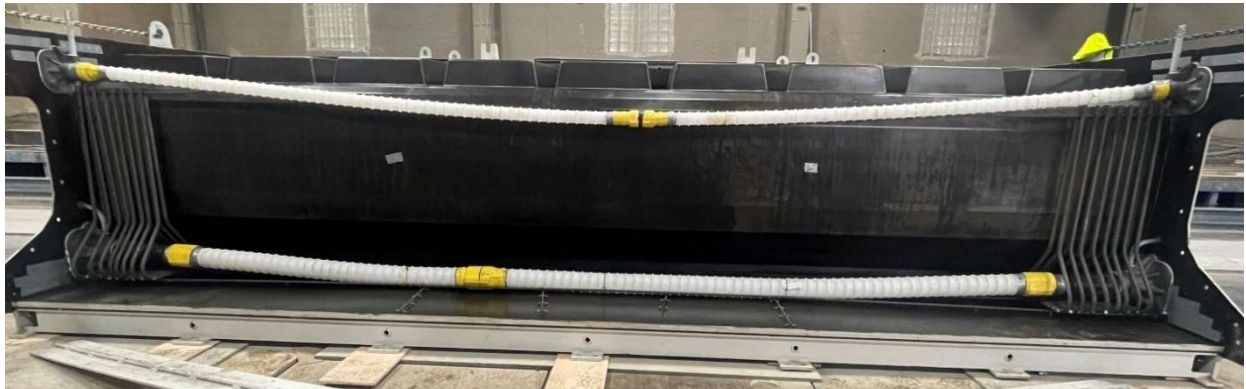


Figure 4.13: Top and bottom post-tensioned ducts and end zone reinforcement



Figure 4.14: End zone reinforcement for PT specimen (left) and edge form with lip (right)



Figure 4.15: Casting UHPC from one end using bucket

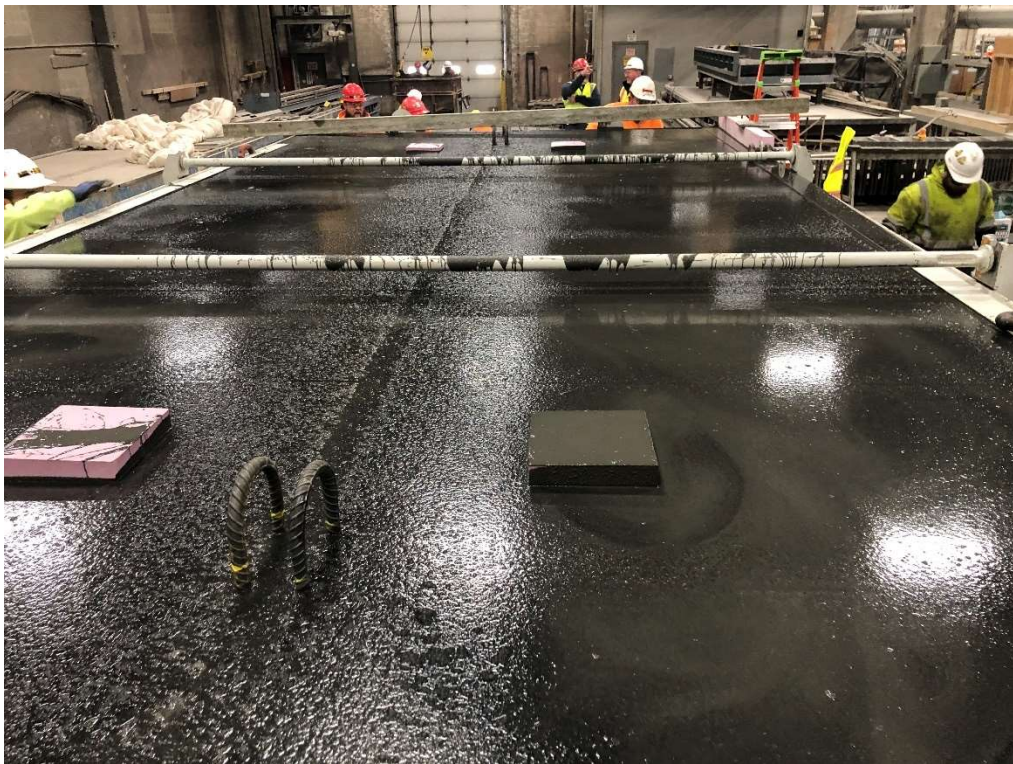


Figure 4.16: Top surface of UHPC showing no signs of fibers

Table 4.7 shows the compressive strength test results of 3 x 6 in. cylinders taken from the combined batches and tested at 2, 6, 14 and 28 days. Specimen tested at Concrete Industries were cured using the Exact Cure System that simulates the temperature of the specimen, while the specimens tested by UNL were moist cured. These results indicate that UHPC compressive strength had high 2-day early strength of 16.5 ksi probably due to the use of Exact Cure System, which exposes the cylinders to the same temperature and humidity regime of the cast specimen. On the other hand, moist cured specimens tested at the university lab curing room had lower compressive strength. The 28-day compressive strength of 18.8 ksi exceeded the minimum requirement of 17.4 ksi. Figure 4.17 shows saw cut cylinder that indicated severe fiber segregation, which significantly affected the flexural strength as evident in Figure 4.18. Table 4.8 summarizes the cracking, peak, and residual strengths, which do not meet the minimum requirements.

Table 4.7: UHPC compressive strength at different ages

Cast Date	Test Date	Sample #	Age (Days)	Compressive Strength (ksi)	Average Strength (ksi)	Tested By
3/9/2022	3/11/2022	1	2	16.47	16.51	Concrete Industries
		2		16.02		
		3		17.04		
	3/15/2022	1	6	14.63	14.67	UNL
		2		14.7		
	3/23/2022	1	14	12.96	14.90	
		2		14.9		
	4/6/2022	1	28	18.35	18.82	
		2		19.29		



Figure 4.17: Saw cut cylinder showing severe fiber segregation (left) and failure mode (right)

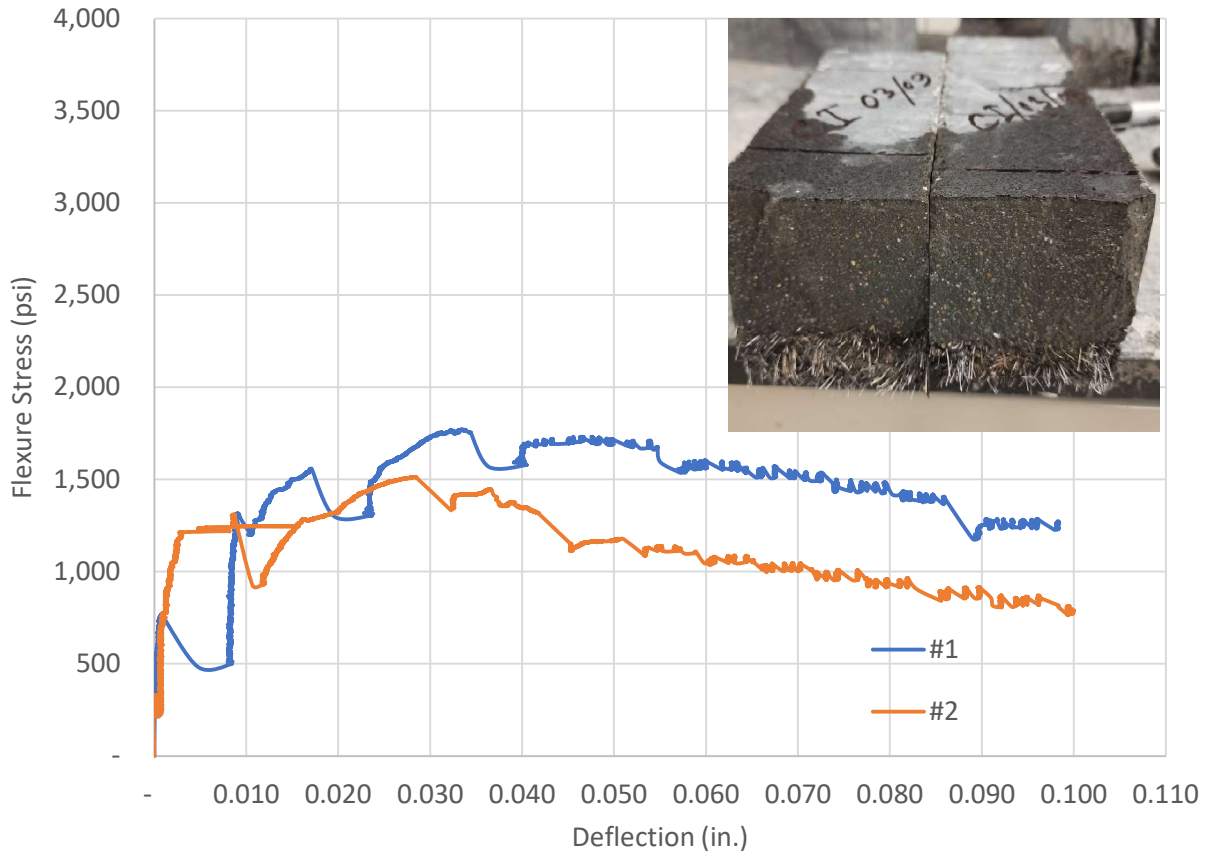


Figure 4.18: Flexure stress versus deflection of two prisms with severe segregation at 28 days

Table 4.8: UHPC flexure strength data and minimum requirements.

Cast Date	Specimen No.	28-Day Flexural Strength (ksi)				
		Cracking	Peak	Peak/Cracking	Residual	Residual/Cracking
3/9/2022	1	766	1,772	231%	1,484	194%
	2	1,311	1,515	116%	920	70%
	Average	1,039	1,644	158%	1,202	116%
<i>Minimum Requirement</i>		1500	2000	125%	N/A	75%

This UHPC DIB specimen was discarded due to the damage occurred while stripping edge forms as shown in Figure 4.19 as well as the severe cracking occurred in the top flange and upper half of the web due to shrinkage and fiber segregation as shown in Figure 4.20. A second specimen was decided to be cast by the same producer to replace the discarded specimen.



Table 4.19: Specimen damage while stripping edge form and surface cracking due to fiber segregation



Table 4.20: Shrinkage cracking at the upper half of the web due to absence of fibers

Second Trial (05/16/2022)

The second post-tensioned DIB specimen was produced by Concrete Industries Inc. (Lincoln) on Monday May 16, 2022. Three changes to the first specimen were made: 1) revised UHPC mix proportions to improve fiber stability; 2) elimination of ribbed slab void forms to simplify form erection and stripping; and 3) changing the edge form to eliminate the lip and use a simpler edge form with a shear key. The total quantity required for producing the specimen with solid slab was estimated at 6.4 cy, which is only 12% more than the quantity for the specimen with ribbed slab. The producer decided to make three batches, each batch is 2.2 cy for a total quantity of 6.6 cy as in the first specimen. Table 4.9 shows the revised UHPC mix proportions per cubic yard and for the batched quantity of 2.2 cy. The main change in the mix proportions is the reduced dosage of chemical admixtures. Also, water quantity was adjusted to compensate for the moisture in sand and loss of flowability between batches due to the long mixing time. Figure 4.21 shows the flow measured for samples taken from the truck mixer as it wasn't safe to sample from the mixer. These significant differences in the flow among batches were due to the adjustments in ice and HRWRA dosages. Ambient temperature was 55°F at the time of batching. Table 4.10 lists the steps of mixing the three batches along with the duration of each step. It should be noted that initial amount of water was intentionally less than calculated, which resulted in a stiff mix. Additional bags of ices and HRWRA were added gradually to achieve the required flowability while avoiding fiber segregation occurred in the first trial.

Table 4.9: UHPC mixture proportions for the second post-tensioned DIB specimen

Ingredient	Type	Specific Gravity	Absorption, %	Moisture Content, %	Quantity, lb/cy	Absolute Volume ft ³	Moisture Corrected Quantity, lb	Quantity per yd ³	2.20 yd ³
Cement					1,206.0	6.14	1,206.0		
Silica Fume					161.1	1.17	161.1		14.2 bags
Slag					585.9	3.24	585.9		
Fine Sand					1,666.0	9.89	1,682.7		
Water					315.5	5.06	315.5		83.2 gal.
Air					-	0.41	-		
Workability Retaining Admixture (WRA)					11.0	0.17	11.0		24.2 lbs
High Range Water Reducer (HRWR)					26.5	0.40	26.5		58.4 lbs
Fibers					263.0	0.54	263.0		11.6 bags
TOTAL					27.00	4,251.7	4,252		



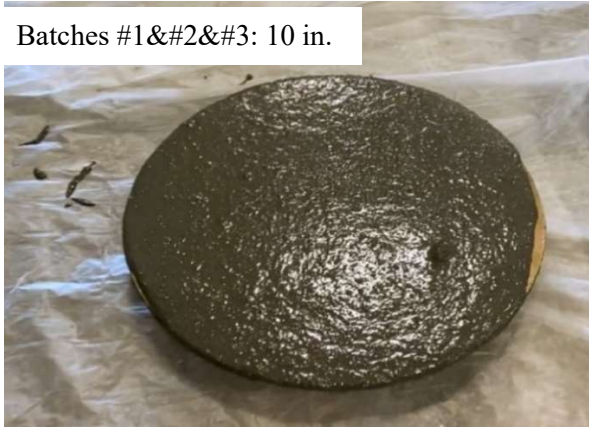


Figure 4.21: Flow of samples taken from the truck mixer after each batch

Table 4.10: UHPC mixing steps for the second post-tensioned DIB specimen

Batch	Time	Notes
#1	8:45 AM	Sand was added into the mixer (3730 lb) with moisture prob reading 4%
	8:52 AM	14 bags of Silica Fume were added
	8:59 AM	290 lb of Water and 13 bags of Ice was added
	9:00 AM	Both Premia 150 and 100 Admixtures were added
	9:04 AM	Concrete Mix was still too dry
	9:07 AM	1 Gal of Premia 150 & 1 bag of Ice was added
	9:09 AM	The concrete mix showed noticeable flowability
	9:12 AM	The mixer was stopped for a brief moment to grab a sample but was still stiff.
	9:16 AM	Two bags of ice were added and Fiber was sieved in to the mixer over 4 to 5 minutes.
#2	9:32 AM	Discharge and A sample was tested for truck flowability with 6 3/4 in smallest and 7 1/2 in the largest
	9:35 AM	The second batch mix had already started sand and silica fume was already in the mixer
	9:38 AM	16 bags of Ice, water and admix were already added to the mixer
	9:40 AM	1 Gal of Premia 150 was added
	9:44 AM	1 bag of ice was added, I was informed that a total of 17 bags of ice including this.
	9:49 AM	The mix was too dry and so another 2 gal of Optima 100 were added
	10:00 AM	Flow test showed no flowability
	10:05 AM	2 Gal of premia 150 was added and mixed for 5 min in the truck
#3	10:10 AM	Flow test showed only a little improvement
	10:10 AM	The third batch mix had already started sand and silica fume was already in the mixer
	10:15 AM	18 bags of Ice, water and admix were already added to the mixer
	10:20 AM	2 Gal of Premia 150 was added with Fibers
	10:25 AM	2 bag of ice was added and Discharged
	10:30 AM	2 Gal of Premia 150 was added and mixed in the truck for 3 minutes but a flow test was not performed
	10:35 AM	Flow test was performed at the bed and showed 10 in.
11:00 AM	Pouring the specimen was completed	

Figure 4.22 shows the plan, elevation, and section views of the second UHPC DIB post-tensioned specimen. The specimen was formed using the same custom forms used earlier but without the pans used to form ribbed slab voids and with different edge form that does not have a lip. The specimen does not have either transverse reinforcement in the web or longitudinal reinforcement in the flange. Figure 4.23 shows the top and bottom transverse reinforcement (#5@12 in.) in the slab and end zone reinforcement (8#6) at both girder ends. This reinforcement had an L-shape to reinforce around the post-tensioning anchorage as the conventional spiral reinforcement was eliminated due to limited space. The specimen has a 4.25 in. diameter bottom plastic duct to host 19-0.6 in. bottom strands. No duct for top strands is used in this specimen.

Figures 4.22 also shows the location of the lifting loops and foam block outs in the web for bracing chains to stabilize the specimen during transportation. Figure 4.23 shows the details of the edge form.

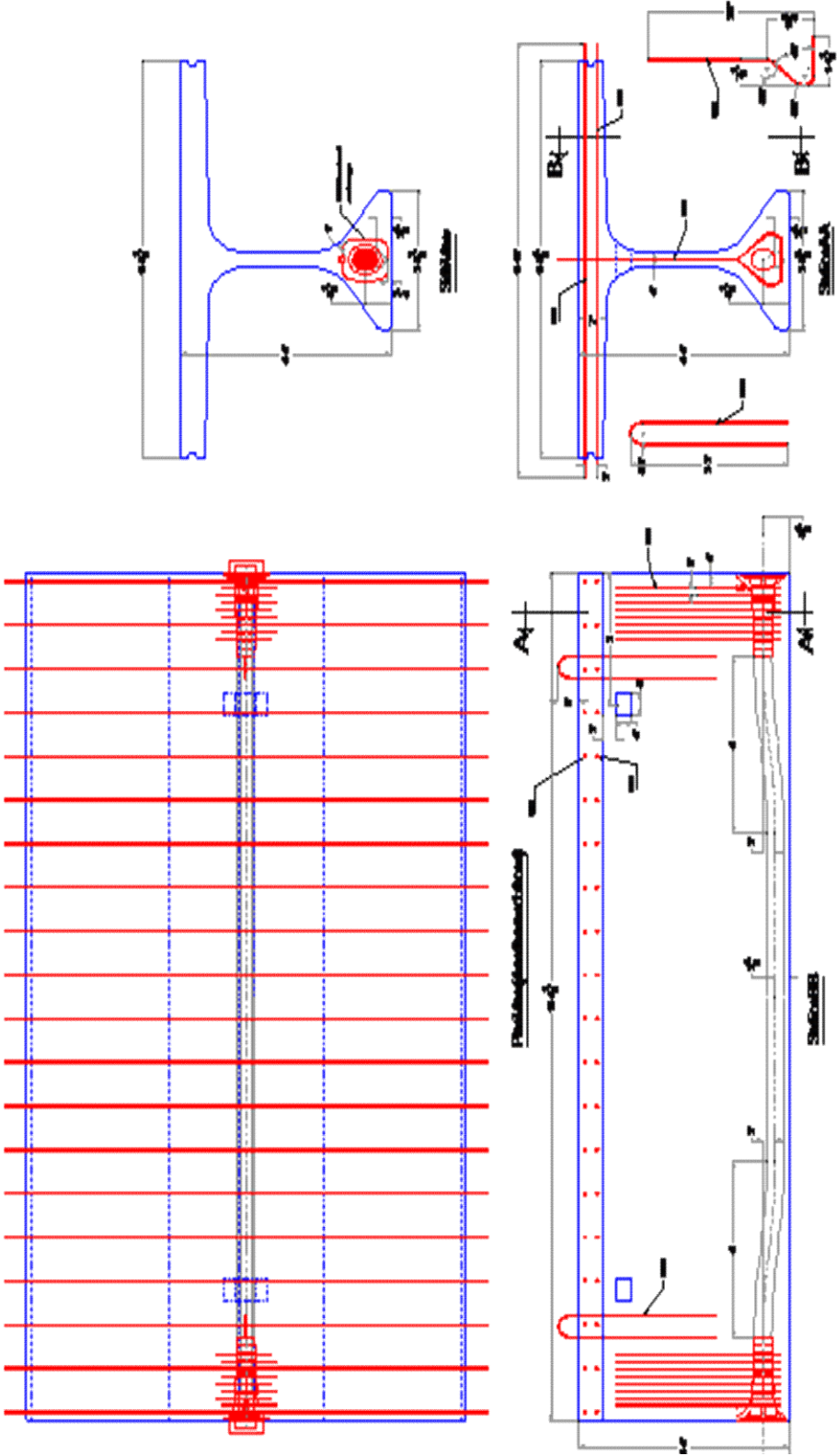


Figure 4.22: UHPC second post-tensioned specimen

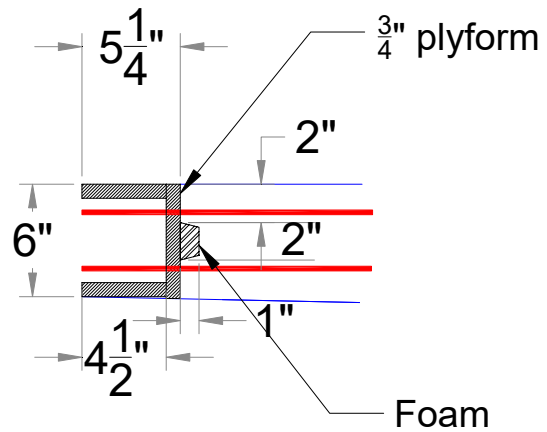


Figure 4.23: Forms for DIB specimen with solid slab

Casting UHPC into the forms was done using a concrete bucket filled by the truck chute as shown in Figure 4.24 and moved over the form for placing UHPC into the form. At the beginning, UHPC was flowable yet stable, which made filling the bottom flange and web easy and quick. Later, UHPC started to lose flowability, which required adding more HRWRA for casting the top flange. Also, screed and shovels were used to level and finish the top flange surface as shown in Figure 4.24. The producer ran out of UHPC to entirely fill the form because significant amount of UHPC was lost due to the bucket leakage. Figure 4.25 shows the unfilled corners of the form, which should not affect the testing presented later. Plastic sheets were placed over the top surface immediately to prevent moisture loss and early-age cracking.



Figure 4.24: UHPC flowability during casting



Figure 4.25: Unfilled corner of the form

Form stripping was done after two days as UHPC early strength exceeded 10 ksi, which went very smoothly due to the absence of pans and ribs. First, edge forms were easily removed. Second, end forms were strips, then soffit forms were easily dropped an inch. Third, crane was used to remove the side forms as shown in Figure 4.26. Visual inspection of the specimen indicated that there is no shrinkage cracks and steel fibers were stable as shown in the photo of the top surface in Figure 4.27. The figure also shows that the top flange thickness was approximately 5.75 in. instead of 6 in.



Figure 4.26: Stripping side forms of DIB with solid slab

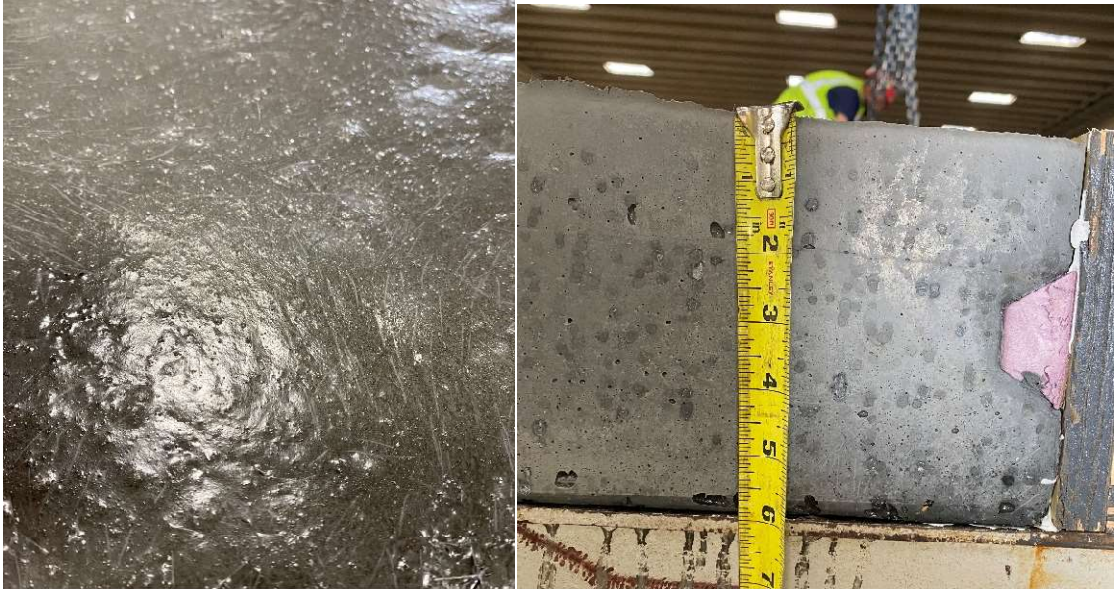


Figure 4.27: DIB with solid slab top surface (left) and flange thickness (right)

Table 4.11 and Figure 4.28 show the compressive strength test results of 3 x 6 in. cylinders taken from the combined batches and tested at 1, 2, 3, 7, 14, 28, 39 and 51 days. Specimen tested at Concrete Industries were ambient cured, while the specimens tested by UNL were moist cured. These results indicate that UHPC compressive strength exceeded the minimum final strength of 17.4 ksi and minimum stripping strength of 10 ksi. It should be noted that applying heat curing at early age could significantly increases the compressive strength gain. Also, it is recommended to test cylinders after 28 days as UHPC continues to gain strength by time as evident in these results.

Table 4.11: UHPC compressive strength at different ages

Cast Date	Test Date	Sample #	Age (day)	Compressive Strength (ksi)	Average (ksi)	Tested By
05/16/2022	05/17/22	1	1	7.8	7.8	Concrete Industries
	05/18/22	1	2	10.6	10.6	
	05/19/22	1	3	11.66	11.35	UNL
		2		11.03		
	05/23/22	1	7	13.36	13.38	
		2		13.39		
	05/30/22	1	14	14.18	15.40	
		2		16.62		
	06/13/22	1	28	16.42	16.59	
		2		16.75		
	06/24/22	1	39	17.03	16.81	
		2		16.59		
	07/06/22	1	51	20.73	21.64	
		2		22.23		
3		21.97				

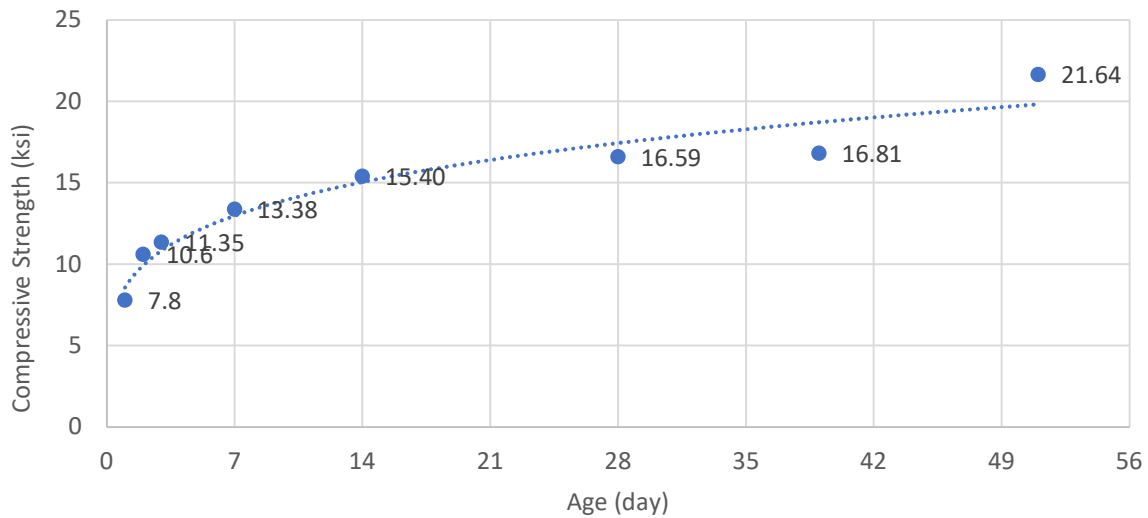


Figure 4.28: UHPC compressive strength gain

Figure 4.29 plots the flexural strength of three 3x3x14 in. prisms tested at 28 days versus deflection, while Table 4.12 summarizes the cracking, peak, and residual strengths, which significantly exceed all the minimum requirements. Figure 4.30 shows a saw cut cylinder and a tested prism to demonstrate fiber distribution, which indicate the excellent fiber stability of the used UHPC mix. The UHPC DIB was shipped to the structural laboratory of UNL in Omaha to be post-tensioned. Specimen was braced during transportation using chains through the web opening as shown in Figure 4.31.

Table 4.12: UHPC flexural strength at 28 days

Cast Date	Specimen No.	28-Day Flexural Strength (ksi)				
		Cracking	Peak	Peak/Cracking	Residual	Residual/Cracking
5/16/2022	1	1,729	3,611	209%	2,384	138%
	2	2,517	4,215	167%	3,695	147%
	3	2,530	4,607	182%	4,019	159%
	Average	2,130	4,109	193%	3,202	150%
<i>Minimum Requirement</i>		1500	2000	125%	N/A	75%

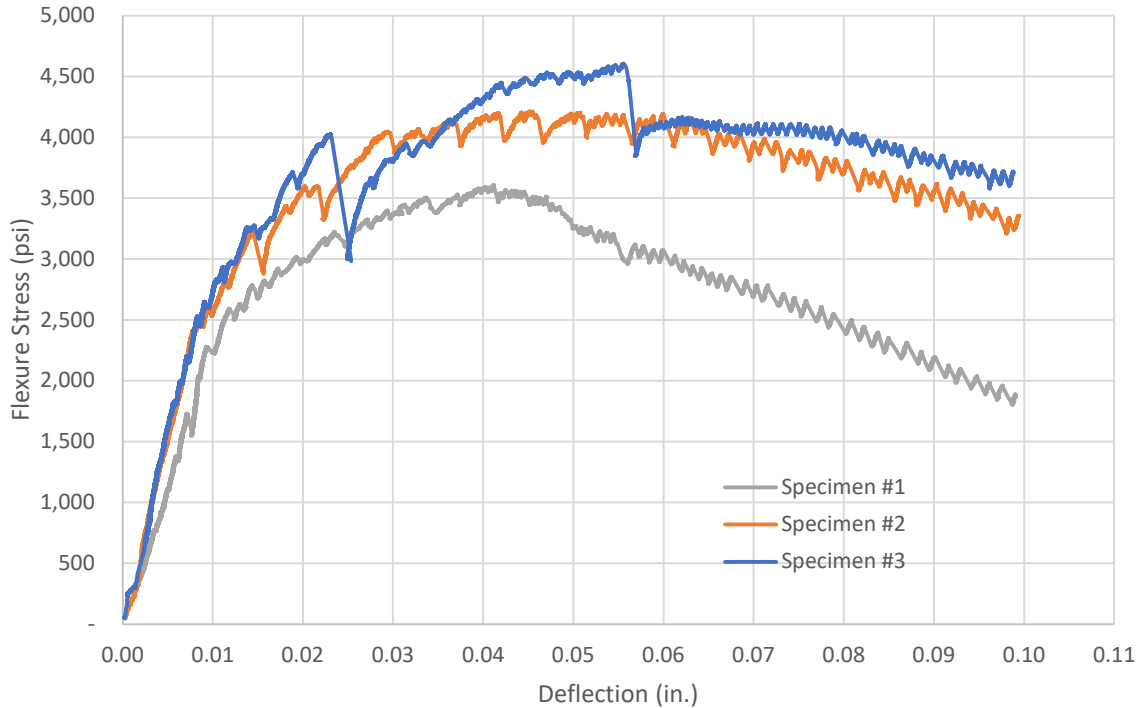


Figure 4.29: Flexure stress versus deflection of three prisms at 28 days

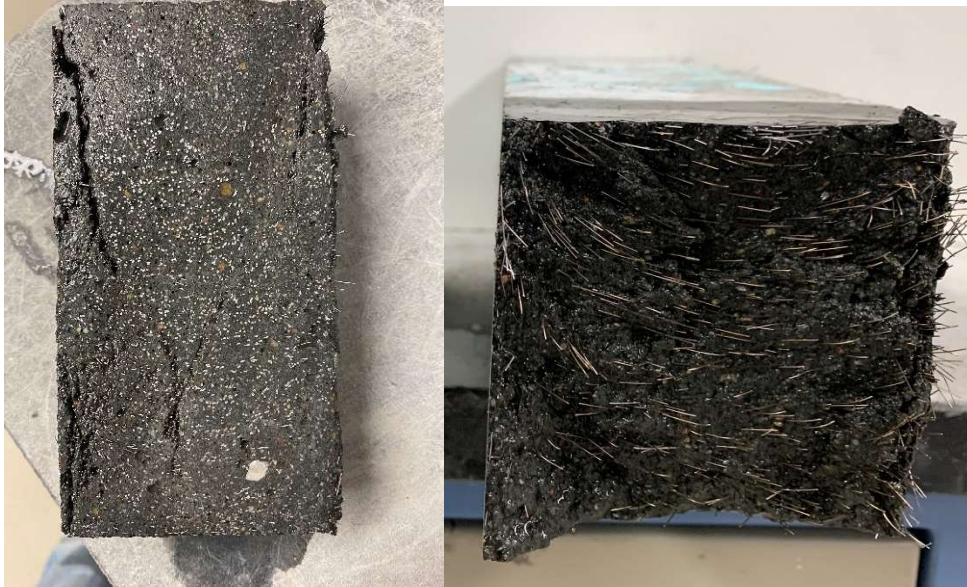


Figure 4.30: UHPC fiber stability as shown in cut cylinder (left) and prism (right)



Figure 4.31: UHPC DIB specimen bracing during transportation

Chapter 5. Experimental Investigation

5.1 Introduction

This chapter presents the several tests conducted to evaluate the structural performance of the proposed superstructure system. Two main groups of tests were conducted: a) component testing, which includes flexural testing of the ribbed slab (positive and negative moment capacities) and punching shear of the ribbed slab; b) full-scale specimen testing, which includes vertical shear of the DIB, load distribution in the transverse direction of DIB with both ribbed and solid slabs, and post-tensioning of DIB for segmental construction.

5.2 Component Testing

5.2.1 Ribbed Slab Positive Moment Capacity

A flexure test of a UHPC ribbed slab was conducted to evaluate its positive moment capacity and validate the accuracy of the predicted capacity. Figure 5.1 shows the dimensions and detailing of the ribbed slab specimen formed using plywood and foam; and reinforced with 2#5 top reinforcement and 2#6 bottom reinforcement Grade 60 A615 steel. Table 5.1 shows the constituents and proportions of the UHPC used in fabricating the ribbed slab with fiber volume fraction equals to 2%. The 28-day compressive strength test was conducted using 3x6 in. cylinders according to ASTM C1856 and resulted in average strength of 18.4 ksi. The 28-day flexural strength test was conducted using 3 x 3 x 14 in prisms according to ASTM C1609 and the results are shown in Table 5.2 and Figure 5.2. These results indicate that UHPC meets the requirements of PCI-UHPC as specified by PCI Guidelines TR-9-22. Figure 5.3 shows the test setup where a mid-span spreader beam was used to apply a concentrated load on the ribbed slab up to failure. String potentiometers and strain gauges were installed to measure mid-span deflection and strain in UHPC.

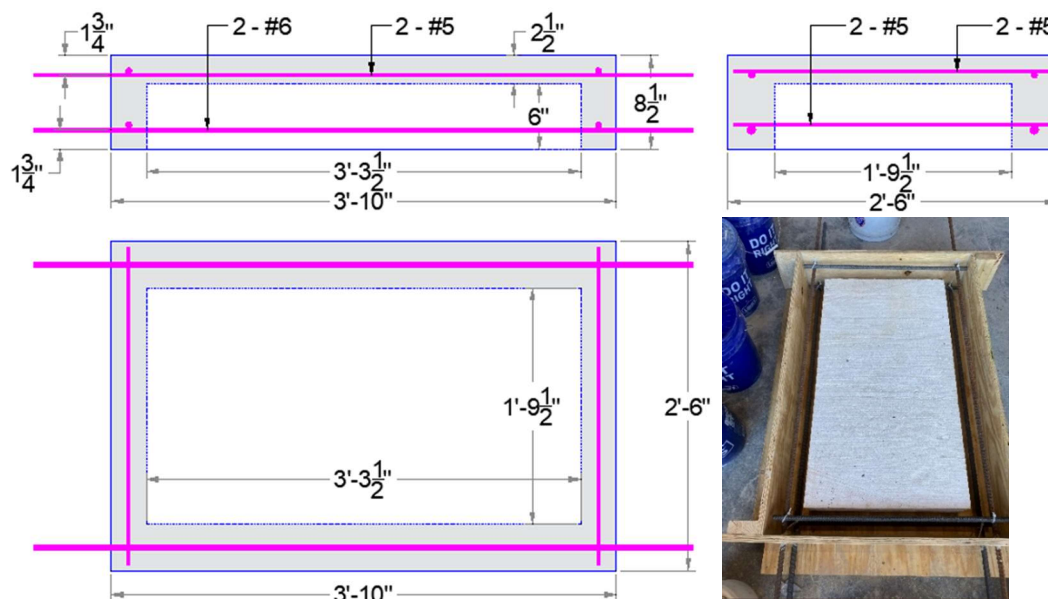


Figure 5.1: Ribbed slab dimensions and reinforcement

Table 5.1: UHPC Mix Proportions Used for Specimen Production

Ingredient	Quantity (lb/y ³)
Cement (Type I/II)	1,206.6
Silica Fume	161.2
Slag (GGBFS)	586.2
Fine Aggregate (#10 Sand)	1631.4
Water + Ice	315.7
Workability Retaining Admixture (WRA)	12.0
High Range Water Reducer (HRWRA)	45.0
Steel Fibers (13 mm long)	263.0

Table 5.2: UHPC Flexure Test Results

Specimen #	Cracking Stress (ksi)	Peak Stress (ksi)	Residual Stress (ksi)	Peak-to-Cracking Stress	Residual-to-Cracking Stress
1	1.7	2.3	1.7	134%	100%
2	2.0	4.2	4.1	215%	210%
3	1.9	3.0	2.5	158%	132%
Average	1.9	3.2	2.8	169%	147%

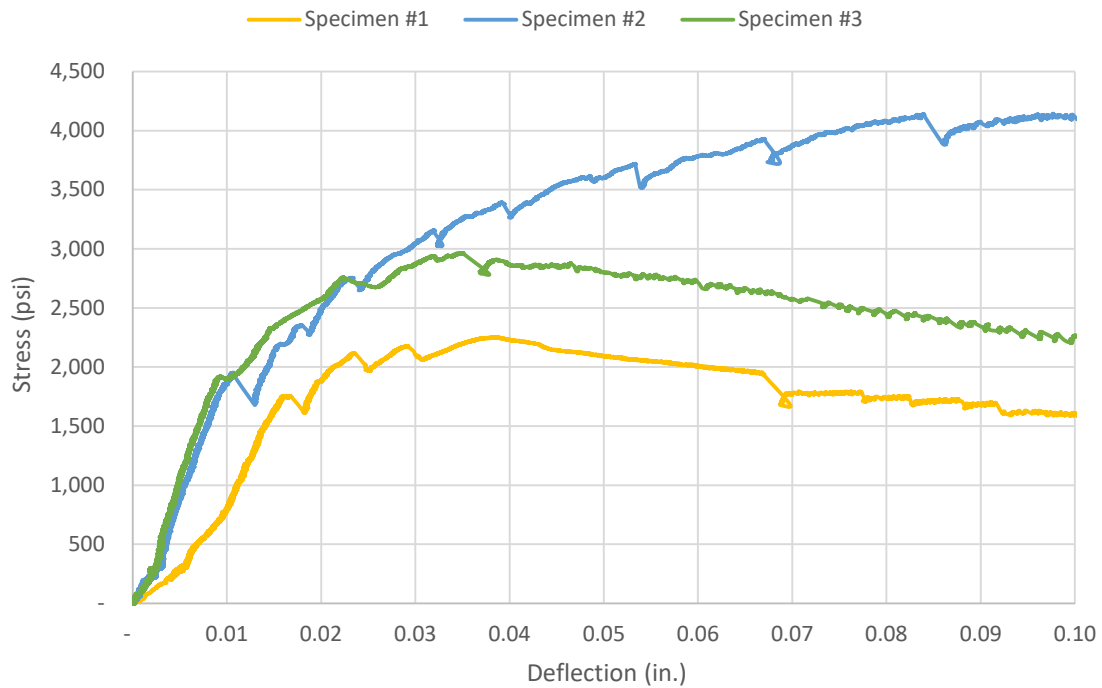


Figure 5.2: UHPC Flexure Test Plots

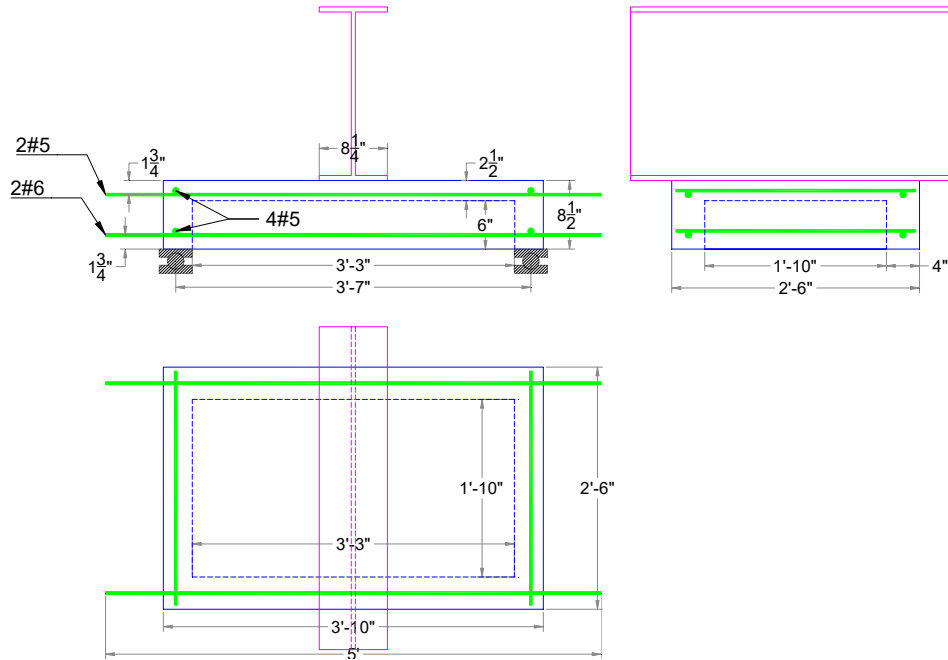


Figure 5.3: Positive Moment Test setup of the Ribbed Slab

Figure 5.4 shows the load-deflection plot of the ribbed slab where the peak load reached 87.3 kip resulting in a moment of 63.2 kip.ft at a deflection of 0.46 in. The plot shows that the slab sustained the peak moment for a significant amount of deformation, which is attributed to UHPC tensile capacity after cracking. The load application was stopped after a wide flexural crack was noticed in the tension area and signs of UHPC crushing in compression started to appear under the spreader beam as shown in Figure 5.5. The predicted first peak nominal moment (at crack localization) was estimated at 46.3 kip.ft. as shown in the moment-curvature plot in Figure 5.6. This results in a measured-to-predicted flexural strength of 1.37, which indicates high margin of safety even without using resistance reduction factor. Figure 5.6 plots the nominal

and factored moment-curvature relationship of the ribbed slab tested in positive moment, which shows and ultimate nominal moment of 36 kip.ft that is approximately 20% less than the peak nominal moment.

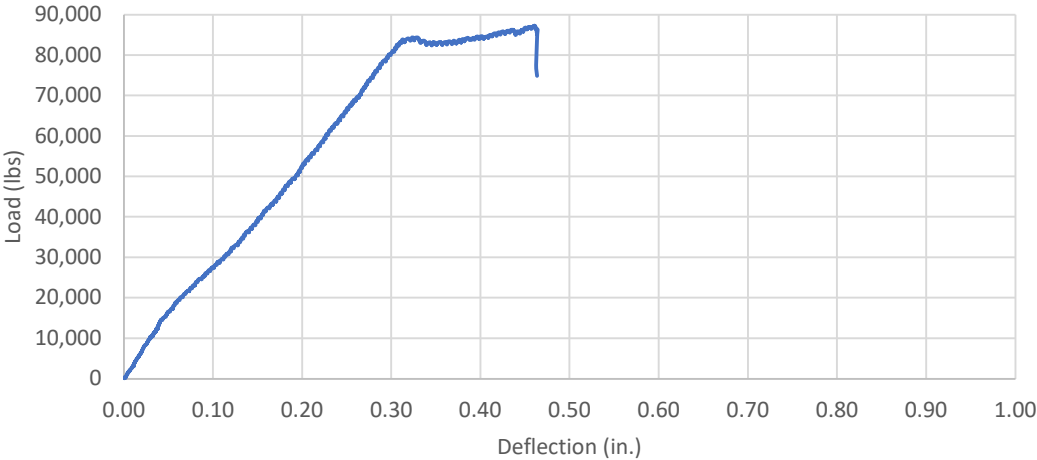


Figure 5.4: Load-deflection plot of the positive flexure test of the UHPC ribbed slab



Figure 5.5: Flexure failure mode of the UHPC ribbed slab in positive moment

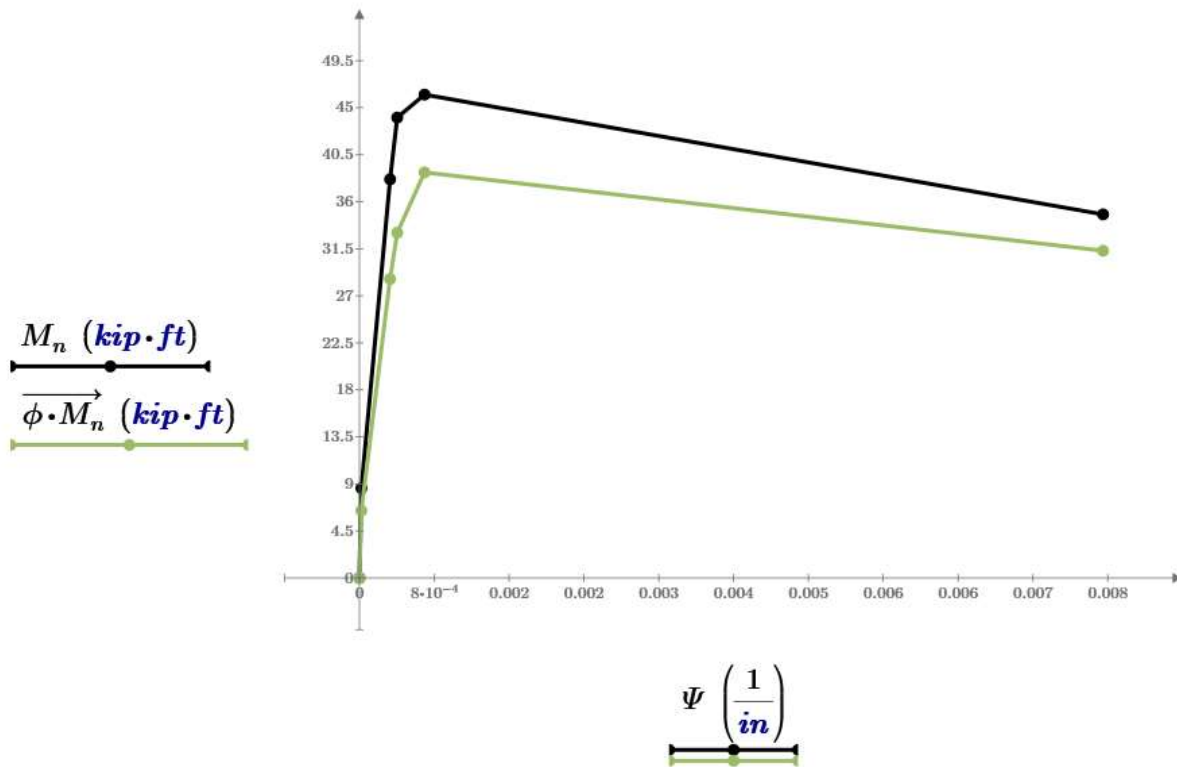


Figure 5.6: Moment-curvature relationship of UHPC ribbed slab in positive moment

5.2.2 Ribbed Slab Negative Moment Capacity

A flexure test of a UHPC ribbed slab was conducted to evaluate its negative moment capacity and validate the accuracy of the predicted capacity. The specimen has the same dimension and reinforcement as the one presented earlier in Figure 5.1, however, the specimen was turned upside down to evaluate its negative moment capacity using the same setup as shown in Figure 5.7. The same UHPC mix constituents and proportions were used for this specimen, which has the properties shown in Table 5.2 and Figure 5.2. Figure 5.7 shows the test setup where a mid-span spreader beam was used to apply a concentrated load on the slab up to failure in the tension zone. String potentiometers were used to measure the mid-span deflection and strain gauges were installed to measure the strain in UHPC.

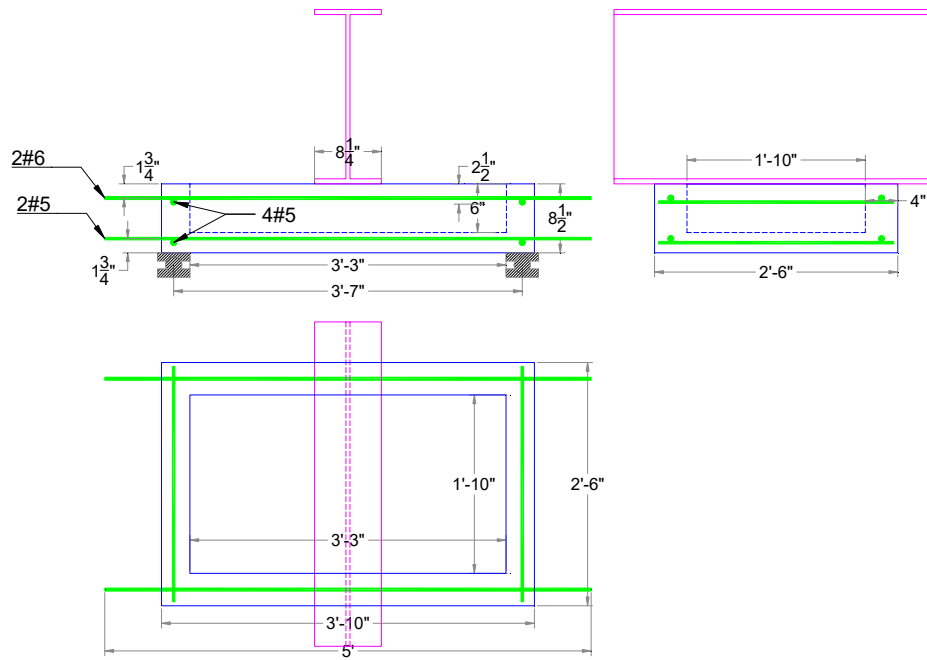


Figure 5.7: Negative Moment Test setup of the Ribbed Slab

Figure 5.8 shows the load-deflection plot of the ribbed slab where the peak load reached 80.2 kip resulting in a moment of 58.1 kip.ft. at a deflection of 0.34 in. The plot also shows that the slab had a significant moment capacity after localization, which is attributed to UHPC residual tensile capacity after reaching the peak moment. The load application was stopped after a wide flexural crack was noticed in the tension area and signs of UHPC crushing in compression started to appear under the spreader beam as shown in Figure 5.9. The predicted first peak nominal moment (at crack localization) was estimated at 54.3 kip.ft. resulting in a measured-to-predicted flexural strength of 1.07. This indicates acceptable prediction accuracy that is much lower than that achieved in the previous test. This could be attributed to the lack of fibers at the tension side as the specimen was cast upside down and flipped over. Figure 5.10 plots the nominal and

factored moment-curvature relationship of the ribbed slab tested in negative moment, which shows an ultimate nominal moment of 27 kip.ft that is approximately 50% less than the peak nominal moment. This large difference in capacity is due to the large tension flange and contribution of its fibers to the flexural capacity of the reinforced concrete section.

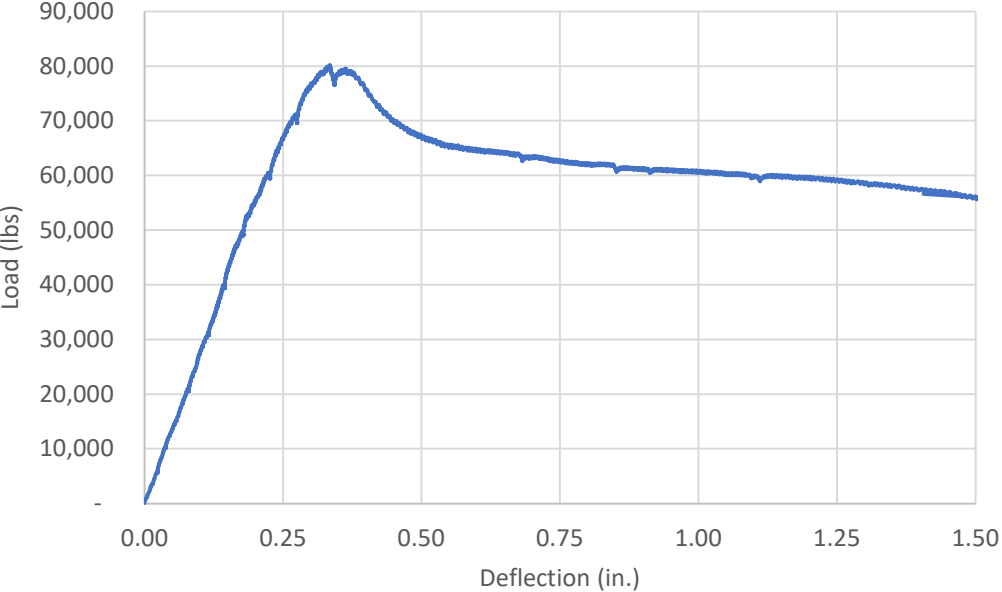


Figure 5.8: Load-deflection plot of the negative flexure test of the UHPC ribbed slab



Figure 5.9: Flexure failure mode of the UHPC ribbed slab in negative moment

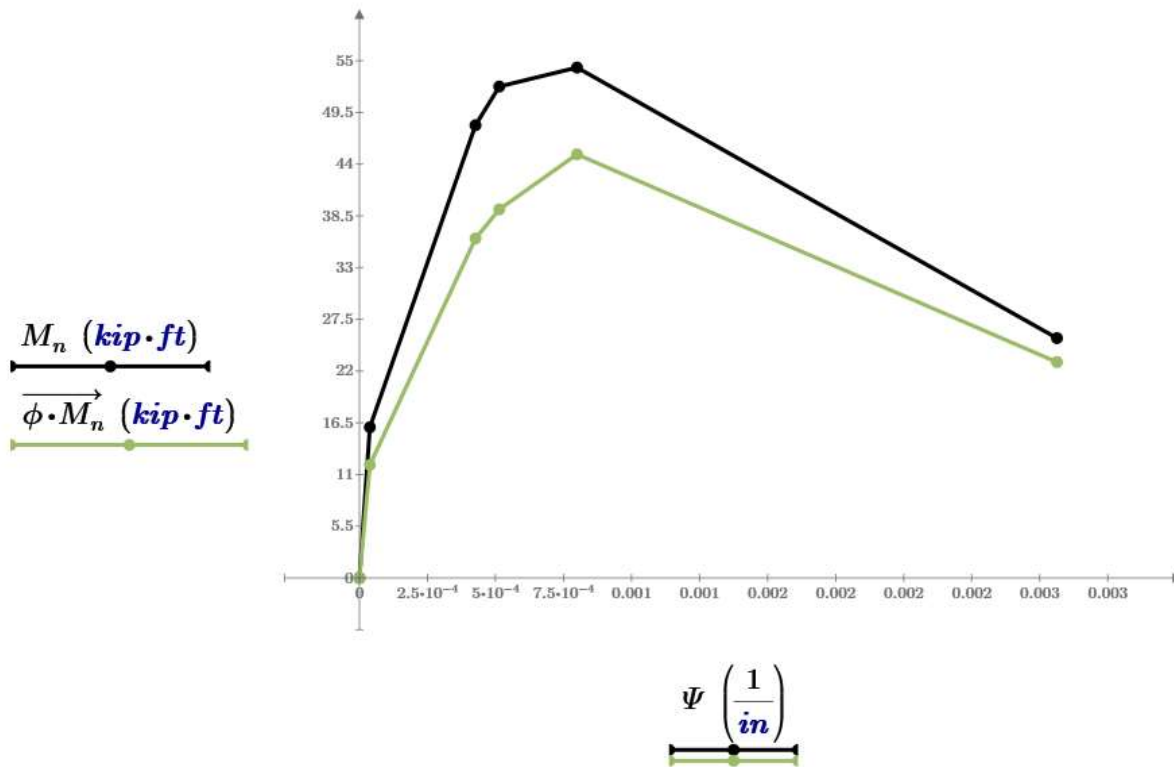


Figure 5.10: Moment-curvature relationship of UHPC ribbed slab in negative moment

5.2.3 Ribbed Slab Punching Shear Capacity

A punching shear test of a UHPC ribbed slab skin was conducted to evaluate its punching shear capacity and validate the accuracy of the predicted capacity. Figure 5.11 shows the dimensions and detailing of the ribbed slab specimen and the punching shear test setup that simulates the wheel footprint of HL93 design truck (10 in. x 20 in.) in the most critical orientation. The figure also shows the loading plates and beam used to apply a concentrated load on the center of the ribbed slab skin up to failure. String potentiometer was installed at the center to measure deflection. An identical specimen was made using conventional concrete (4000 psi 47BD mix) to be tested in the same manner for comparison.

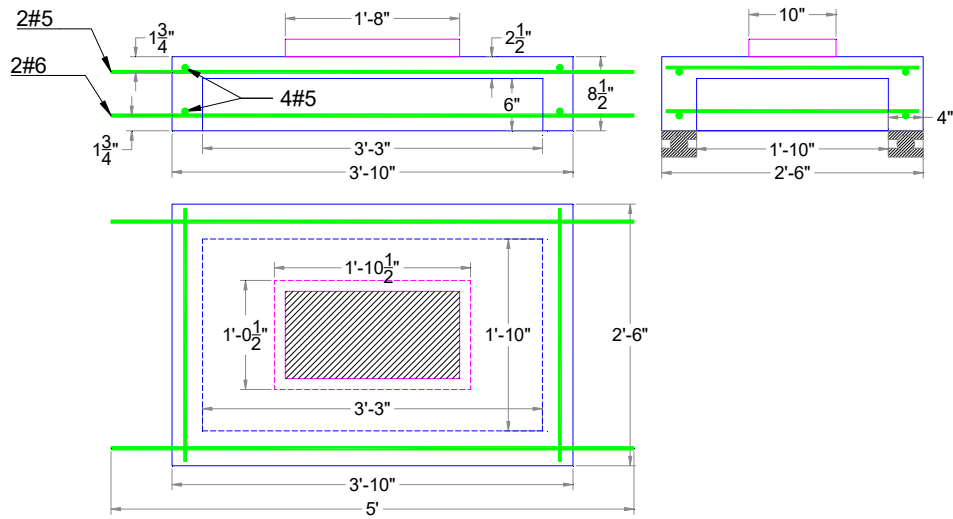


Figure 5.11: Punching Shear Test setup of the Ribbed Slab Skin

Figure 5.12 shows the load-deflection plots of the two specimens side by side. The figure shows that the UHPC and CC ribbed slabs had punching shear capacity of 72.02 kip and 17.94 kip, respectively, which indicates that UHPC ribbed slab punching shear capacity is four times that of conventional concrete ribbed slab. This is also significantly higher than the demand calculated at $1.75 * 1.33 * 8 \text{ kip} = 18.62 \text{ kip}$. It should be noted that nominal punching shear capacity of a 2.5 in. thick UHPC slab is predicted at 65.6 kip, which is very close to the measured capacity. Figure 5.13 shows the mode of failure of both specimens due to punching shear. Although the cracking patterns of both specimens are similar, the conventional concrete showed complete separation of the sheared area due to absence of reinforcement. Fiber reinforcement of UHPC controlled the cracking and prevented the complete separation of the sheared area. Detailed calculations are shown in Appendix B.

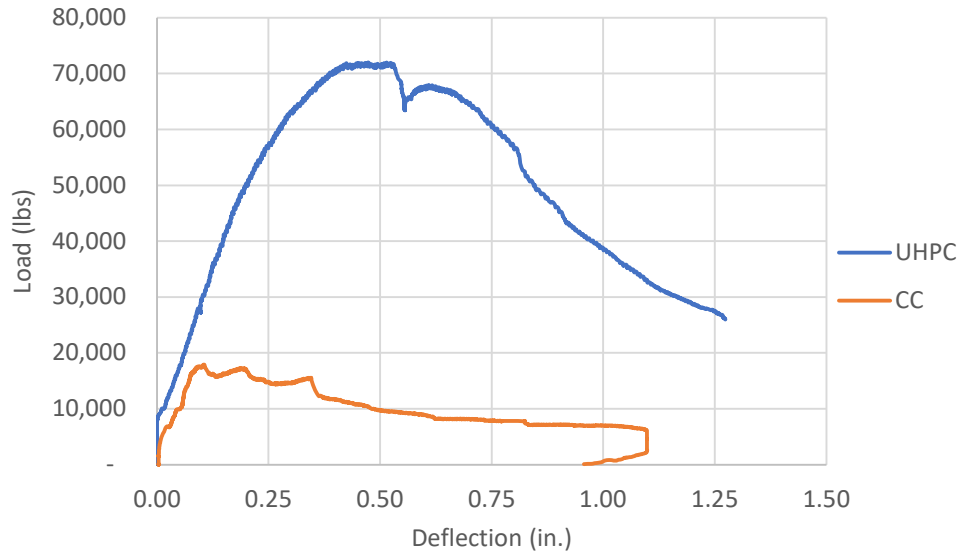


Figure 5.12: Punching Shear Test Results of the UHPC and CC Ribbed Slabs

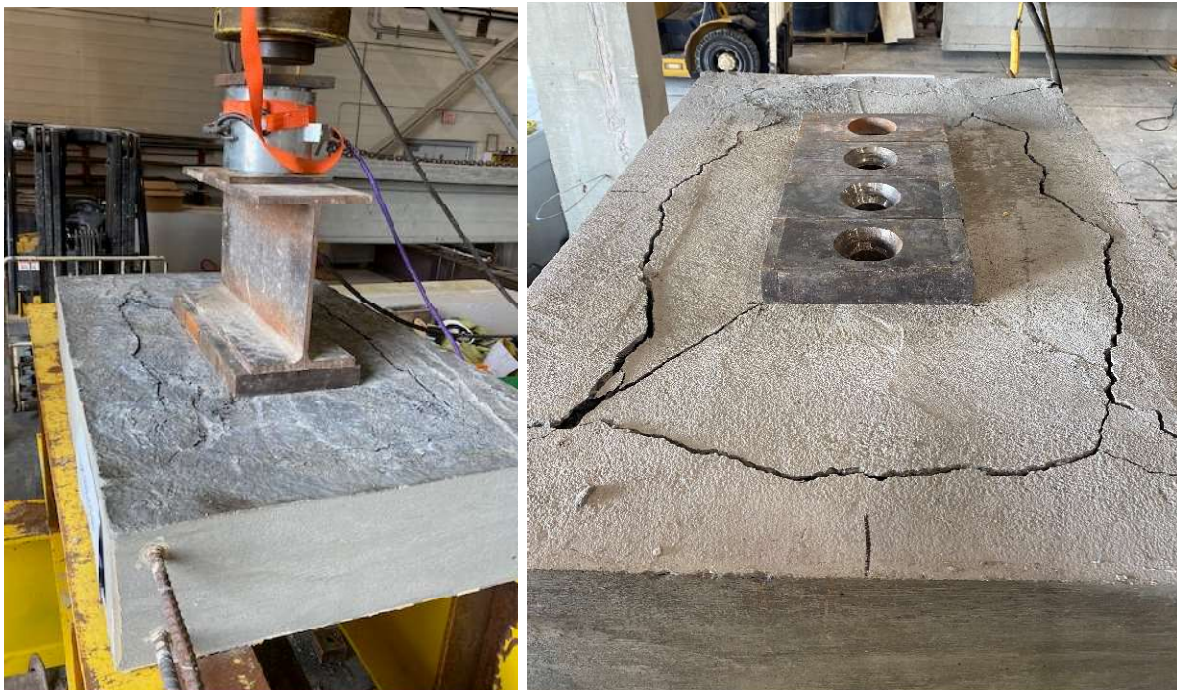


Figure 5.13: Punching Shear Failure Mode in UHPC Slab (left) and CC Slab (right)

5.2.4 DIB Longitudinal Joint

The longitudinal UHPC joint between adjacent DIBs is subjected to both positive bending moment and shearing force due to wheel load of the design truck (HL93), which is the same as calculated earlier for punching shear (18.62 kip). Figure 5.14 shows a section view of the proposed longitudinal joint reinforcement, shear key and bottom form after casting in-situ UHPC. Mild steel reinforcement extending from DIB ribbed slabs has non-contact lap splices using short loose bars in the transverse direction in addition to longitudinal bars (black dots in Figure 5.14) tied to the transverse bars to hold them during UHPC placement. Figure 5.15 shows the lab specimen made to simulate the longitudinal joint around one rib from adjacent DIBs with 1#5 bar at the top and another 1#5 at the bottom. The specimen also has 4#5 short bars for non-contact lap splices and 4#5 longitudinal bars to hold them in place. The smooth finish of the shear key was roughened after hardening via sandblasting as shown in Figure 5.16.

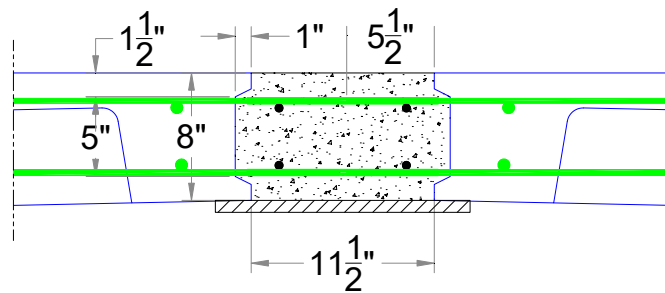


Figure 5.14: Section View of the Proposed UHPC Longitudinal Joint

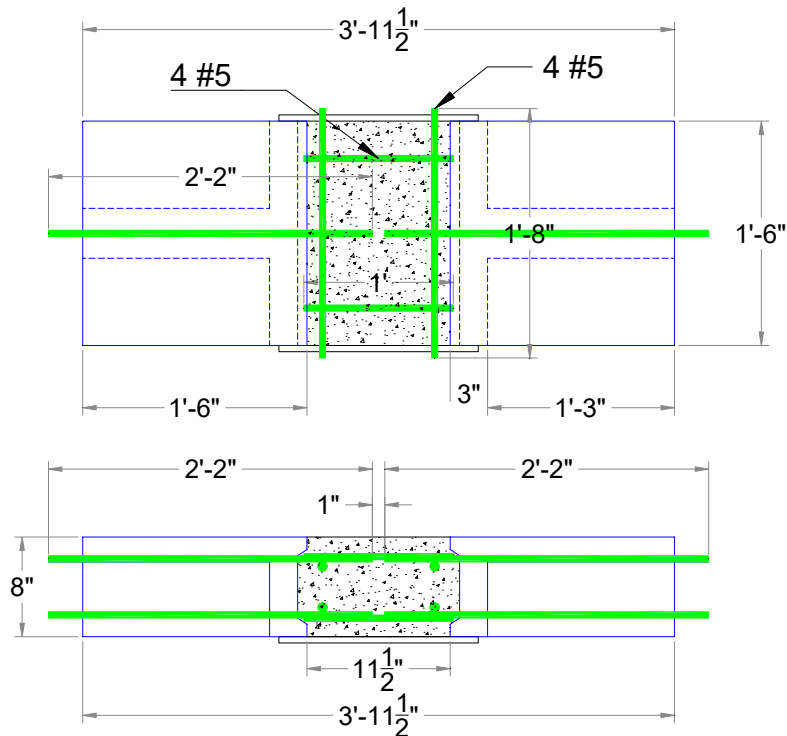




Figure 5.15: UHPC Longitudinal Joint Specimen



Figure 5.16: Finishing UHPC Shear key Surface: Smooth (left) and Sandblast (right)

A flexure test was conducted to evaluate its positive moment capacity of the longitudinal joint and ensure that the proposed non-contact lap splices are adequate to fully develop the transverse reinforcement of the ribbed slab. Figure 5.17 shows the test setup where a mid-span spreader beam was used to apply a concentrated load on the longitudinal joint up to failure. String potentiometers and strain gauges were installed to measure mid-span deflection and strains in interface between UHPC joint and shear key.

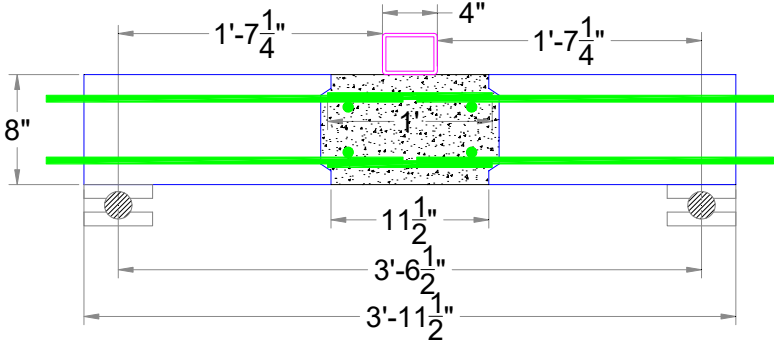


Figure 5.17: Longitudinal Joint Test Setup

Figure 5.18 shows the load-deflection and load-strain plots of the flexure test indicating that the longitudinal joint was able to carry a load up to 33.1 kip, which corresponds to a moment of 17.93 kip.ft. The joint failed by the rupture of bottom transverse bar, which indicates that the proposed non-contact lap splices using loose bars is adequate to fully develop the transverse reinforcement. Also, these plots indicate that the yielding of transverse bars occurred at a load of approximately 22 kip, while the joint started to open at much lower load of approximately 7.5 kips. Calculations of the applied moment and predicted capacity are shown in Appendix B.

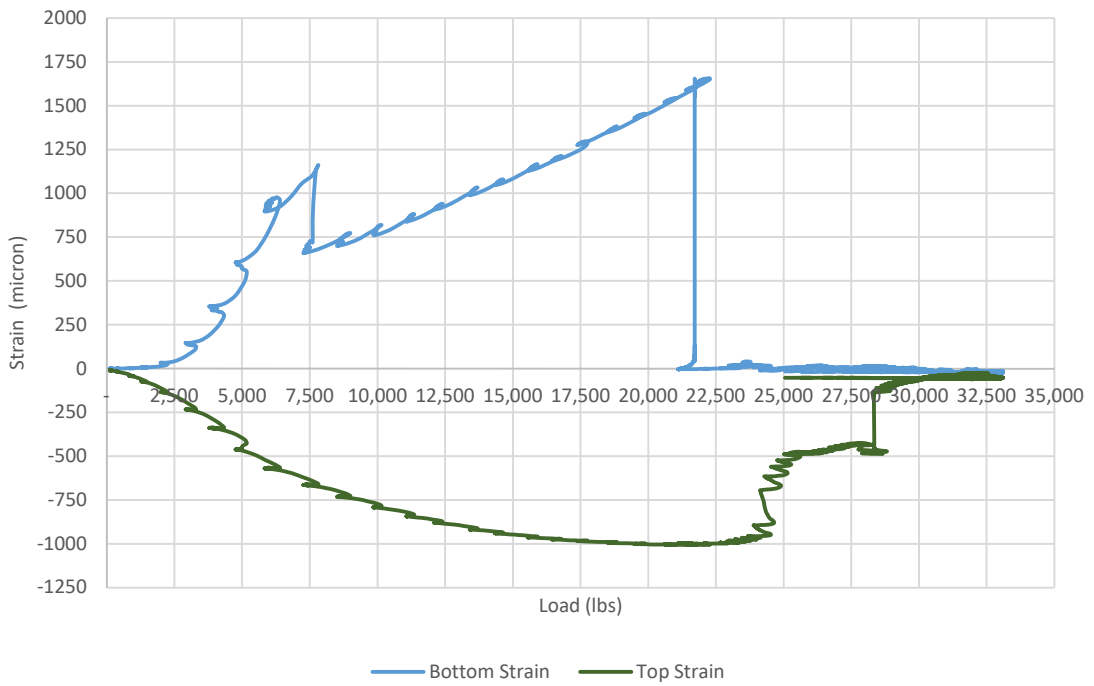
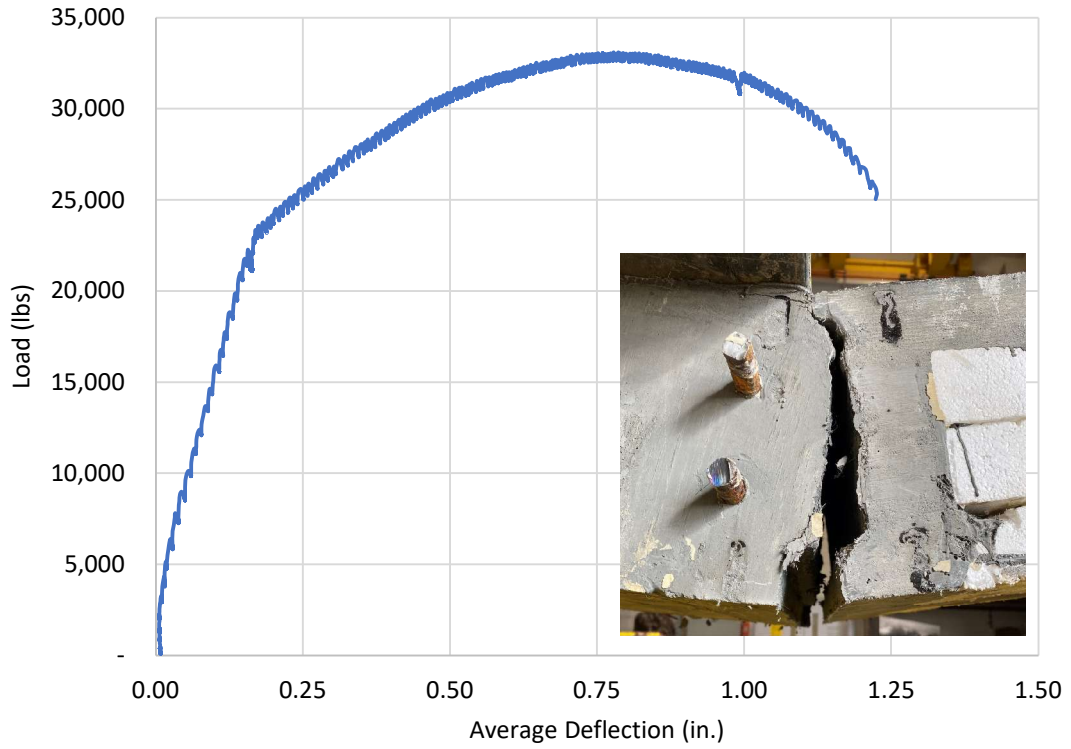


Figure 5.18: Test Results: Load-Deflection Plot (top) and Load-Strain Plot (bottom)

5.3 Full-Scale Testing

This section presents the testing conducted on the two full-scale UHPC DIB specimens fabricated by Coreslab Structures Inc. and Concrete Industries Inc. This includes measuring the transfer length, vertical shear test, transverse load distribution test, and post-tensioning anchorage test.

5.3.1 Transfer Length Test

A total of 12 DEMEC gauges were attached to one end of the pretensioned DIB specimen at the level of prestressing strands and at 4 in. spacing as shown in Figure 5.19. Measurements were taken before and after prestress release to calculate the elastic strain in the end 4 ft of the DIB. Figure 5.20 plots strain measurements and the 95% of the maximum average strain is used to estimate the transfer length, which was found to be approximately 13 in. This is in agreement with the prediction methods as the PCI method suggests $20 d_b$ (12 in.) and FHWA method suggests $24 d_b$ (14.4 in.).



Figure 5.19: DEMEC gauges installed for strain measurements at girder end

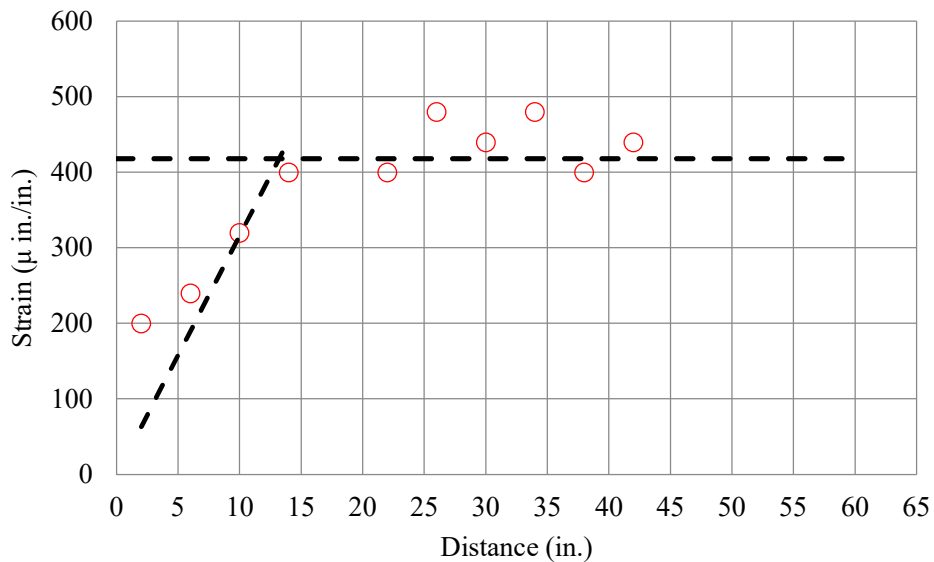


Figure 5.20: Strain measurements used in estimating the transfer length

5.3.2 Vertical Shear Test

To evaluate the shear capacity of UHPC DIB without any transverse reinforcement in the web, the pre-tensioned specimen was loaded at the mid span as shown in Figure 5.21. The setup is acceptable as it results in a shear span to depth ratio 2.1 and ensures that the shear failure occurs before the flexural failure of the specimen. Two hydraulic rams were used with a steel spreader beam to load the middle section of the beam, while strain gauges were used to measure the strains at locations A and B shown in Figure 5.21. LVDTs were used at beam ends to measure strand slippage, while string potentiometers were used at beam midspan to measure specimen deflection.

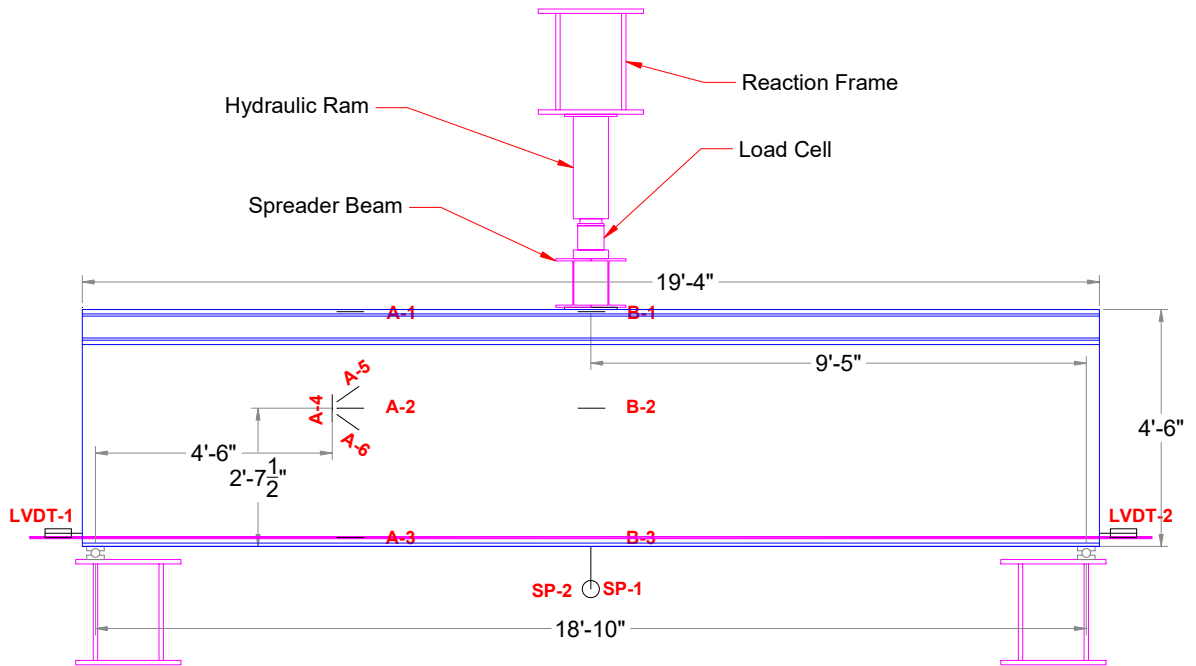


Figure 5.21: Vertical shear test setup and instrumentation

Figure 5.22 plots load-deflection relationship and Figure 5.23 plots load-strain relationships at section A. No strand slippage was detected. These figures indicate that a maximum load of 612 kip was achieved, which corresponds to a shearing force of 317 kip including the self-weight. Loading was stopped at this level as it reached the maximum capacity of the loading frame before reaching the maximum shear capacity of the specimen, which was estimated at 338 kip. This is acceptable as the measured load already exceeds the shear demand of 285 kip estimated for a 100 ft long simply supported bridge with 10 ft girder spacing.

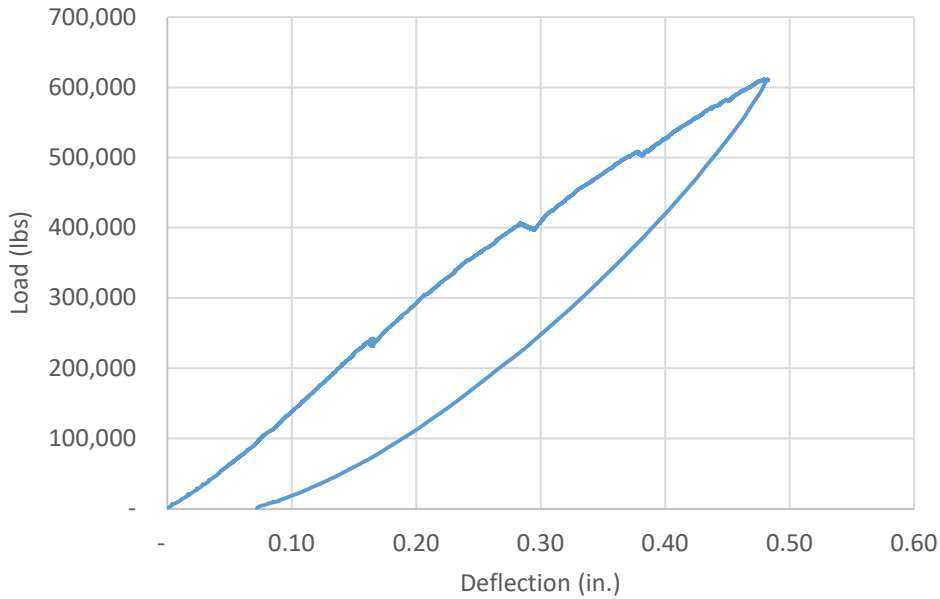


Figure 5.22: Load-deflection plot of vertical shear test

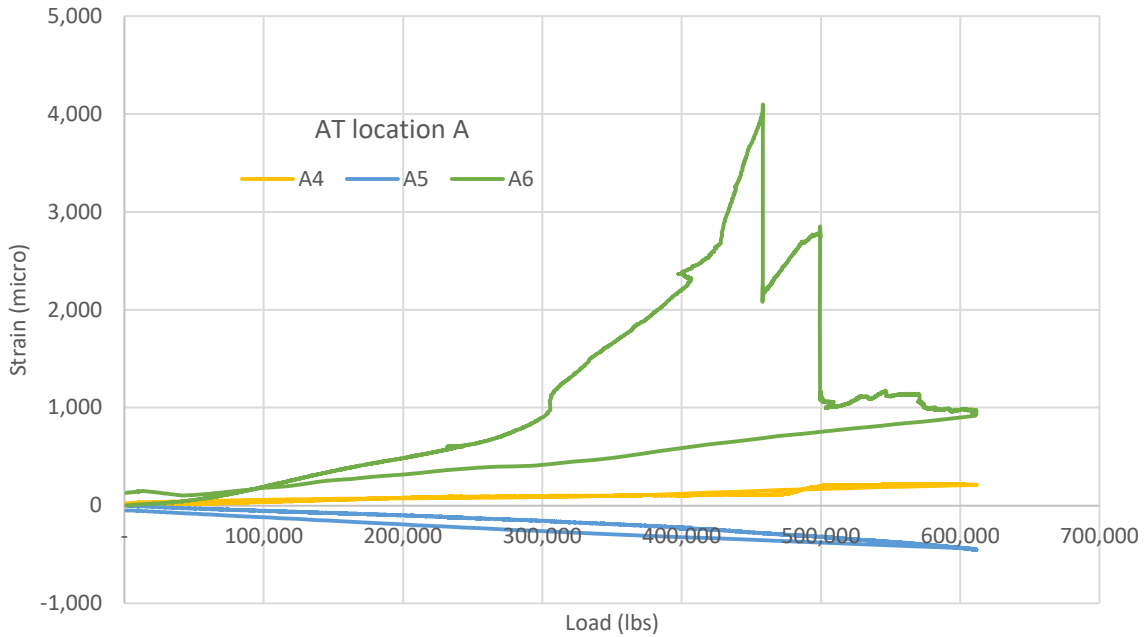


Figure 5.23: Load-strain plots of vertical shear test

Diagonal tension cracks were observed at the middle of the shear span in both sides of the beam as shown in Figure 5.24. The measured crack angle was found to be approximately 32°deg., which is very close to the crack angle of 30.8 deg. predicted using the PCI design approach. It was also observed that end zone cracking occurred only at the girder end that does not have bursting reinforcement, while the other end that had 2#6 is crack free as shown in Figure 5.25.



Figure 5.24: Diagonal tension cracks at both girder sides



Figure 5.25: End zone cracking at both girder ends

5.3.3 Wheel Load Distribution in the Transverse Direction

There are two types of live load distribution to be considered in design: in the longitudinal direction for design of beams, and in the transverse direction for design of deck slabs. The AASHTO LRFD Bridge Design Specifications do not have distribution factors for ribbed slab decks as they are not commonly used in US. Accordingly, for the longitudinal design of the beams, it is possible to use the distribution factors for conventional I-beams with cast-in-place solid composite deck slabs. This can be achieved by determining the equivalent slab thickness that produces the same transverse moment of inertia as a ribbed slab. For the UHPC beams being considered the equivalent solid slab thickness is about 5.4 inches. This is the value used to establish the LL distribution factors for bending and for shear.

In the transverse direction, values of two-way moments and shears are needed to determine adequacy of the ribbed slab flange and to determine the amount of reinforcement needed in both the transverse direction (in the transverse ribs) and in the longitudinal direction in the skin and longitudinal ribs. This type of analysis is similar to the “strip method” in Section 9 of AASHTO, which assumes a solid slab. This system behavior is hard to model in a lab testing of individual segments of UHPC DIB. However, it was decided to proceed with testing of the two specimens made separately by the two precasters without longitudinal joints or rail to determine a conservative estimate of the capacity of the overhang. The first specimen had a ribbed slab with longitudinal edge ribs that were not reinforced. The transverse ribs were 8 in. thick at the edge and 9 in. thick at the face of the web and had 2#5 bars/rib as top and bottom reinforcement. The second specimen had a solid slab with a nominal thickness of 6 in. at the edge and 7 in. at the face of the web. The solid slab beam had #5 at 12 in. top and bottom transverse bars and no longitudinal bars. These tests were conducted to get an idea about behavior of the top flange when subjected to wheel load at the edge. However, it should be emphasized that the tests cannot be used as a measure of the capacity of the deck for either the ribbed or solid slab. The continuity between flanges would be missing, the longitudinal bars in the longitudinal edge ribs and in the CIP closure pour would be missing. Only a finite element analysis or a more comprehensive testing program would account for these primary effects.

Figure 5.26 shows the AASHTO LRFD design truck wheel patch for front and rear axles. In the test, a 20”x 10” wheel patch was used with a design service load of 8 kips per wheel, which results in a factored load of 37.24 kips per group including 33% dynamic load allowance. Table 5.3 shows the existing formula for calculating the width of the primary strip. The formula for an overhang is used to predict the strip width for load distribution in the transverse direction as it is the most critical case. The following two subsections present the results of testing UHPC DIB ribbed and solid slab overhangs to determine their load carrying capacity compared to predicted values.

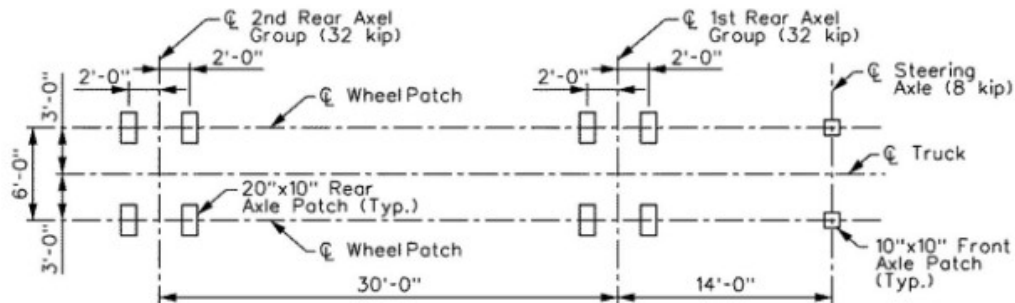


Figure 5.26: AASHTO LRFD Design truck axle loads, wheel loads, and wheel patches

Table 5.3: AASHTO LRFD width of primary strip for wheel load distribution

Type of Deck	Direction of Primary Strip Relative to Traffic	Width of Primary Strip (in.)
Concrete:		
<ul style="list-style-type: none"> Cast-in-place 	Overhang	$45.0 + 10.0X$
	Either Parallel or Perpendicular	+M: $26.0 + 6.6S$ -M: $48.0 + 3.0S$
<ul style="list-style-type: none"> Cast-in-place with stay-in-place concrete formwork 	Either Parallel or Perpendicular	+M: $26.0 + 6.6S$ -M: $48.0 + 3.0S$
	Either Parallel or Perpendicular	+M: $26.0 + 6.6S$ -M: $48.0 + 3.0S$
<ul style="list-style-type: none"> Precast, post-tensioned 	Either Parallel or Perpendicular	+M: $26.0 + 6.6S$ -M: $48.0 + 3.0S$
	Either Parallel or Perpendicular	+M: $26.0 + 6.6S$ -M: $48.0 + 3.0S$

Ribbed Slab Test

The UHPC DIB pretensioned specimen with ribbed slab was tested for flexure in the transverse direction directly after being tested in vertical shear using the same loading frame and rams. A longer steel spreader beam was used as shown in Figure 5.27 and steel loading plates were used to simulate the wheel patches. Load was applied at the location shown in Figure 5.27 and between the slab ribs as it is the most critical position. The DIB was supported at the midspan in the longitudinal direction to prevent its deflection while loading. String potentiometers were attached under each loaded side to measure overhang deflections.



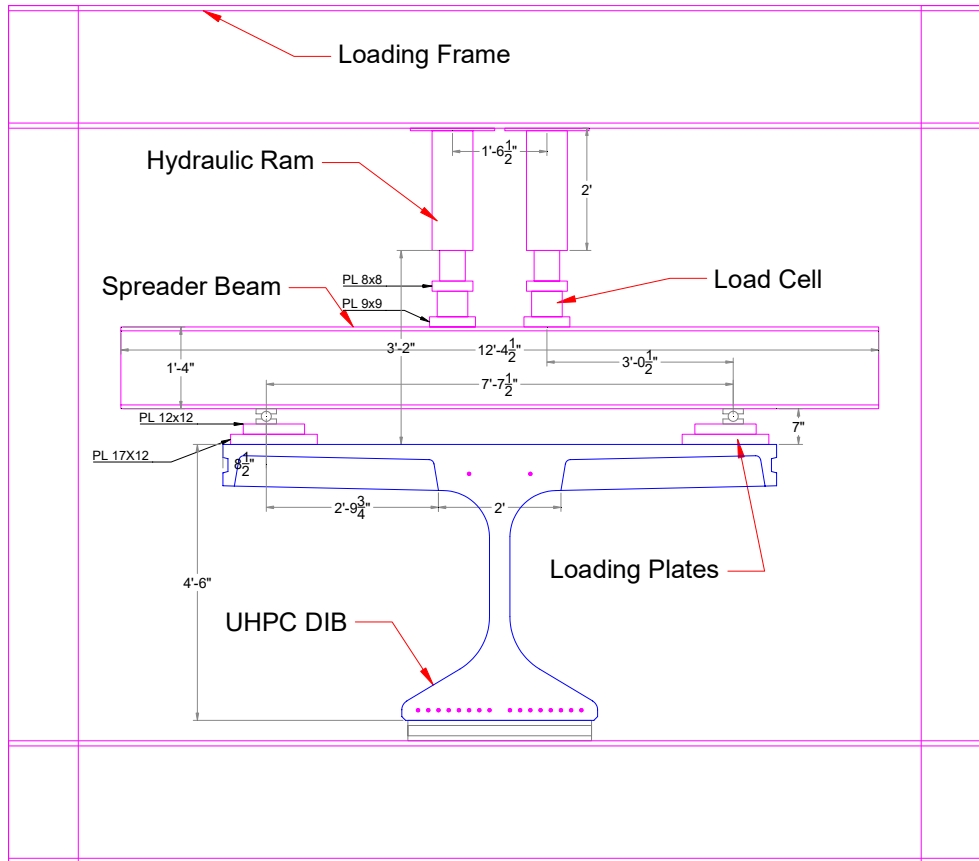


Figure 5.27: Ribbed slab test setup

Figure 5.28 shows the load-deflection plots of the two loaded sides (north and south). The plots indicate that the loading was balanced and the maximum load achieved was 78 kips. This is more than twice the demand of 37.24 kips and 70% more than the predicted load of 45.23 kip using the AASHTO LRFD primary strip width of 6.1 ft. Prediction calculations are shown in Appendix B. Figure 5.29 shows the cracking of the edge rib at early loading due to flexure and absence of continuous reinforcement in the edge rib. This test is conservative as the actual bridge section has longitudinal joints or rail connection with top and bottom longitudinal reinforcement that distributes the wheel load not just the edge rib as tested. Similar specimen tested by North Carolina State University had better performance when 2#5 longitudinal bars are used in each edge rib. Figure 5.30 show several photos of the ribbed slab failure by punching shear. This is consistent with the punching shear test presented earlier as it showed a load capacity of 72 kips, which is close to the maximum load of 78 kip achieved in this test.

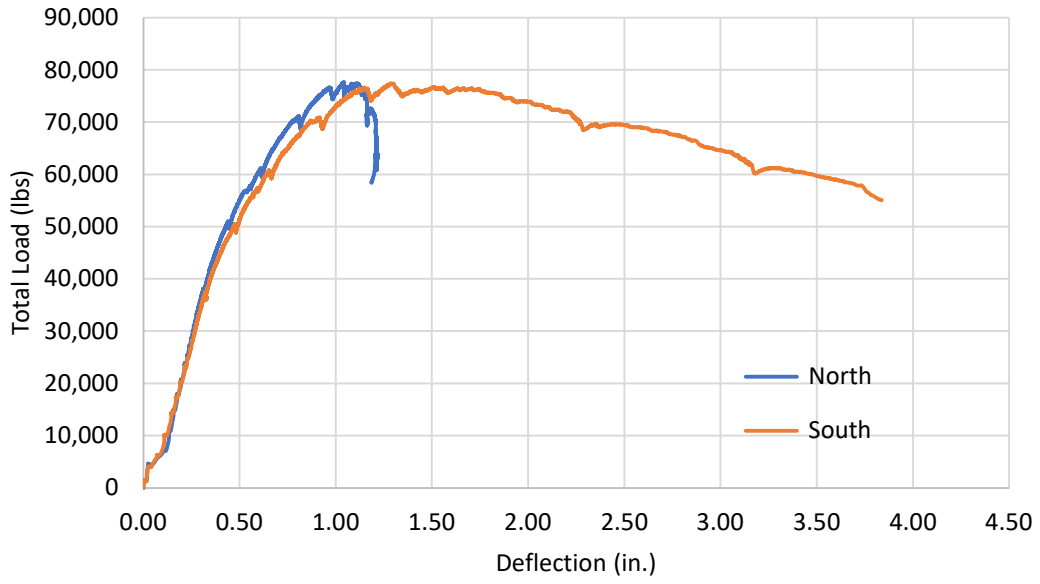


Figure 5.28: Load-deflection plots of ribbed slab overhang



Figure 5.29: Cracking of unreinforced edge rib at early loading



Figure 5.30: Ribbed slab overhang failure by punching shear

Solid Slab Test

The UHPC DIB post-tensioned specimen with solid slab was tested for flexure in the transverse direction prior to being post-tensioned and using the same loading frame, rams, spreader beam, and loading plates used in testing the ribbed slab specimen. Figure 5.31 shows the loading location, which was identical to that used in testing the ribbed slab. The DIB was supported at the midspan in the longitudinal direction to prevent its bending and deflection while loading. String potentiometers were attached under each loaded side to measure overhang deflections. This test is conservative as the actual bridge section has longitudinal joints or rail connection with top and bottom longitudinal reinforcement that distributes the wheel load.

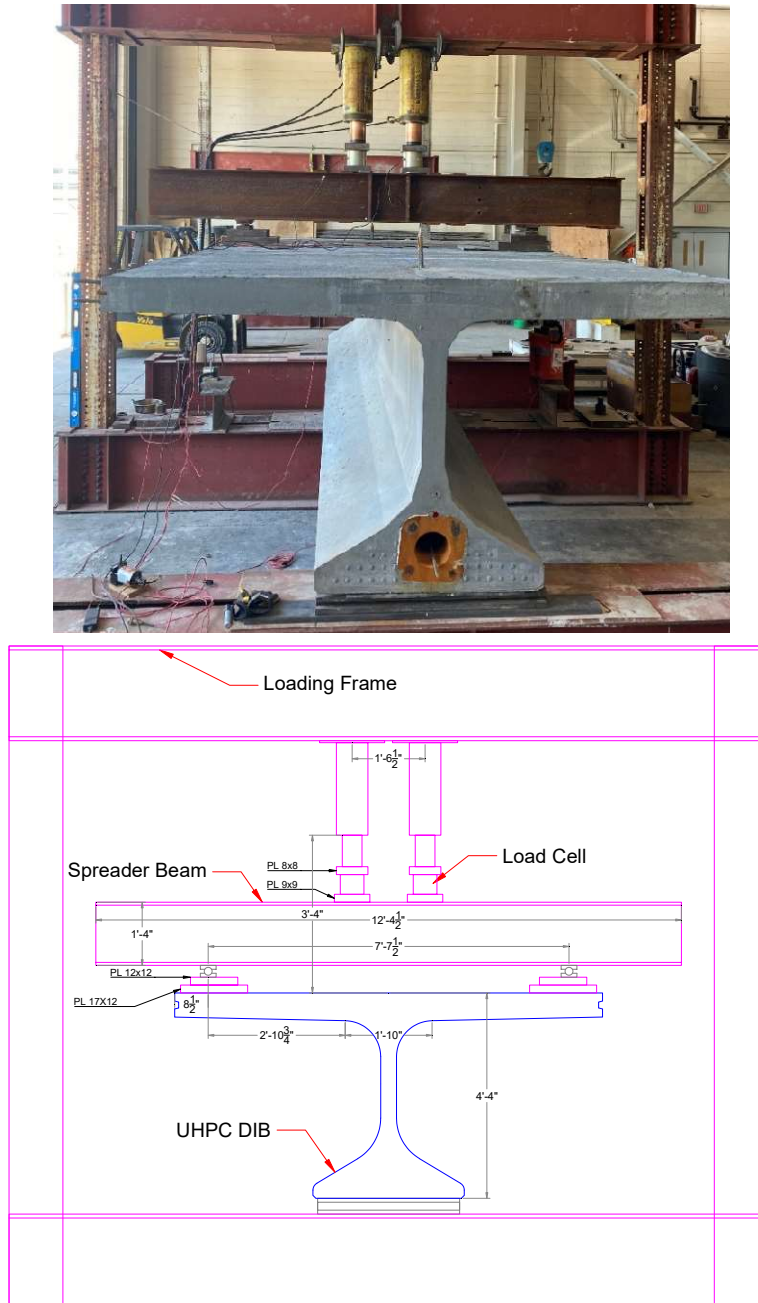


Figure 5.31: Solid slab test setup

Figure 5.32 shows the load-deflection plots of the two loaded sides (north and south). The plots indicate that the loading was similar in both sides with slightly higher deflection in south side than the north side. Loading continued up to 120 kips then stopped to preserve the specimen for further testing. This load is 3.2 times the demand of 37.24 kips and 2.3 than the predicted capacity of 52.14 kip using the AASHTO LRFD primary strip width of 6.2 ft. Prediction calculations are shown in Appendix B. Figure 5.33 shows the negative moment longitudinal top cracking of the overhang, while Figure 5.34 shows the bottom and side transverse cracking, which is considered insignificant given the magnitude of the load of 120 kips.

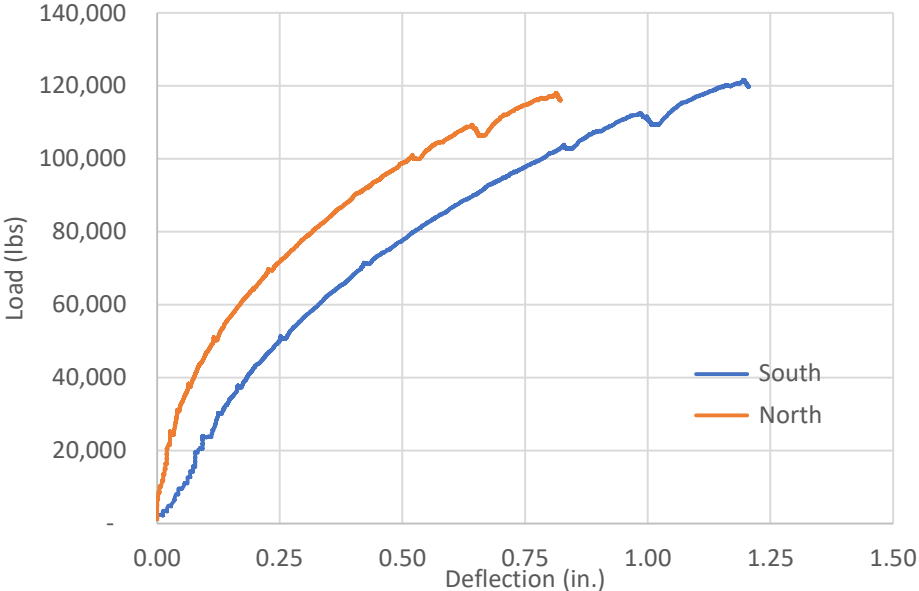


Figure 5.32: Load-deflection of the solid slab overhang



Figure 5.33: Longitudinal flexure cracks at the top of the solid slab

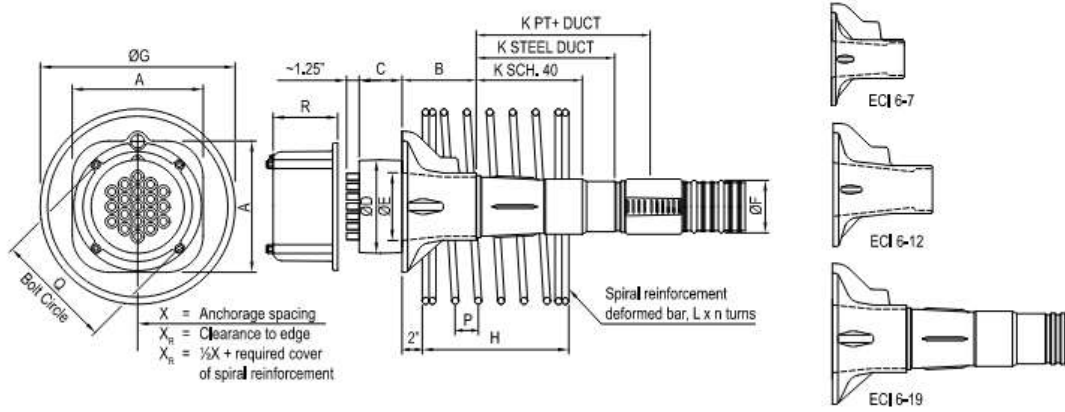


Figure 5.34: Transverse flexure cracks at the side and bottom of the solid slab

5.3.4 Post-Tensioning Anchorage Test

For the post-tensioned option, DIB segments will be fabricated using match cast and post-tensioned either at the precast yard or in the site. Due to the limited space at the bottom flange of the DIB, standard PT anchorage was modified by eliminating the standard spiral reinforcement in order to fit in the bottom flange without casting a special anchorage block. This will simplify the production of DIB segments by using the same prismatic forms used for the pretensioned option. To evaluate the performance of the modified PT anchorage hardware, a test was conducted by post-tensioning the second specimen fabricated by Concrete Industries to the full tensioning force at the Structural Laboratory of UNL. The multistrand standard ECI 6-19 anchorage from VSL, shown in Figure 5.36, was used in this specimen but without the standard spiral reinforcement around the trumpet. Instead, a special L-shape end zone bursting reinforcement (8#6) was used around the trumpet as shown earlier in Chapter 4. Figure 5.36 shows the sketch and dimensions of the ECI 6-19 anchorage used with 4 in. polypropylene plastic duct in the bottom flange. Also, the multistrand ECI 6-7 anchorage is proposed to be used in the top flange to connect the segments and control the camber. Figure 5.37 shows the DIB specimen with the anchorage plate and the 19-0.6 in. strands before tensioning.

Type ECI Stressing Anchorage



		Dimensions (Inches)																		
Tendon Unit	F _{ci} (psi)	A	B	C	øD	øE	øF PT+ Duct	øF Steel Duct	øF SCH 40 Pipe	øG	H	K PT+ Duct	K Steel Duct	K SCH 40 Pipe	L	n	P	Q	R	X
6-7	3500	8.54	6.69	2.37	5.33	3.31	2.87	2.88	3.00	11.00	12.00	No Trumpet on 6-7			#4	6.50	3.00	7.40	4.17	13.00
6-7	5500	8.54	6.69	2.37	5.33	3.31	2.87	2.88	3.00	11.00	12.00	No Trumpet on 6-7			#4	6.50	3.00	7.40	4.17	13.00
6-12	3500	9.88	8.66	3.00	6.85	4.62	3.58	3.24	3.50	13.00	14.00	No Trumpet on 6-12			#5	7.00	3.00	8.66	4.90	15.00
6-12	5500	9.88	8.66	3.00	6.85	4.62	3.58	3.24	3.50	13.00	13.50	No Trumpet on 6-12			#4	7.00	3.00	8.66	4.90	15.00
6-19	3500	11.42	6.91	3.75	8.13	5.90	4.57	4.10	4.50	17.00	19.00	15.19	12.09	9.29	#5	11.50	2.00	10.24	5.63	19.00
6-19	5500	11.42	6.91	3.75	8.13	5.90	4.57	4.10	4.50	15.00	17.00	15.19	12.09	9.29	#5	10.50	2.00	10.24	5.63	17.00

Figure 5.36: ECI 6-19 Anchorage used in the tested specimen

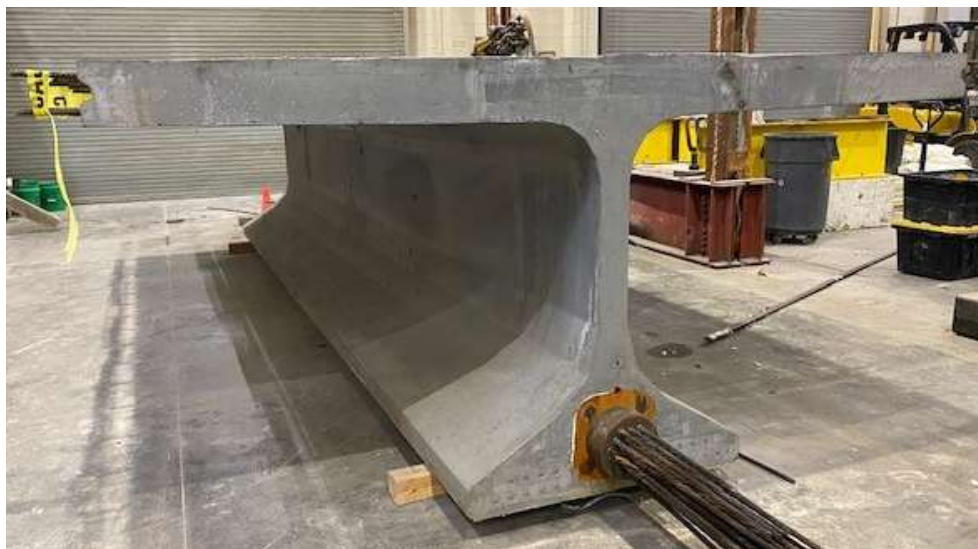


Figure 5.37: UHPC DIB with solid slab before post-tensioning

A total of 6 DEMEC gauges were installed to the middle section of the specimen at 2.5 in. from the bottom as shown in Figure 5.38 to measure the strain due to post-tensioning and verify the applied force. Figure 5.39 shows the anchorage plate and special plates used to post-tension 19-0.6” strands using a mono-strand hydraulic ram and ensure that wedge seating loss is only ¼ in. Tensioning was completed in a symmetrical manner and in two stages 50% then 100% of the full prestressing force to minimize elastic shortening losses. Also, tensioning was conducted from both ends of the specimen to minimize friction losses. Figure 5.39 shows the anchorage plate with the seated wedges after completing PT at both ends of the specimens. Marking were made on the strands to measure the actual elongation and compare to the predicted elongation of 1.65 in. as a verification that the design PT force was achieved. Figure 5.40 shows the two specimen ends after post-tensioning indicating that no cracking or any signs of distress was observed, which confirms the adequacy of the provided end zone reinforcement. Also, Table 5.4 shows the strain measurements at midspan using DEMEC gauges, which resulted in an average strain of 0.00024 directly after post-tensioning. This slightly less than predicted strain of 0.00026, which could be attributed to normal variability in stress measurements and/or friction losses that were not counted for. Strain calculations are shown in Appendix B.



Figure 5.38: DEMEC gauges attached to bottom flange to measure strains due to post-tensioning





Figure 5.39: Anchorage plates and the hardware used for post-tensioning.



Figure 5.40: Specimen ends after post-tensioning showing no cracking

Table 5.4: Strain measurements using DEMEC gauges at midspan

Date	Stage	DEMEC Location				Average Difference
		West-South	West-North	East-North	East-South	
27-Sep-22	Before Tensioned	19.40	21.80	16.60	19.65	
10-Oct-22	50% tensioned	19.20	21.65	16.45	19.45	
11-Oct-22	100% tensioned	19.10	21.50	16.35	19.35	
Difference		0.30	0.30	0.25	0.30	0.3

Conversion Factor 0.0008
Average Strain 0.00024

Chapter 6. Conclusions

6.1 Production Conclusions

- a. Production of NDOT-UNL UHPC in precast plant in a quantity of 6.6 yd³ was successful and material properties met all the minimum requirements for a structural design according to PCI Phase II report.
- b. Mixing multiple small batches of UHPC in a truck mixer before casting is a good practice as it ensures consistency, allows adjusting workability, and prevents the formation of cold joints (elephant skin) between batches.
- c. Mixture temperature, sand moisture content, and dosage of admixtures must be carefully monitored to ensure adequate UHPC workability and stability of fibers.
- d. Flow test and VSI should be performed before casting to determine whether the workability and stability are acceptable. Admixtures can be added to improve the mix rheology.
- e. Unstable UHPC demonstrates significant early age cracking, very low flexural strength, and brittle failure in compression.
- f. Edge form with a bottom lip are challenging to strip due to the presence of transverse bars. Modified edge form without a lip and with vertical shear key was easier to strip.
- g. DIB pans for forming ribbed slab voids are difficult to strip due to friction, suction and shrinkage effects. A modified forming system to allow for simplified pan removal and using shrinkage reducing admixtures are recommended.
- h. Removing the pans and using 6 in. solid slab is a feasible option to simplify production. DIB with solid slab will have a slightly higher weight compared to ribbed slab.

6.2 Design Conclusions

- a. UHPC DIB with 4 in. web has adequate shear capacity for 100 ft simple span at 10 ft spacing without the need for shear reinforcement. It is possible that DIBs made continuous for live load would require small amount of shear reinforcement near the piers.
- b. No spiral reinforcement is needed in the local zone of PT anchorage as the random steel fibers are adequate for providing the necessary confinement.
- c. End zone reinforcement of the AASHTO LRFD are needed to provide the required splitting resistance for both pretensioned and post-tensioned options.

- d. UHPC DIB with either 8 in. ribbed slab or 6 in. solid slab have adequate flexural capacity for wheel load distribution in the transverse direction.
- e. No longitudinal reinforcement is needed in the solid slab as the random steel fibers are adequate for load distribution in the transverse direction.
- f. Longitudinal reinforcement in the edge rib, in addition to longitudinal joint, is recommended to control cracking under service load and improve load distribution in the transverse direction under ultimate load.
- g. The 2.5 in. unreinforced UHPC slab between ribs has adequate punching shear capacity for design truck wheel load.
- h. Non-contact lap splices at the longitudinal joints between DIBs are adequate to fully develop transverse reinforcement over $8d_b$ distance.

REFERENCES

- American Association of State Highway and Transportation Officials (AASHTO) (2017) "LRFD Bridge Design Specifications." AASHTO LRFD, 8th Edition, AASHTO, Washington, D.C.
- American Association of State Highway and Transportation Officials (AASHTO) T397-22 (2022) "Standard Method of Test for Uniaxial Tensile Response of Ultra-High-Performance Concrete", Technical Committee: 3C, Hardened Concrete, Washington, DC.
- American Association of State Highway and Transportation Officials (AASHTO) (2023) "Structural Design with Ultra-High-Performance Concrete: AASHTO Guide Specifications; Document developed for consideration by AASHTO CBS T-10 committee (Structural Concrete Design), Draft", Washington, DC.
- American Concrete Institute (ACI) Committee 239 (2018) "Ultra-High-Performance Concrete: (ACI 239-18). Farmington Hills, MI.
- ASTM C1609 / C1609M-19, (2019) "Standard Test Method for Flexural Performance of Fiber-Reinforced Concrete (Using Beam with Third-Point Loading)", ASTM International, West Conshohocken, PA.
- ASTM C1856 / C1856M-17 (2017) "Standard Practice for Fabricating and Testing Specimens of Ultra-High-Performance Concrete", ASTM International, West Conshohocken, PA.
- Bierwagen, D., Moore, B., Keierlieber, B., Sritharan, S., Wipf, T., and Abu-Hawash, A. (2010) "Design of Buchanan County Bridge Using Ultra-High-Performance Concrete and Pi-Girder Cross Section", 2010 PCI National Bridge Convention.
- El-Helou, R. G., and Graybeal, B. A. (2022) "Flexural Behavior and Design of Ultra-High-Performance Concrete Beams", ASCE Journal of Structural Engineering, 148(4).
- Federal Highway Administration (FHWA) (2023) "Deployment of UHPC in Highway Bridge Construction", website accessed on February 2023, <https://highways.dot.gov/research/structures/ultra-high-performance-concrete/deployments>
- Graybeal, B. A. (2006) "Structural behavior of ultra-high-performance concrete prestressed I-girders" No. FHWA-HRT-06-115. United States. Federal Highway Administration. Office of Infrastructure Research and Development.
- Graybeal, B. A. (2009) "Flexural behavior of a Prototype Ultra-High-Performance Concrete Pi-Girder." No. FHWA-HRT-10-027. United States. Federal Highway Administration. Office of Infrastructure Research and Development.
- Hajar, Z., Simon, A., Lecointre, D., Petitjean, J. (2003) "Construction of the First Road Bridges Made of Ultra-High-Performance Concrete", 2003 ISHPC.
- Kodsy, A.; Morcous, G. (2021) "Flexural strength prediction models of non-prestressed Ultra-High-Performance Concrete (UHPC) components." Structures, 34, 4532–4547, <https://doi.org/10.1016/j.istruc.2021.10.047>.

- Mendonca, F., Abo El-Khier, M., Morcous, G., and Hu, J. (2020) “Feasibility Study of Development of Ultra-High-Performance Concrete (UHPC) for Highway Bridge Applications in Nebraska.” No. SPR-P1 (18) M072. Nebraska Department of Transportation, Lincoln, NE.
- Ozyildirim, C. (2011) “Evaluation of Ultra-High-Performance Fiber Reinforced Concrete”, Technical Report VCTIR 12-R1.
- Park, S., Kim, S., Cho, J., Lee, J., and Kim, B. (2013) “Trial Construction of UHPC Highway Bridge”, 2013 UHPCFRC, France.
- Precast/Prestressed Concrete Institute (PCI) TR-9-22 (2022) “Guidelines for the Use of Ultra-High-Performance Concrete (UHPC) in Precast and Prestressed Concrete”, PCI Concrete Materials Technology Committee, Chicago, IL
- Sim, C., Tadros, M.K., Gee, D. and Asaad, M. (2020) “Flexural design of precast, prestressed ultra-high-performance concrete members.” PCI Journal, 65(6).
- Tadros, M. K., Sevenker, A., Gardonio, D., and Loh, P. (2020) “ABC Design of UHPC Decked I-Beam Vehicular Bridge in Ontario, Canada”, Florida International University (FIU), Accelerated Bridge Construction Conference, Miami, FL, Paper 48.
- Tadros, M.K., Lawler, J., Abo El-Khier, M., Gee, D., Kurt, A., Lucier, G. and Wagner, E. (2022) “Implementation of Ultra-High-Performance Concrete in Long-Span Precast Pretensioned Elements for Concrete Buildings and Bridges” Phase II Report v2.0; Precast/Prestressed Concrete Institute, Chicago, IL.
- Tadros, M.K., Lawler, J., Morcous, G., Klein, G., Lucier, G. (2019), “Implementation of Ultra High-Performance Concrete in Precast Pretension Long Span Bridge and Building Beams, Phase I Report, Precast Prestressed Concrete Institute, Chicago, IL.
- Voo, Y. L., Foster, S. J., and Voo, C. C. (2015) “Ultra-High Performance Concrete Segmental Bridge Technology: Toward Sustainable Bridge Construction”, ASCE Journal of Bridge Engineering, 20(8).
- Voo, Y. L., Foster, S. J., Faiz, M., and Hassan, A. (2014) “The Current State of Art of Ultra-High Performance Concrete Bridge Construction in Malaysia”, Proceedings of the 12th International Conference on Concrete Engineering and Technology, Selangor, Malaysia.

APPENDIX A: UHPC DIB FORMS

The forms shown in this appendix were fabricated by the company Kessab Steel in the United Arab Emirates. Two twenty-foot sections were ordered and paid for as a contribution from e.construct.USA as a means of encouraging the two Nebraska producers to participate in the UHPC initiative without the risk of paying for new forms. The forms have achieved their purpose. The two producers participated in the research program. Concrete Industries was not familiar with UHPC production. The exercise, while costing them to repeat production of their first specimen, ended up creating valuable experience. The second specimen by Concrete Industries was of high quality and was used for lab testing. However, due to difficulty in stripping the block-outs for the top flange ribs, it was decided to produce a solid slab top flange for the second specimen. Coreslab Structures (Omaha) had significant experience with UHPC before this project as they had participated in demonstration projects for Iowa DOT and FHWA, and also produced all the full scale shear testing specimens for the PCI-UHPC Project.



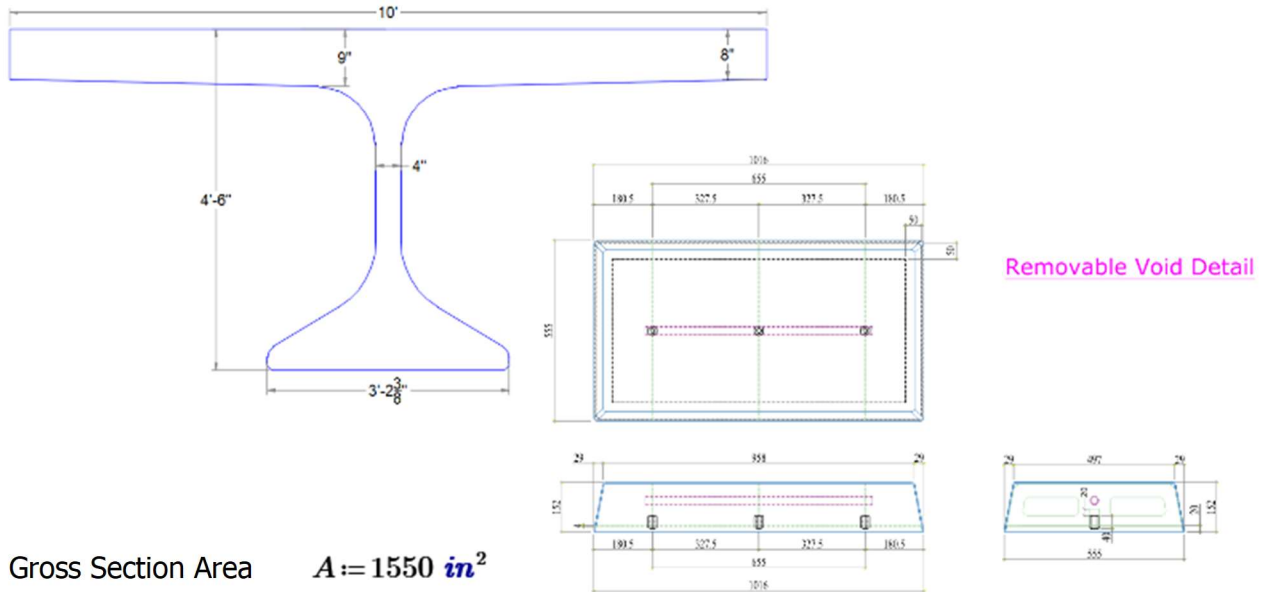






APPENDIX B: TEST CALCULATIONS

UHPC Volume in Ribbed and Solid Slab Options



Gross Section Area $A := 1550 \text{ in}^2$

Segment Length $l := 19.35 \text{ ft}$

Gross Volume $V_g := l \cdot A = 7.71 \text{ yd}^3$

Volume of a Void $v := 152 \text{ mm} \cdot \left(\frac{555 \text{ mm} + 497 \text{ mm}}{2} \right) \cdot \left(\frac{958 \text{ mm} + 1016 \text{ mm}}{2} \right) = 2.787 \text{ ft}^3$

No. of Voids $n := 18$

Volume of Voids $V_o := n \cdot v = 1.86 \text{ yd}^3$

Ribbed DIB Volume $V := V_g - V_o = 5.86 \text{ yd}^3$

New Thickness $t := 6 \text{ in}$

Segment Width $w := 10 \text{ ft}$

Volume Reduction $\Delta V := w \cdot l \cdot (8 \text{ in} - t) = 1.19 \text{ yd}^3$

New Volume $V_n := V + V_o - \Delta V = 6.52 \text{ yd}^3$

$\frac{V_n}{V} = 111\%$

Punching Shear Capacity of Ribbed Slab

Wheel Patch Width $w_{wheel} := 10 \text{ in}$

Wheel Patch Length $l_{wheel} := 20 \text{ in}$

Average Thickness $h := 2.5 \text{ in}$

Critical Section Perimeter $b_o := 2 \cdot (l_{wheel} + w_{wheel} + 2 h) = 70 \text{ in}$

Post-Cracking Residual Tensile Strength $f_{rr} := 0.75 \text{ ksi}$

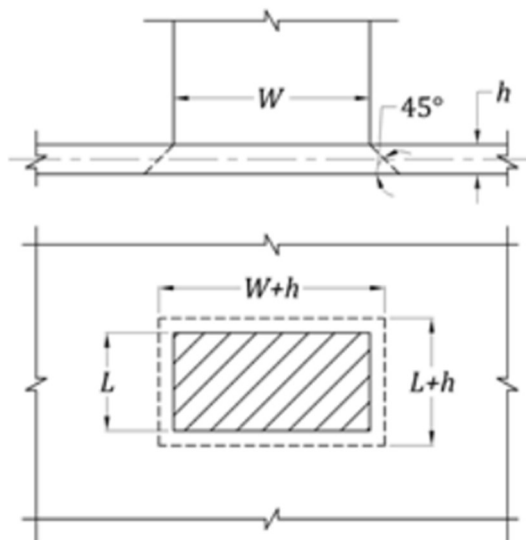
Nominal Punching Shear Capacity $V_{np} := \frac{1}{2} \cdot f_{rr} \cdot h \cdot b_o = 65.6 \text{ kip}$

Measured Capacity $V_{test} := 72 \text{ kip}$

Factored Load (Demand) $V_u := 8 \text{ kip} \cdot 1.75 \cdot (1 + 0.33) = 18.62 \text{ kip}$

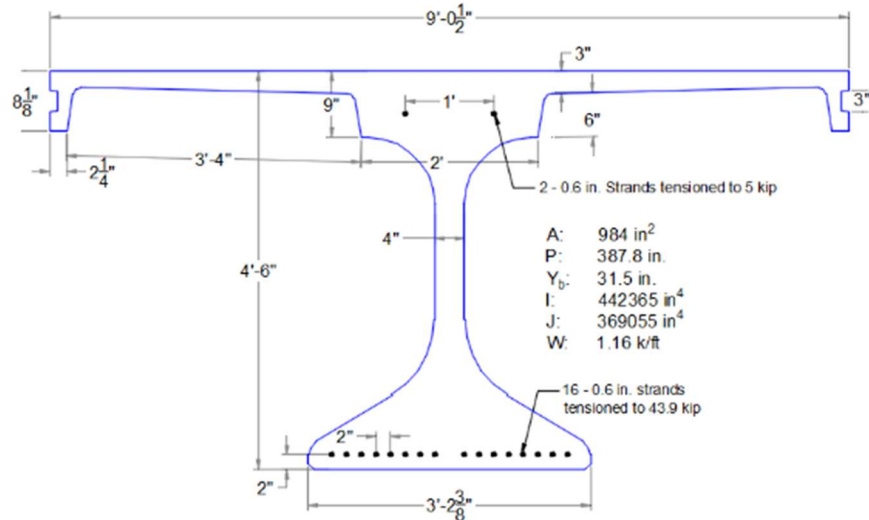
Measured-to-Predicted $\frac{V_{test}}{V_{np}} = 1.1$

Measured-to-Demand $\frac{V_{test}}{V_u} = 3.87$



Shear Strength Predictions of Prestressed UHPC Beams

Coreslab DIB
with Ribbed Slab



Concrete Properties

Girder Compressive Strength $f_c' := 17.4 \text{ ksi}$

Girder Height $h := 54 \text{ in}$

Girder Cross-sectional Area $A_g := 984 \text{ in}^2$

Shear Width $b_v := 4 \text{ in}$

Prestressing Properties

Prestressing MOE $E_p := 29000 \text{ ksi}$

Prestressing Ultimate Strength $f_{pu} := 270 \text{ ksi}$

Locked-in Stress in Prestressing $f_{po} := 0.7 \cdot f_{pu} = 189 \text{ ksi}$

Area of Prestressing $A_{ps} := 16 \cdot 0.217 \text{ in}^2 = 3.47 \text{ in}^2$

Vertical Component of Prestress $V_p := 0 \text{ kip}$

C.G. of Strands from Top of Girder $d_e := h - 2 \text{ in} = 52 \text{ in}$

Shear Depth $d_v := d_e - 0.5 \text{ in} = 51.5 \text{ in}$

$$d_v := \max(d_v, 0.72 h, 0.9 d_e) = 51.5 \text{ in}$$

Prestressing Ratio $\rho := \frac{A_{ps}}{b_v \cdot d_e} = 1.7\%$

Steel Properties

Steel MOE $E_s := 29000 \text{ ksi}$

Steel Yield Strength $f_y := 60 \text{ ksi}$

Longitudinal Reinforcement Area $A_s := 0 \cdot \text{in}^2$

Transverse Reinforcement Area $A_v := 0 \text{ in}^2$

Transverse Reinforcement Spacing
(1.0 in if no reinforcement) $s := 1 \text{ in}$

Transverse Reinforcement Angle $\alpha := 90 \text{ deg}$

Transverse Reinforcement Ratio $\rho_v := \frac{A_v}{b_v \cdot s} = 0$

Load Data

Specimen Span $L := 18 \text{ ft} + 10 \text{ in}$

Ultimate Shear Force $V_u := 317 \text{ kip}$

Ultimate Axial Force $N_u := 0 \cdot \text{kip}$ -ve if Compression

Ultimate Moment $M_u := V_u \cdot \left(\frac{L}{2} - d_v \right) = 1624.6 \text{ kip} \cdot \text{ft}$

$M_u := \max(M_u, |V_u - V_p| \cdot d_v) = 1624.6 \text{ kip} \cdot \text{ft}$

Resistance Factors

For Shear $\phi_v := 0.9$

For Flexure $\phi_f := 1.0$

For Axial $\phi_c := 0.75$

PCI Phase II Report, Version 2.0 (2022)

MOE Correction Factor $K_1 := 1.013$

Modulus of Elasticity $E_c := 2500 \text{ ksi} \cdot K_1 \cdot \left(\frac{f'_c}{\text{ksi}}\right)^{0.33} = 6500.3 \text{ ksi}$

Effective Tensile Strength of UHPC $f_t := 1 \text{ ksi}$

UHPC Area in Flexural Tension Side $A_{ct} := \frac{A_g}{2} = 492 \text{ in}^2$

Longitudinal Strain $\varepsilon_s := \min\left(\frac{\left|\frac{M_u}{d_v}\right| + 0.5 N_u + |V_u - V_p| - A_{ps} \cdot f_{po}}{E_p \cdot A_{ps} + E_s \cdot A_s}, 0.006\right)$

$\varepsilon_s := \text{if}\left(\varepsilon_s < 0, \max\left(\frac{\left|\frac{M_u}{d_v}\right| + 0.5 N_u + |V_u - V_p| - A_{ps} \cdot f_{po}}{E_p \cdot A_{ps} + E_s \cdot A_s + E_c \cdot A_{ct}}, -0.0004\right), \varepsilon_s\right) \quad \varepsilon_s = 3.91 \cdot 10^{-4}$

Crack Angle $\theta := (29 + 3500 \cdot \varepsilon_s) \cdot \text{deg} \quad \theta = 30.4 \text{ deg}$

UHPC Shear Resistance $V_{cf} := f_t \cdot b_v \cdot d_v \cdot \cot(\theta) \quad V_{cf} = 351.573 \text{ kip}$

Transverse Steel Contribution $V_s := \frac{A_v \cdot f_y \cdot d_v \cdot (\cot(\theta) + \cot(\alpha)) \cdot \sin(\alpha)}{s} \quad V_s = 0 \text{ kip}$

Predicted Shear Strength $V_n := V_{cf} + V_s + V_p \quad V_n = 351.6 \text{ kip}$

Maximum Shear Resistance $V_{nmax} := 0.25 f'_c \cdot b_v \cdot d_v + V_p \quad V_{nmax} = 896.1 \text{ kip}$

Measured-to-Predicted Ratio $\frac{V_u}{V_n} = 0.9$

Longitudinal Reinforcement Check $f_{ps} := f_{pu}$

$check := \text{if}\left((A_{ps} \cdot f_{ps} + A_s \cdot f_y) \geq \left(\frac{|M_u|}{d_v \cdot \phi_f} + 0.5 \frac{N_u}{\phi_c} \downarrow + \left(\left|\frac{V_u}{\phi_v} - V_p\right| - 0.5 V_s\right) \cdot \cot(\theta)\right), \text{"OK"}, \text{"NG"}\right) = \text{"NG"}$

AASHTO Guide Specification for Structural Design with UHPC, Version 1.2 (2022)

Tensile Strength at Crack Localization	$f_{t.loc} := 1 \text{ ksi}$
Cracking Tensile Strength	$f_{t.cr} := 1 \text{ ksi}$
Tensile Strength Reduction Factor	$\gamma_u := 0.85$ $\gamma_u \cdot f_{t.loc} = 0.85 \text{ ksi}$
Tensile Strain at Crack Localization	$\epsilon_{t.loc} := 0.005$
Cracking Tensile Strain	$\epsilon_{t.cr} := \frac{\gamma_u \cdot f_{t.cr}}{E_c} = 1.308 \cdot 10^{-4}$

Longitudinal Strain

$$\epsilon_s := \min \left(\frac{\left| \frac{M_u}{d_v} \right| + 0.5 N_u + |V_u - V_p| - A_{ps} \cdot f_{po} - \gamma_u \cdot f_{t.cr} \cdot A_{ct}}{E_s \cdot A_s + E_p \cdot A_{ps}}, \epsilon_{t.loc} \right)$$

$$\epsilon_s := \text{if} \left(\epsilon_s < \epsilon_{t.cr}, \frac{\left| \frac{M_u}{d_v} \right| + 0.5 N_u + |V_u - V_p| - A_{ps} \cdot f_{po}}{E_p \cdot A_{ps} + E_s \cdot A_s + E_c \cdot A_{ct}}, \epsilon_s \right) \quad \epsilon_s = 1.193 \cdot 10^{-5}$$

Guess Values	$\theta := 32 \text{ deg}$ $\epsilon_v := 0.002$
Constraints	$\epsilon_{t.loc} = \frac{\epsilon_s}{2} \cdot \left(1 + (\cot(\theta))^2 \right) + \frac{2 \cdot f_{t.loc}}{E_c} \cdot (\cot(\theta))^4 \downarrow$ $+ \frac{2 \cdot \rho_v \cdot \min(E_s \cdot \epsilon_v, f_y)}{E_c} \cdot \sin(\alpha) \cdot (\cot(\theta))^2 \cdot \left(1 + (\cot(\theta))^2 + \cot(\alpha) \cdot (\tan(\theta) + \cot(\theta)) \right)$ $\epsilon_v - \epsilon_{t.loc} + 0.5 \cdot \epsilon_s = \frac{-2 \cdot f_{t.loc}}{E_c} \cdot (\cot(\theta))^2 \downarrow$ $- \frac{2 \cdot \rho_v \cdot \min(E_s \cdot \epsilon_v, f_y)}{E_c} \cdot \sin(\alpha) \cdot \left(1 + (\cot(\theta))^2 + \cot(\alpha) \cdot (\tan(\theta) + \cot(\theta)) \right)$
Solver	$Solution := \text{find}(\epsilon_v, \theta) = \begin{bmatrix} 0.004 \\ 0.463 \end{bmatrix}$

$$\theta := Solution_1 = 26.5 \text{ deg} \quad \epsilon_v := Solution_0 = 0.0038$$

Stress Limit in Transverse Reinforcement $f_v := \min(E_s \cdot \epsilon_v, f_y) = 60 \text{ ksi}$

UHPC Shear Strength $V_{UHPC} := \gamma_u \cdot f_{t.loc} \cdot b_v \cdot d_v \cdot \cot(\theta)$ $V_{UHPC} = 351 \text{ kip}$

Transverse Steel Contribution	$V_s := \frac{A_v \cdot f_v \cdot d_v \cdot (\cot(\theta) + \cot(\alpha)) \cdot \sin(\alpha)}{s}$	$V_s = 0 \text{ kip}$
Predicted Shear Resistance	$V_n := V_{UHPC} + V_s + V_p$	$V_n = 351 \text{ kip}$
Maximum Shear Resistance	$V_{nmax} := 0.25 f_c' \cdot b_v \cdot d_v + V_p$	$V_{nmax} = 896.1 \text{ kip}$
Measured-to-Predicted Ratio	$\frac{V_u}{V_n} = 0.9$	

Longitudinal Reinforcement Check

$$check := \text{if} \left(\left(\begin{array}{l} A_{ps} \cdot f_{ps} + A_s \cdot E_s \cdot \varepsilon_{t.loc} \uparrow \\ + A_{ct} \cdot \gamma_u \cdot f_{t.cr} \end{array} \right) \geq \left(\begin{array}{l} \frac{|M_u|}{d_v \cdot \phi_f} + 0.5 \frac{N_u}{\phi_c} \uparrow \\ + \left(\left| \frac{V_u}{\phi_v} - V_p \right| - 0.5 V_s \right) \cdot \cot(\theta) \end{array} \right), \text{"OK"}, \text{"NG"} \right) = \text{"OK"}$$

Solid Slab Transverse Load Prediction

Wheel Load	$P := 16 \text{ kip}$
Dynamic Load Allowance	$IM := 1.33$
Service Load	$P_a := IM \cdot P = 21.28 \text{ kip}$
Factored Load (Demand)	$P_u := 1.75 \cdot P_a = 37.24 \text{ kip}$
Distance Between Load and Support	$X := \frac{108.5 \text{ in} - 22 \text{ in}}{2} - 8.5 \text{ in} = 34.75 \text{ in}$
Width of Overhang Strip	$W := 45 \text{ in} + \frac{10}{12} X = 6.16 \text{ ft}$
Capacity of One Foot	$M_{n1} := 24.5 \text{ kip} \cdot \text{ft}$
Moment Capacity of Strip	$M_n := M_{n1} \cdot \frac{W}{12 \text{ in}} = 151 \text{ kip} \cdot \text{ft}$
Theoretical Load	$P_n := \frac{M_n}{X} = 52.14 \text{ kip}$
Test Load	$P_{test} := 120 \text{ kip}$
Measured-to-Predicted Ratio	$\frac{P_{test}}{P_n} = 2.3$
Measured-to-Demand Ratio	$\frac{P_{test}}{P_u} = 3.22$

Ribbed Slab Transverse Load Prediction

Wheel Load	$P := 16 \text{ kip}$
Dynamic Load Allowance	$IM := 1.33$
Service Load	$P_a := IM \cdot P = 21.28 \text{ kip}$
Factored Load (Demand)	$P_u := 1.75 \cdot P_a = 37.24 \text{ kip}$
Distance Between Load and Support	$X := \frac{108.5 \text{ in} - 24 \text{ in}}{2} - 8.5 \text{ in} = 33.75 \text{ in}$
Width of Overhang Strip	$W := 45 \text{ in} + \frac{10}{12} X = 6.09 \text{ ft}$
Spacing Between Ribs	$S := 25.75 \text{ in}$
No. of Ribs in the Strip	$n := \frac{W}{S} = 2.84$
Capacity of One Rib	$M_{n1} := 44.8 \text{ kip} \cdot \text{ft}$
Moment Capacity of Strip	$M_n := M_{n1} \cdot n = 127.2 \text{ kip} \cdot \text{ft}$
Theoretical Load	$P_n := \frac{M_n}{X} = 45.23 \text{ kip}$
Test Load	$P_{test} := 78 \text{ kip}$
Measured-to-Predicted Ratio	$\frac{P_{test}}{P_n} = 1.72$
Measured-to-Demand Ratio	$\frac{P_{test}}{P_u} = 2.09$

Post-Tensioning Calculations for UHPC DIB Specimen

Specimen Length	$L := 19.35 \text{ ft}$	
Section Area	$A := 1236 \text{ in}^2$	
Section Weight	$w := A \cdot 155 \text{ pcf} = 1.33 \text{ klf}$	
Mid-Section Moment	$M_g := \frac{w \cdot L^2}{8} = 62.267 \text{ kip} \cdot \text{ft}$	
Section C.G. from Bottom	$y_b := 34.09 \text{ in}$	
Section Inertia	$I := 469424 \text{ in}^4$	
UHPC MOE	$E_c := 6500 \text{ ksi}$	
Strand C.G. from Bottom	$cg := 7.5 \text{ in}$	Due to duct moving upward while casting
Strand Eccentricity	$e := y_b - cg = 26.59 \text{ in}$	
Jacking Stress	$f_{pi} := 0.75 \cdot 270 \text{ ksi} = 202.5 \text{ ksi}$	
Strand MOE	$E_p := 28500 \text{ ksi}$	
Area of Strands	$A_{ps} := 19 \cdot 0.217 \text{ in}^2 = 4.123 \text{ in}^2$	
Jacking Prestress Force	$P := A_{ps} \cdot f_{pi} = 834.9 \text{ kip}$	
Total Instantaneous Losses	$TL := 18.5\%$	
Effective Pre-stressing	$f_{pe} := (1 - TL) \cdot f_{pi} = 165.038 \text{ ksi}$	
Effective Prestress Force	$P_e := (1 - TL) \cdot P = 680.4 \text{ kip}$	
Effective Strain	$\epsilon_{pi} := \frac{f_{pe}}{E_p} = 0.006$	
Expected Strand Elongation	$\delta := \epsilon_{pi} \cdot L = 1.34 \text{ in}$	
Anchorage Set Loss	$AS := \frac{0.25 \text{ in}}{L} \cdot E_p = 30.685 \text{ ksi}$	$\frac{AS}{f_{pi}} = 15.2\%$
Elastic Shortening Loss	$ES := \left(\frac{P_e}{A} + \frac{P_e \cdot e^2}{I} - \frac{M_g \cdot e}{I} \right) \cdot \frac{E_p}{E_c} = 6.72 \text{ ksi}$	$\frac{ES}{f_{pi}} = 3.3\%$

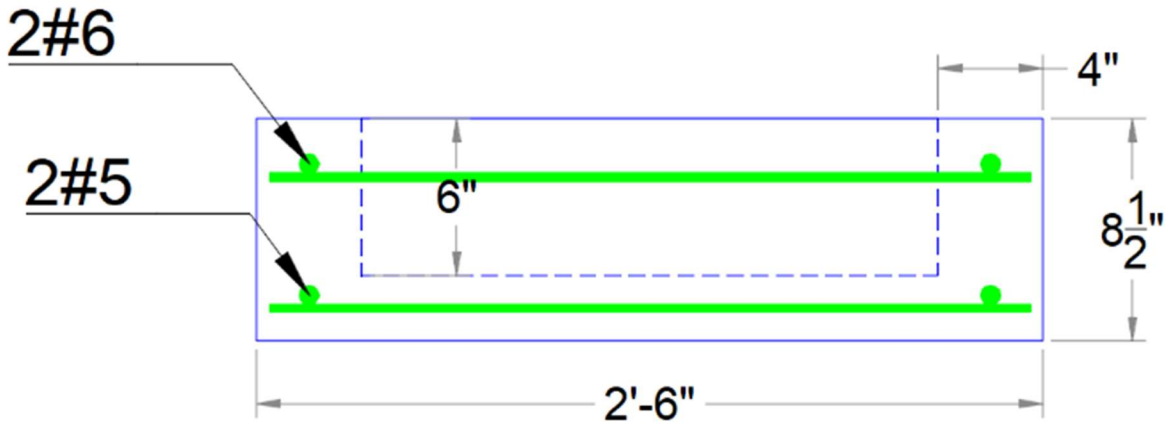
Stress at DEMEC Location

$$f_b := \frac{P_e}{A} + \frac{P_e \cdot e \cdot (y_b - 2.5 \text{ in})}{I} - \frac{M_g \cdot (y_b - 2.5 \text{ in})}{I} = 1.72 \text{ ksi}$$

Strain at DEMEC Location

$$\varepsilon_c := \frac{f_b}{E_c} = 0.00026$$

Flexure Strength of Prestressed/Reinforced UHPC Ribbed Slab Specimen
(Negative Moment) According to PCI & FHWA Methods



Maximum Load $P_{test} := 80.23 \text{ kip}$

Beam Span $L := 43 \text{ in}$

Width of Loading Pad $a := 8.25 \text{ in}$

Test Moment $M_{test} := \frac{P_{test}}{4} (L - a) = 58.1 \text{ kip} \cdot \text{ft}$

Nominal Capacity $M_n := 54.3 \text{ kip} \cdot \text{ft}$ $\frac{M_{test}}{M_n} = 1.07$

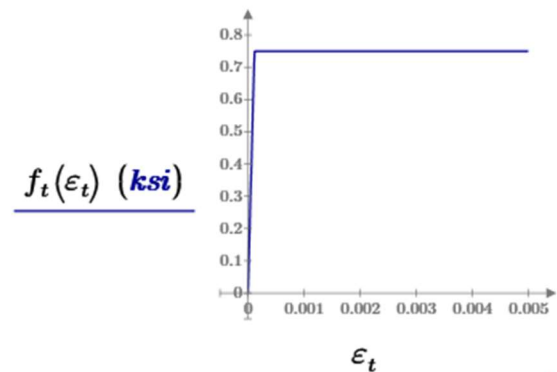
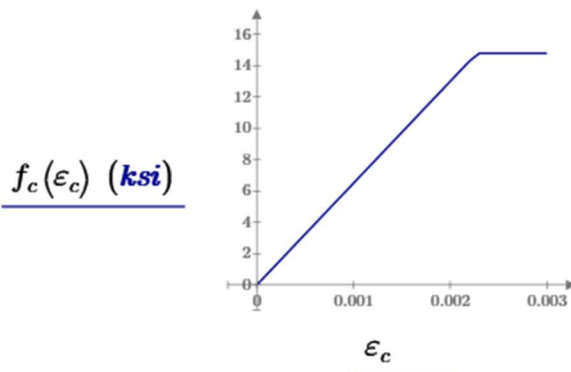
Demand $M_u := 4.41 \frac{\text{kip} \cdot \text{ft}}{\text{ft}} \cdot 1.75 \cdot 4 \text{ ft} = 30.87 \text{ kip} \cdot \text{ft}$ $\frac{M_{test}}{M_u} = 1.882$

UHPC Compression Model

Design Compressive Strength	$f'_c := 17.4 \text{ ksi}$
Correction Factor for MOE	$K_1 := 1.013$
Modulus of Elasticity	$E_c := 2500 \text{ ksi } K_1 \cdot \left(\frac{f'_c}{\text{ksi}}\right)^{0.33} = 6500 \text{ ksi}$
Reduction Factor for Compression	$\alpha := 0.85$
Elastic Compressive Strain	$\varepsilon_{cp} := \frac{\alpha \cdot f'_c}{E_c} = 0.0023$
Ultimate Compressive Strain	$\varepsilon_{cu} := 0.003$
Compressive Stress-Strain Relationship	$f_c(\varepsilon_c) := \text{if}(0 \leq \varepsilon_c < \varepsilon_{cp}, \varepsilon_c \cdot E_c, \text{if}(\varepsilon_{cp} \leq \varepsilon_c \leq \varepsilon_{cu}, \alpha \cdot f'_c, 0 \text{ ksi}))$

UHPC Tension Model

Effective Cracking Strength	$f_{t.cr} := 0.882 \text{ ksi}$
Crack Localization Stress	$f_{t.loc} := 0.882 \text{ ksi}$
Reduction Factor for Tension	$\gamma := 0.85$ $\gamma \cdot f_{t.loc} = 0.75 \text{ ksi}$
Elastic Tensile Strain	$\varepsilon_{t.cr} := \frac{\gamma \cdot f_{t.cr}}{E_c} = 0.000115$
Crack Localization Strain	$\varepsilon_{t.loc} := 0.005$
Tensile Stress-Strain Relationship	$f_t(\varepsilon_t) := \text{if}\left(0 \leq \varepsilon_t \leq \varepsilon_{t.cr}, \varepsilon_t \cdot E_c, \text{if}\left(\varepsilon_{t.cr} < \varepsilon_t \leq \varepsilon_{t.loc}, \gamma \cdot f_{t.cr} + (\varepsilon_t - \varepsilon_{t.cr}) \cdot \frac{\gamma \cdot (f_{t.loc} - f_{t.cr})}{(\varepsilon_{t.loc} - \varepsilon_{t.cr})}, 0 \text{ ksi}\right)\right)$
	$\varepsilon_c := 0, 0.0001 \dots \varepsilon_{cu}$ $\varepsilon_t := 0, 0.00001 \dots \varepsilon_{t.loc}$



Section Geometry

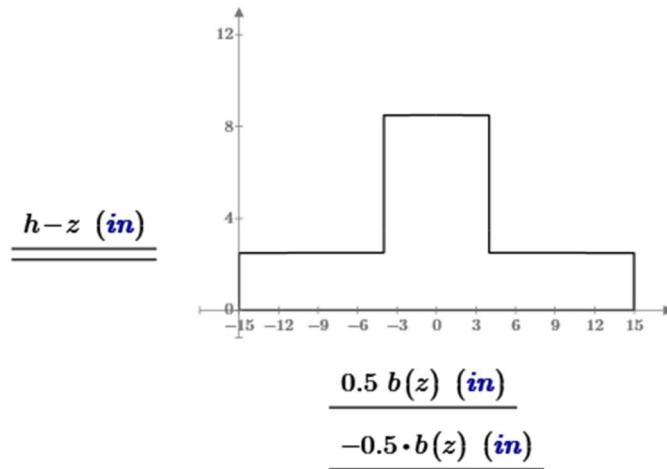
Section Height

$$h := 8.5 \text{ in}$$

Section Width
(z from compression side)

$$b(z) := \begin{cases} \text{if } 0 < z \leq 6 \text{ in} \\ \quad \parallel 8 \text{ in} \\ \text{else if } 6 \text{ in} < z \leq h \\ \quad \parallel 30 \text{ in} \\ \text{else} \\ \quad \parallel 0 \text{ in} \end{cases}$$

$$z := 0, 0.01 \text{ in} \dots h + 0.01 \text{ in}$$



Section Area

$$A_g := \int_{0 \text{ in}}^h b(z) dz = 123 \text{ in}^2$$

Section C.G. from
Compression Side

$$y_t := \frac{\int_{0 \text{ in}}^h b(z) \cdot z dz}{A_g} = 5.59 \text{ in}$$

Section C.G. from
Tension Side

$$y_b := h - y_t = 2.908 \text{ in}$$

Section Inertia

$$I_g := \int_{0 \text{ in}}^h b(z) \cdot (y_t - z)^2 dz = 712.3 \text{ in}^4$$

Non-Pre-stressing Reinforcement

Steel MOE	$E_s := 29000 \text{ ksi}$											
Steel Yield Strength	$f_y := 60 \text{ ksi}$											
Strain at Service Stress Limit	$\epsilon_{sl} := \frac{0.8 f_y}{E_s} = 0.00166$											
Rupture Strain of Steel	$\epsilon_{su} := 9\%$											
Stress of Non-prestressing steel	$f_s(\epsilon_s) := \text{if}(\epsilon_s \geq 0, \min(\epsilon_s \cdot E_s, f_y), \max(\epsilon_s \cdot E_s, -f_y))$											
Steel Layers (at least 2) (d from compression side)	<table style="margin-left: 40px;"> <tr> <td>A_s</td> <td>d</td> <td></td> </tr> <tr> <td>(in^2)</td> <td>(in)</td> <td></td> </tr> <tr> <td>$2 \cdot 0.44$</td> <td>1.75</td> <td rowspan="2">$\sum A_s = 1.5 \text{ in}^2$</td> </tr> <tr> <td>$2 \cdot 0.31$</td> <td>$6.75$</td> </tr> </table>	A_s	d		(in^2)	(in)		$2 \cdot 0.44$	1.75	$\sum A_s = 1.5 \text{ in}^2$	$2 \cdot 0.31$	6.75
A_s	d											
(in^2)	(in)											
$2 \cdot 0.44$	1.75	$\sum A_s = 1.5 \text{ in}^2$										
$2 \cdot 0.31$	6.75											

Pre-stressing Reinforcement

Ultimate Strength of Strands	$f_{pu} := 270 \text{ ksi}$
Rupture Strain of Strands	$\epsilon_{pu} := 3.5\%$
Strand MOE	$E_p := 28500 \text{ ksi}$
Yield Strength of Strands	$f_{py} := 0.9 \cdot f_{pu} = 243 \text{ ksi}$
Power Formula Factors	$Q := 0.031$ $K := 1.043$ $R := 7.36$
Stress of Low-Relaxation Pre-stressing Steel	$f_p(\epsilon_p) := \min \left(f_{pu}, E_p \cdot \epsilon_p \cdot \left(Q + \frac{1-Q}{\left(1 + \left(\frac{E_p \cdot \epsilon_p }{K \cdot f_{py}} \right)^R \right)^{\frac{1}{R}}} \right) \right)$
Estimated Total Losses	$TL := 18\%$
Effective Pre-stressing	$f_{se} := 75\% \cdot (1 - TL) \cdot f_{pu} = 166.05 \text{ ksi}$
Effective Strain of Strands	$\epsilon_{se} := \frac{f_{se}}{E_p} = 0.00583$
Strain at Service Stress Limit	$\epsilon_{pl} := \text{root}(f_p(\epsilon_p) - 0.8 f_{py}, \epsilon_p, 0, \epsilon_{pu}) = 0.00696$

Strand Diameter

$$d_b := 0.6 \text{ in}$$

One Strand Area

$$A_{s1} := \begin{cases} \text{if } d_b = 0.375 \text{ in} \\ \quad \parallel 0.085 \text{ in}^2 \\ \text{else if } d_b = 0.5 \text{ in} \\ \quad \parallel 0.153 \text{ in}^2 \\ \text{else if } d_b = 0.6 \text{ in} \\ \quad \parallel 0.217 \text{ in}^2 \\ \text{else if } d_b = 0.7 \text{ in} \\ \quad \parallel 0.294 \text{ in}^2 \\ \text{else} \\ \quad \parallel 0 \text{ in}^2 \end{cases} = 0.217 \text{ in}^2$$

Strand Layers (at least 2)
(d from compression side)

$$\begin{array}{cc} n_{ps} & d_p \\ & (\text{in}) \\ \hline 0 & 1.75 \\ 0 & 6.75 \end{array} \quad \sum n_{ps} = 0$$

Area of Prestressing Steel

$$A_{ps} := A_{s1} \cdot n_{ps} = \begin{bmatrix} 0 \\ 0 \end{bmatrix} \text{ in}^2 \quad \sum A_{ps} = 0 \text{ in}^2$$

Depth of most tension Steel

$$d_t := \max(d_p, d) = 6.75 \text{ in}$$

Resistance Factor

Comp-Control Strain Limit

$$\varepsilon_{cl} := 0.002$$

Tension-Control Strain Limit

$$\varepsilon_{ul} := 0.005$$

Lower Limit of Phi Factor

$$\phi_l := 0.75$$

Upper Limit of Phi Factor

$$\phi_u := 0.9 \quad \text{Use 1.0 for Prestressed and 0.9 otherwise}$$

Resistance Reduction Factor

$$\phi(\varepsilon_t) := \min\left(\phi_u, \max\left(\phi_l, \phi_l + (\phi_u - \phi_l) \cdot \frac{\varepsilon_t - \varepsilon_{cl}}{\varepsilon_{ul} - \varepsilon_{cl}}\right)\right)$$

Ductility Ratio Limit

$$\mu_l := 3.0$$

Cracking Point

Curvature

$$\psi(c) := \frac{\varepsilon_{t.cr}}{h-c}$$

UHPC Compression Force

$$C_c(c) := \int_{0 \text{ in}}^c b(c-y) \cdot f_c(\psi(c) \cdot y) dy$$

Compression Force C.G. from N.A.

$$Z(c) := \frac{1}{C_c(c)} \cdot \int_{0 \text{ in}}^c b(c-y) \cdot f_c(\psi(c) \cdot y) \cdot y dy$$

UHPC Tension Force

$$T_c(c) := \int_{0 \text{ in}}^{h-c} b(c+x) \cdot f_t(\psi(c) \cdot x) dx$$

Tension Force C.G. from N.A.

$$X(c) := \frac{1}{T_c(c)} \cdot \int_{0 \text{ in}}^{h-c} b(c+x) \cdot f_t(\psi(c) \cdot x) \cdot x dx$$

Strain in Non-Pre-stressing Steel

$$\varepsilon_s(c) := (d-c) \cdot \psi(c)$$

Stress in Non-Pre-stressing Steel

$$f_{ss}(c) := \left\| \begin{array}{l} \text{for } i \in 0 \dots \text{last}(d) \\ \left\| \begin{array}{l} R_i \leftarrow \text{if } d_i > c \\ \left\| \begin{array}{l} f_s(\varepsilon_s(c)_i) - f_t(\varepsilon_s(c)_i) \\ \text{else} \\ f_s(\varepsilon_s(c)_i) + f_c(\varepsilon_s(c)_i) \end{array} \right\| \end{array} \right\| \\ R \end{array} \right\|$$

Force in Non-Pre-stressing Steel

$$T_s(c) := \overrightarrow{A_s \cdot f_{ss}(c)}$$

Strain in Pre-stressing Strands

$$\varepsilon_{ps}(c) := \psi(c) \cdot (d_p - c) + \varepsilon_{se}$$

Stress in Pre-stressing Strands

$$f_{ps}(c) := \left\| \begin{array}{l} \text{for } i \in 0 \dots \text{last}(d_p) \\ \left\| \begin{array}{l} R_i \leftarrow \text{if } d_{p_i} > c \\ \left\| \begin{array}{l} f_p(\varepsilon_{ps}(c)_i) - f_t(\varepsilon_{ps}(c)_i - \varepsilon_{se}) \\ \text{else} \\ f_p(\varepsilon_{ps}(c)_i) + f_c(\varepsilon_{ps}(c)_i - \varepsilon_{se}) \end{array} \right\| \end{array} \right\| \\ R \end{array} \right\|$$

Force in Pre-stressing Strands

$$T_{ps}(c) := \overrightarrow{A_{ps} \cdot f_{ps}(c)}$$

Initial Guess of c

$$c := \frac{h}{2}$$

Neutral Axis Location

$$c_e := \text{root} \left(T_c(c) + \sum T_s(c) + \sum T_{ps}(c) - C_c(c), c \right) = 5.494 \text{ in}$$

Nominal Flexural Strength

$$M_n(c) := C_c(c) \cdot Z(c) + T_c(c) \cdot X(c) + T_{ps}(c) \cdot (d_p - c) + T_s(c) \cdot (d - c)$$

$$\varepsilon_t := \psi(c_e) \cdot (d_t - c_e) = 0$$

$$\varepsilon_c := \psi(c_e) \cdot c_e = 0.0002$$

$$\Phi_1 := \phi(\varepsilon_t) = 0.75$$

$$\Psi_1 := \psi(c_e) = 0.00004 \frac{1}{\text{in}}$$

$$M_1 := M_n(c_e) = 16 \text{ kip} \cdot \text{ft}$$

$$\Phi_{\mu_1} := 0.75$$

Service Stress Point

Curvature

$$\psi(c) := \frac{\varepsilon_{sl}}{d_t - c}$$

Use $\varepsilon_{pl} - \varepsilon_{se}$ for prestressed, ε_{sl} otherwise

UHPC Compression Force

$$C_c(c) := \int_{0 \text{ in}}^c b(c-y) \cdot f_c(\psi(c) \cdot y) dy$$

Compression Force C.G. from N.A.

$$Z(c) := \frac{1}{C_c(c)} \cdot \int_{0 \text{ in}}^c b(c-y) \cdot f_c(\psi(c) \cdot y) \cdot y dy$$

UHPC Tension Force

$$T_c(c) := \int_{0 \text{ in}}^{h-c} b(c+x) \cdot f_t(\psi(c) \cdot x) dx$$

Tension Force C.G. from N.A.

$$X(c) := \frac{1}{T_c(c)} \cdot \int_{0 \text{ in}}^{h-c} b(c+x) \cdot f_t(\psi(c) \cdot x) \cdot x dx$$

Strain in Non-Pre-stressing Steel

$$\varepsilon_s(c) := (d - c) \cdot \psi(c)$$

Stress in Non-Pre-stressing Steel

$$f_{ss}(c) := \left\| \begin{array}{l} \text{for } i \in 0 \dots \text{last}(d) \\ \left\| \begin{array}{l} R_i \leftarrow \text{if } d_i > c \\ \left\| \begin{array}{l} f_s(\varepsilon_s(c)_i) - f_t(\varepsilon_s(c)_i) \\ \text{else} \\ f_s(\varepsilon_s(c)_i) + f_c(\varepsilon_s(c)_i) \end{array} \right\| \end{array} \right\| \\ R \end{array} \right\|$$

Force in Non-Pre-stressing Steel

$$T_s(c) := \overline{A_s \cdot f_{ss}(c)}$$

Strain in Pre-stressing Strands

$$\varepsilon_{ps}(c) := \psi(c) \cdot (d_p - c) + \varepsilon_{se}$$

Stress in Pre-stressing Strands

$$f_{ps}(c) := \begin{cases} \text{for } i \in 0 \dots \text{last}(d_p) \\ \left\| \begin{array}{l} R_i \leftarrow \text{if } d_{p_i} > c \\ \left\| \begin{array}{l} f_p(\varepsilon_{ps}(c)_i) - f_t(\varepsilon_{ps}(c)_i - \varepsilon_{se}) \\ \text{else} \\ f_p(\varepsilon_{ps}(c)_i) + f_c(\varepsilon_{ps}(c)_i - \varepsilon_{se}) \end{array} \right\| \\ R \end{array} \right\| \end{cases}$$

Force in Pre-stressing Strands

$$T_{ps}(c) := \overrightarrow{A_{ps} \cdot f_{ps}(c)}$$

Initial Guess of c

$$c := \frac{h}{4}$$

Neutral Axis Location

$$c_e := \text{root}\left(T_c(c) + \sum T_s(c) + \sum T_{ps}(c) - C_c(c), c\right) = 2.869 \text{ in}$$

Nominal Flexural Strength

$$M_n(c) := C_c(c) \cdot Z(c) + T_c(c) \cdot X(c) + T_{ps}(c) \cdot (d_p - c) + T_s(c) \cdot (d - c)$$

$$\varepsilon_t := \psi(c_e) \cdot (d_t - c_e) = 0.0017$$

$$\varepsilon_c := \psi(c_e) \cdot c_e = 0.0012$$

$$\Phi_2 := \phi(\varepsilon_t) = 0.75$$

$$\Psi_2 := \psi(c_e) = 0.00043 \frac{1}{\text{in}}$$

$$M_2 := M_n(c_e) = 48.1 \text{ kip} \cdot \text{ft}$$

$$\Phi_{\mu_2} := 0.75$$

1st Peak Point (Crack Localization)

Curvature

$$\psi(c) := \frac{\varepsilon_{t,loc}}{h - c}$$

UHPC Compression Force

$$C_c(c) := \int_{0 \text{ in}}^c b(c - y) \cdot f_c(\psi(c) \cdot y) \, dy$$

Compression Force C.G. from N.A.

$$Z(c) := \frac{1}{C_c(c)} \cdot \int_{0 \text{ in}}^c b(c - y) \cdot f_c(\psi(c) \cdot y) \cdot y \, dy$$

UHPC Tension Force

$$T_c(c) := \int_{0 \text{ in}}^{h-c} b(c + x) \cdot f_t(\psi(c) \cdot x) \, dx$$

Tension Force C.G. from N.A.

$$X(c) := \frac{1}{T_c(c)} \cdot \int_{0 \text{ in}}^{h-c} b(c + x) \cdot f_t(\psi(c) \cdot x) \cdot x \, dx$$

Strain in Non-Pre-stressing Steel

$$\varepsilon_s(c) := (d - c) \cdot \psi(c)$$

Stress in Non-Pre-stressing Steel

$$f_{ss}(c) := \begin{array}{l} \text{for } i \in 0 \dots \text{last}(d) \\ \quad R_i \leftarrow \text{if } d_i > c \\ \quad \quad \left\| \begin{array}{l} f_s(\varepsilon_s(c)_i) - f_t(\varepsilon_s(c)_i) \\ \text{else} \\ f_s(\varepsilon_s(c)_i) + f_c(\varepsilon_s(c)_i) \end{array} \right\| \\ R \end{array}$$

Force in Non-Pre-stressing Steel

$$T_s(c) := \overline{A_s \cdot f_{ss}(c)}$$

Strain in Pre-stressing Strands

$$\varepsilon_{ps}(c) := \psi(c) \cdot (d_p - c) + \varepsilon_{se}$$

Stress in Pre-stressing Strands

$$f_{ps}(c) := \begin{array}{l} \text{for } i \in 0 \dots \text{last}(d_p) \\ \quad R_i \leftarrow \text{if } d_{p_i} > c \\ \quad \quad \left\| \begin{array}{l} f_p(\varepsilon_{ps}(c)_i) - f_t(\varepsilon_{ps}(c)_i - \varepsilon_{se}) \\ \text{else} \\ f_p(\varepsilon_{ps}(c)_i) + f_c(\varepsilon_{ps}(c)_i - \varepsilon_{se}) \end{array} \right\| \\ R \end{array}$$

Force in Pre-stressing Strands

$$T_{ps}(c) := \overline{A_{ps} \cdot f_{ps}(c)}$$

Initial Guess of c

$$c := \frac{h}{8}$$

Neutral Axis Location

$$c_e := \text{root}\left(T_c(c) + \sum T_s(c) + \sum T_{ps}(c) - C_c(c), c\right) = 2.246 \text{ in}$$

Nominal Flexural Strength

$$M_n(c) := C_c(c) \cdot Z(c) + T_c(c) \cdot X(c) + T_{ps}(c) \cdot (d_p - c) + T_s(c) \cdot (d - c)$$

$$\varepsilon_t := \psi(c_e) \cdot (d_t - c_e) = 0.004$$

$$\varepsilon_c := \psi(c_e) \cdot c_e = 0.0018$$

$$\Phi_3 := \phi(\varepsilon_t) = 0.83$$

$$\Psi_3 := \psi(c_e) = 0.0008 \frac{1}{\text{in}}$$

$$M_3 := M_n(c_e) = 54.3 \text{ kip} \cdot \text{ft}$$

Curvature Ductility Ratio

$$\mu := \frac{\Psi_3}{\Psi_2} = 1.875$$

Curvature Ductility
Resistance Factor

$$\Phi_{\mu_3} := \text{if}\left(\mu < 1, 0.75, \text{if}\left(\mu > \mu_l, 0.9, 0.75 + 0.15 \cdot \frac{(\mu - 1)}{(\mu_l - 1)}\right)\right) = 0.816$$

2nd Peak Point (Ultimate)

Curvature $\psi(c) := \min\left(\frac{\epsilon_{su}}{d_t - c}, \frac{\epsilon_{cu}}{c}\right)$ Use $\epsilon_{pu} - \epsilon_{se}$ for prestressed, ϵ_{su} otherwise

UHPC Compression Force $C_c(c) := \int_{0 \text{ in}}^c b(c-y) \cdot f_c(\psi(c) \cdot y) dy$

Compression Force C.G. from N.A. $Z(c) := \frac{1}{C_c(c)} \cdot \int_{0 \text{ in}}^c b(c-y) \cdot f_c(\psi(c) \cdot y) \cdot y dy$

UHPC Tension Force $T_c(c) := \int_{0 \text{ in}}^{h-c} b(c+x) \cdot f_t(\psi(c) \cdot x) dx$

Tension Force C.G. from N.A. $X(c) := \frac{1}{T_c(c)} \cdot \int_{0 \text{ in}}^{h-c} b(c+x) \cdot f_t(\psi(c) \cdot x) \cdot x dx$

Strain in Non-Pre-stressing Steel $\epsilon_s(c) := (d-c) \cdot \psi(c)$

Stress in Non-Pre-stressing Steel $f_{ss}(c) := \left\| \begin{array}{l} \text{for } i \in 0 \dots \text{last}(d) \\ \left\| \begin{array}{l} R_i \leftarrow \text{if } d_i > c \\ \left\| \begin{array}{l} f_s(\epsilon_s(c)_i) - f_t(\epsilon_s(c)_i) \\ \text{else} \\ f_s(\epsilon_s(c)_i) + f_c(\epsilon_s(c)_i) \end{array} \right\| \end{array} \right\| \\ R \end{array} \right\|$

Force in Non-Pre-stressing Steel $T_s(c) := \overrightarrow{A_s \cdot f_{ss}(c)}$

Strain in Pre-stressing Strands $\epsilon_{ps}(c) := \psi(c) \cdot (d_p - c) + \epsilon_{se}$

Stress in Pre-stressing Strands $f_{ps}(c) := \left\| \begin{array}{l} \text{for } i \in 0 \dots \text{last}(d_p) \\ \left\| \begin{array}{l} R_i \leftarrow \text{if } d_{p_i} > c \\ \left\| \begin{array}{l} f_p(\epsilon_{ps}(c)_i) - f_t(\epsilon_{ps}(c)_i - \epsilon_{se}) \\ \text{else} \\ f_p(\epsilon_{ps}(c)_i) + f_c(\epsilon_{ps}(c)_i - \epsilon_{se}) \end{array} \right\| \end{array} \right\| \\ R \end{array} \right\|$

Force in Pre-stressing Strands $T_{ps}(c) := \overrightarrow{A_{ps} \cdot f_{ps}(c)}$

Initial Guess of c

$$c := \frac{h}{16}$$

Neutral Axis Location

$$c_e := \text{root} \left(T_c(c) + \sum T_s(c) + \sum T_{ps}(c) - C_c(c), c \right) = 1.171 \text{ in}$$

Nominal Flexural Strength

$$M_n(c) := C_c(c) \cdot Z(c) + T_c(c) \cdot X(c) + T_{ps}(c) \cdot (d_p - c) + T_s(c) \cdot (d - c)$$

$$\varepsilon_t := \psi(c_e) \cdot (d_t - c_e) = 0.014$$

$$\varepsilon_c := \psi(c_e) \cdot c_e = 0.003$$

$$\Phi_4 := \phi(\varepsilon_t) = 0.9$$

$$\Psi_4 := \psi(c_e) = 0.00256 \frac{1}{\text{in}}$$

$$M_4 := M_n(c_e) = 25.5 \text{ kip}\cdot\text{ft}$$

Curvature Ductility Ratio

$$\mu := \frac{\Psi_4}{\Psi_2} = 6.008$$

Curvature Ductility Resistance Factor

$$\Phi_{\mu_4} := \text{if} \left(\mu < 1, 0.75, \text{if} \left(\mu > \mu_l, 0.9, 0.75 + 0.15 \cdot \frac{(\mu - 1)}{(\mu_l - 1)} \right) \right) = 0.9$$

PCI Design Flexural Strength

$$M_r := \max(\Phi_3 \cdot M_3, \Phi_4 \cdot M_4) = 45 \text{ kip}\cdot\text{ft}$$

FHWA Design Flexural Strength

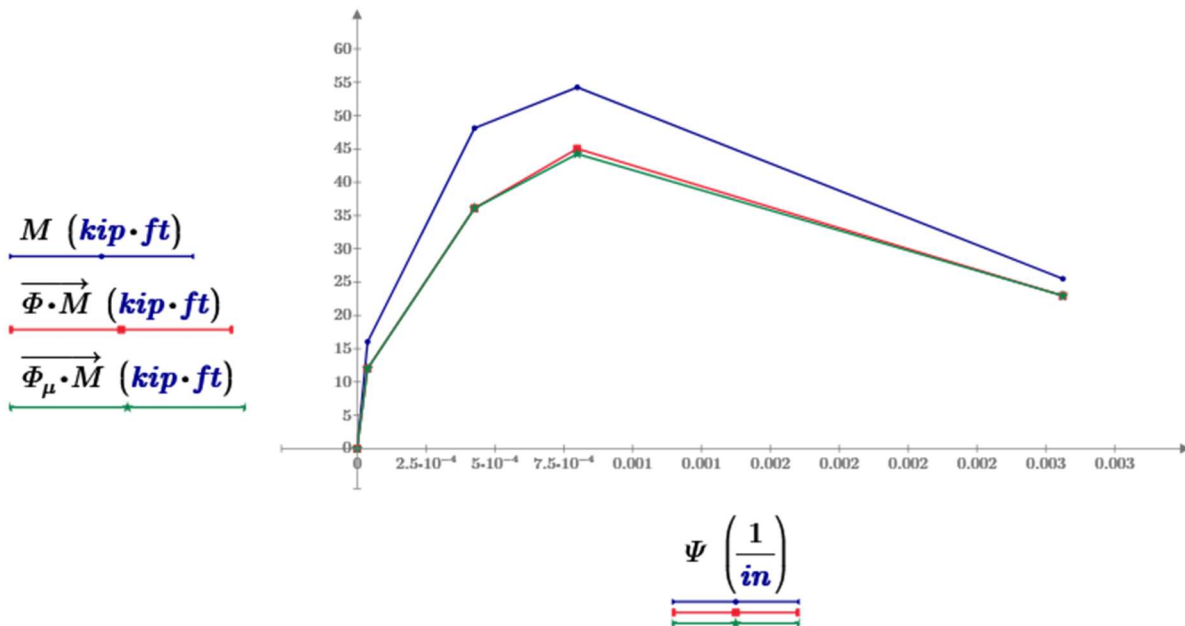
$$M_r := \Phi_{\mu_3} \cdot M_3 = 44.3 \text{ kip}\cdot\text{ft}$$

$$\Psi = \begin{bmatrix} 0 \\ 3.837 \cdot 10^{-5} \\ 4.265 \cdot 10^{-4} \\ 7.995 \cdot 10^{-4} \\ 0.003 \end{bmatrix} \frac{1}{\text{in}}$$

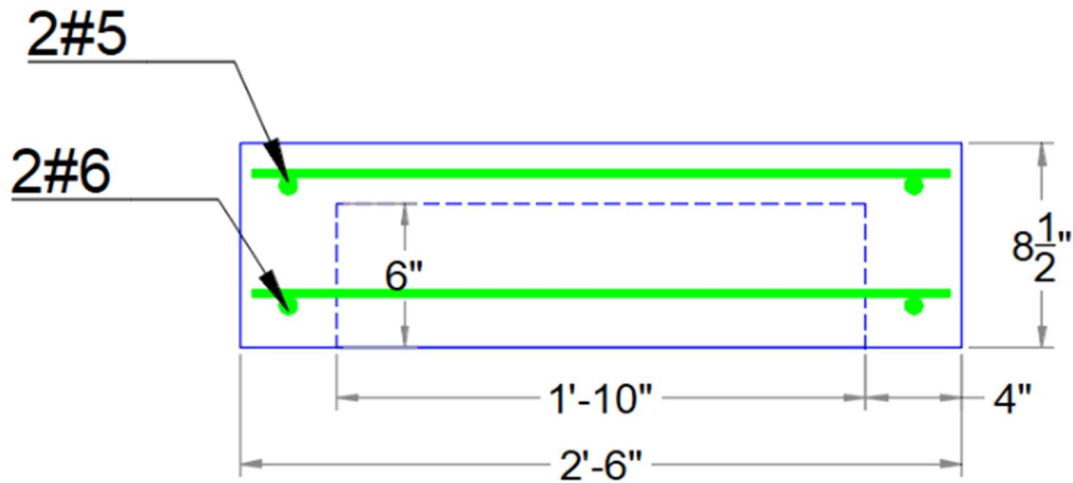
$$M = \begin{bmatrix} 0 \\ 16 \\ 48.1 \\ 54.3 \\ 25.5 \end{bmatrix} \text{ kip}\cdot\text{ft}$$

$$\Phi = \begin{bmatrix} 0 \\ 0.75 \\ 0.75 \\ 0.83 \\ 0.9 \end{bmatrix}$$

$$\Phi_{\mu} = \begin{bmatrix} 0 \\ 0.75 \\ 0.75 \\ 0.816 \\ 0.9 \end{bmatrix}$$



Flexure Strength of Prestressed/Reinforced UHPC Ribbed Slab Specimen
(Positive Moment) According to PCI & FHWA Methods



Beam Span $L := 43 \text{ in}$

Width of Loading Pad $a := 8.25 \text{ in}$

Maximum Load $P_{test} := 87.3 \text{ kip}$

Test Moment $M_{test} := \frac{P_{test}}{4} (L - a) = 63.2 \text{ kip} \cdot \text{ft}$

Nominal Capacity $M_n := 46.3 \text{ kip} \cdot \text{ft}$ $\frac{M_{test}}{M_n} = 1.37$

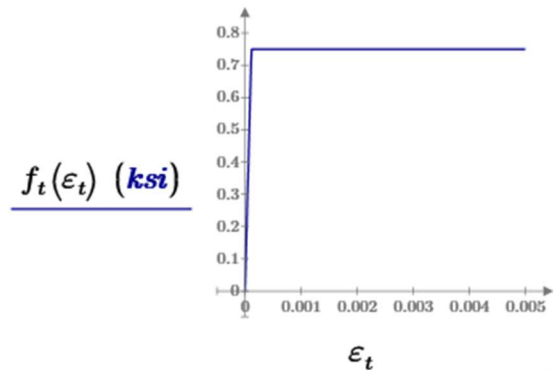
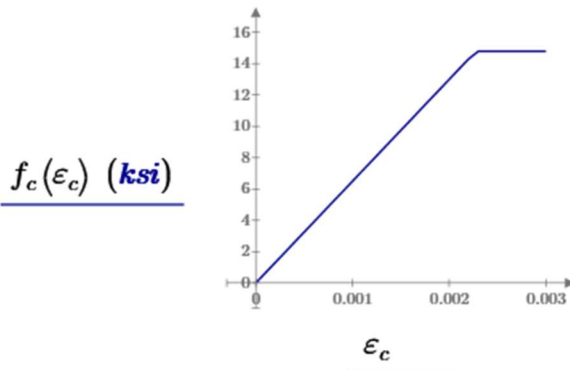
Demand $M_u := 6.89 \frac{\text{kip} \cdot \text{ft}}{\text{ft}} \cdot 1.75 \cdot 4 \text{ ft} = 48.23 \text{ kip} \cdot \text{ft}$ $\frac{M_{test}}{M_u} = 1.31$

UHPC Compression Model

Design Compressive Strength	$f'_c := 17.4 \text{ ksi}$
Correction Factor for MOE	$K_1 := 1.013$
Modulus of Elasticity	$E_c := 2500 \text{ ksi } K_1 \cdot \left(\frac{f'_c}{\text{ksi}}\right)^{0.33} = 6500 \text{ ksi}$
Reduction Factor for Compression	$\alpha := 0.85$
Elastic Compressive Strain	$\varepsilon_{cp} := \frac{\alpha \cdot f'_c}{E_c} = 0.0023$
Ultimate Compressive Strain	$\varepsilon_{cu} := 0.003$
Compressive Stress-Strain Relationship	$f_c(\varepsilon_c) := \text{if}(0 \leq \varepsilon_c < \varepsilon_{cp}, \varepsilon_c \cdot E_c, \text{if}(\varepsilon_{cp} \leq \varepsilon_c \leq \varepsilon_{cu}, \alpha \cdot f'_c, 0 \text{ ksi}))$

UHPC Tension Model

Effective Cracking Strength	$f_{t.cr} := 0.882 \text{ ksi}$
Crack Localization Stress	$f_{t.loc} := 0.882 \text{ ksi}$
Reduction Factor for Tension	$\gamma := 0.85$ $\gamma \cdot f_{t.loc} = 0.75 \text{ ksi}$
Elastic Tensile Strain	$\varepsilon_{t.cr} := \frac{\gamma \cdot f_{t.cr}}{E_c} = 0.000115$
Crack Localization Strain	$\varepsilon_{t.loc} := 0.005$
Tensile Stress-Strain Relationship	$f_t(\varepsilon_t) := \text{if}\left(0 \leq \varepsilon_t \leq \varepsilon_{t.cr}, \varepsilon_t \cdot E_c, \text{if}\left(\varepsilon_{t.cr} < \varepsilon_t \leq \varepsilon_{t.loc}, \gamma \cdot f_{t.cr} + (\varepsilon_t - \varepsilon_{t.cr}) \cdot \frac{\gamma \cdot (f_{t.loc} - f_{t.cr})}{(\varepsilon_{t.loc} - \varepsilon_{t.cr})}, 0 \text{ ksi}\right)\right)$
	$\varepsilon_c := 0, 0.0001 \dots \varepsilon_{cu}$ $\varepsilon_t := 0, 0.00001 \dots \varepsilon_{t.loc}$



Section Geometry

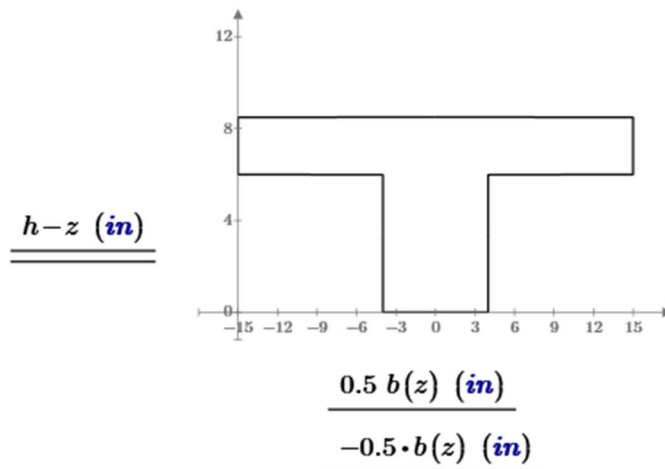
Section Height

$$h := 8.5 \text{ in}$$

Section Width
(z from compression side)

$$b(z) := \begin{cases} 30 \text{ in} & \text{if } 0 < z \leq 2.5 \text{ in} \\ 8 \text{ in} & \text{else if } 2.5 \text{ in} < z \leq h \\ 0 \text{ in} & \text{else} \end{cases}$$

$$z := 0, 0.01 \text{ in} \dots h + 0.01 \text{ in}$$



Section Area

$$A_g := \int_{0 \text{ in}}^h b(z) dz = 123 \text{ in}^2$$

Section C.G. from
Compression Side

$$y_t := \frac{\int_{0 \text{ in}}^h b(z) \cdot z dz}{A_g} = 2.91 \text{ in}$$

Section C.G. from
Tension Side

$$y_b := h - y_t = 5.591 \text{ in}$$

Section Inertia

$$I_g := \int_{0 \text{ in}}^h b(z) \cdot (y_t - z)^2 dz = 712.3 \text{ in}^4$$

Non-Pre-stressing Reinforcement

Steel MOE	$E_s := 29000 \text{ ksi}$											
Steel Yield Strength	$f_y := 60 \text{ ksi}$											
Strain at Service Stress Limit	$\epsilon_{sl} := \frac{0.8 f_y}{E_s} = 0.00166$											
Rupture Strain of Steel	$\epsilon_{su} := 9\%$											
Stress of Non-prestressing steel	$f_s(\epsilon_s) := \text{if}(\epsilon_s \geq 0, \min(\epsilon_s \cdot E_s, f_y), \max(\epsilon_s \cdot E_s, -f_y))$											
Steel Layers (at least 2) (d from compression side)	<table style="margin-left: 40px;"> <tr> <td>A_s</td> <td>d</td> <td></td> </tr> <tr> <td>(in^2)</td> <td>(in)</td> <td></td> </tr> <tr> <td>$2 \cdot 0.31$</td> <td>1.75</td> <td rowspan="2">$\sum A_s = 1.5 \text{ in}^2$</td> </tr> <tr> <td>$2 \cdot 0.44$</td> <td>$6.75$</td> </tr> </table>	A_s	d		(in^2)	(in)		$2 \cdot 0.31$	1.75	$\sum A_s = 1.5 \text{ in}^2$	$2 \cdot 0.44$	6.75
A_s	d											
(in^2)	(in)											
$2 \cdot 0.31$	1.75	$\sum A_s = 1.5 \text{ in}^2$										
$2 \cdot 0.44$	6.75											

Pre-stressing Reinforcement

Ultimate Strength of Strands	$f_{pu} := 270 \text{ ksi}$
Rupture Strain of Strands	$\epsilon_{pu} := 3.5\%$
Strand MOE	$E_p := 28500 \text{ ksi}$
Yield Strength of Strands	$f_{py} := 0.9 \cdot f_{pu} = 243 \text{ ksi}$
Power Formula Factors	$Q := 0.031$ $K := 1.043$ $R := 7.36$
Stress of Low-Relaxation Pre-stressing Steel	$f_p(\epsilon_p) := \min \left(f_{pu}, E_p \cdot \epsilon_p \cdot \left(Q + \frac{1-Q}{\left(1 + \left(\frac{E_p \cdot \epsilon_p }{K \cdot f_{py}} \right)^R \right)^{\frac{1}{R}}} \right) \right)$
Estimated Total Losses	$TL := 18\%$
Effective Pre-stressing	$f_{se} := 75\% \cdot (1 - TL) \cdot f_{pu} = 166.05 \text{ ksi}$
Effective Strain of Strands	$\epsilon_{se} := \frac{f_{se}}{E_p} = 0.00583$
Strain at Service Stress Limit	$\epsilon_{pl} := \text{root}(f_p(\epsilon_p) - 0.8 f_{py}, \epsilon_p, 0, \epsilon_{pu}) = 0.00696$

Strand Diameter

$$d_b := 0.6 \text{ in}$$

One Strand Area

$$A_{s1} := \begin{cases} \text{if } d_b = 0.375 \text{ in} \\ \quad \parallel 0.085 \text{ in}^2 \\ \text{else if } d_b = 0.5 \text{ in} \\ \quad \parallel 0.153 \text{ in}^2 \\ \text{else if } d_b = 0.6 \text{ in} \\ \quad \parallel 0.217 \text{ in}^2 \\ \text{else if } d_b = 0.7 \text{ in} \\ \quad \parallel 0.294 \text{ in}^2 \\ \text{else} \\ \quad \parallel 0 \text{ in}^2 \end{cases} = 0.217 \text{ in}^2$$

Strand Layers (at least 2)
(d from compression side)

$$\begin{array}{cc} n_{ps} & d_p \\ & (\text{in}) \\ \hline 0 & 1.75 \\ 0 & 6.75 \end{array} \quad \sum n_{ps} = 0$$

Area of Prestressing Steel

$$A_{ps} := A_{s1} \cdot n_{ps} = \begin{bmatrix} 0 \\ 0 \end{bmatrix} \text{ in}^2 \quad \sum A_{ps} = 0 \text{ in}^2$$

Depth of most tension Steel

$$d_t := \max(d_p, d) = 6.75 \text{ in}$$

Resistance Factor

Comp-Control Strain Limit

$$\varepsilon_{cl} := 0.002$$

Tension-Control Strain Limit

$$\varepsilon_{ul} := 0.005$$

Lower Limit of Phi Factor

$$\phi_l := 0.75$$

Upper Limit of Phi Factor

$$\phi_u := 0.9 \quad \text{Use 1.0 for Prestressed and 0.9 otherwise}$$

Resistance Reduction Factor

$$\phi(\varepsilon_t) := \min\left(\phi_u, \max\left(\phi_l, \phi_l + (\phi_u - \phi_l) \cdot \frac{\varepsilon_t - \varepsilon_{cl}}{\varepsilon_{ul} - \varepsilon_{cl}}\right)\right)$$

Ductility Ratio Limit

$$\mu_l := 3.0$$

Cracking Point

Curvature

$$\psi(c) := \frac{\varepsilon_{t.cr}}{h-c}$$

UHPC Compression Force

$$C_c(c) := \int_{0 \text{ in}}^c b(c-y) \cdot f_c(\psi(c) \cdot y) dy$$

Compression Force C.G. from N.A.

$$Z(c) := \frac{1}{C_c(c)} \cdot \int_{0 \text{ in}}^c b(c-y) \cdot f_c(\psi(c) \cdot y) \cdot y dy$$

UHPC Tension Force

$$T_c(c) := \int_{0 \text{ in}}^{h-c} b(c+x) \cdot f_t(\psi(c) \cdot x) dx$$

Tension Force C.G. from N.A.

$$X(c) := \frac{1}{T_c(c)} \cdot \int_{0 \text{ in}}^{h-c} b(c+x) \cdot f_t(\psi(c) \cdot x) \cdot x dx$$

Strain in Non-Pre-stressing Steel

$$\varepsilon_s(c) := (d-c) \cdot \psi(c)$$

Stress in Non-Pre-stressing Steel

$$f_{ss}(c) := \left\| \begin{array}{l} \text{for } i \in 0 \dots \text{last}(d) \\ \left\| \begin{array}{l} R_i \leftarrow \text{if } d_i > c \\ \left\| \begin{array}{l} f_s(\varepsilon_s(c)_i) - f_t(\varepsilon_s(c)_i) \\ \text{else} \\ f_s(\varepsilon_s(c)_i) + f_c(\varepsilon_s(c)_i) \end{array} \right\| \end{array} \right\| \\ R \end{array} \right\|$$

Force in Non-Pre-stressing Steel

$$T_s(c) := \overrightarrow{A_s \cdot f_{ss}(c)}$$

Strain in Pre-stressing Strands

$$\varepsilon_{ps}(c) := \psi(c) \cdot (d_p - c) + \varepsilon_{se}$$

Stress in Pre-stressing Strands

$$f_{ps}(c) := \left\| \begin{array}{l} \text{for } i \in 0 \dots \text{last}(d_p) \\ \left\| \begin{array}{l} R_i \leftarrow \text{if } d_{p_i} > c \\ \left\| \begin{array}{l} f_p(\varepsilon_{ps}(c)_i) - f_t(\varepsilon_{ps}(c)_i - \varepsilon_{se}) \\ \text{else} \\ f_p(\varepsilon_{ps}(c)_i) + f_c(\varepsilon_{ps}(c)_i - \varepsilon_{se}) \end{array} \right\| \end{array} \right\| \\ R \end{array} \right\|$$

Force in Pre-stressing Strands

$$T_{ps}(c) := \overrightarrow{A_{ps} \cdot f_{ps}(c)}$$

Initial Guess of c

$$c := \frac{h}{2}$$

Neutral Axis Location

$$c_e := \text{root} \left(T_c(c) + \sum T_s(c) + \sum T_{ps}(c) - C_c(c), c \right) = 2.974 \text{ in}$$

Nominal Flexural Strength

$$M_n(c) := C_c(c) \cdot Z(c) + T_c(c) \cdot X(c) + T_{ps}(c) \cdot (d_p - c) + T_s(c) \cdot (d - c)$$

$$\varepsilon_t := \psi(c_e) \cdot (d_t - c_e) = 0.0001$$

$$\varepsilon_c := \psi(c_e) \cdot c_e = 0.0001$$

$$\Phi_1 := \phi(\varepsilon_t) = 0.75$$

$$\Psi_1 := \psi(c_e) = 0.00002 \frac{1}{\text{in}}$$

$$M_1 := M_n(c_e) = 8.6 \text{ kip} \cdot \text{ft}$$

$$\Phi_{\mu_1} := 0.75$$

Service Stress Point

Curvature

$$\psi(c) := \frac{\varepsilon_{sl}}{d_t - c}$$

Use $\varepsilon_{pl} - \varepsilon_{se}$ for prestressed, ε_{sl} otherwise

UHPC Compression Force

$$C_c(c) := \int_0^c b(c-y) \cdot f_c(\psi(c) \cdot y) dy$$

Compression Force C.G. from N.A.

$$Z(c) := \frac{1}{C_c(c)} \cdot \int_0^c b(c-y) \cdot f_c(\psi(c) \cdot y) \cdot y dy$$

UHPC Tension Force

$$T_c(c) := \int_0^{h-c} b(c+x) \cdot f_t(\psi(c) \cdot x) dx$$

Tension Force C.G. from N.A.

$$X(c) := \frac{1}{T_c(c)} \cdot \int_0^{h-c} b(c+x) \cdot f_t(\psi(c) \cdot x) \cdot x dx$$

Strain in Non-Pre-stressing Steel

$$\varepsilon_s(c) := (d - c) \cdot \psi(c)$$

Stress in Non-Pre-stressing Steel

$$f_{ss}(c) := \left\| \begin{array}{l} \text{for } i \in 0 \dots \text{last}(d) \\ \left\| \begin{array}{l} R_i \leftarrow \text{if } d_i > c \\ \left\| \begin{array}{l} f_s(\varepsilon_s(c)_i) - f_t(\varepsilon_s(c)_i) \\ \text{else} \\ f_s(\varepsilon_s(c)_i) + f_c(\varepsilon_s(c)_i) \end{array} \right\| \end{array} \right\| \\ R \end{array} \right\|$$

Force in Non-Pre-stressing Steel

$$T_s(c) := \overline{A_s \cdot f_{ss}(c)}$$

Strain in Pre-stressing Strands

$$\varepsilon_{ps}(c) := \psi(c) \cdot (d_p - c) + \varepsilon_{se}$$

Stress in Pre-stressing Strands

$$f_{ps}(c) := \begin{cases} \text{for } i \in 0 \dots \text{last}(d_p) \\ \left\| \begin{array}{l} R_i \leftarrow \text{if } d_{p_i} > c \\ \left\| \begin{array}{l} f_p(\varepsilon_{ps}(c)_i) - f_t(\varepsilon_{ps}(c)_i - \varepsilon_{se}) \\ \text{else} \\ f_p(\varepsilon_{ps}(c)_i) + f_c(\varepsilon_{ps}(c)_i - \varepsilon_{se}) \end{array} \right\| \\ R \end{array} \right\| \end{cases}$$

Force in Pre-stressing Strands

$$T_{ps}(c) := \overrightarrow{A_{ps} \cdot f_{ps}(c)}$$

Initial Guess of c

$$c := \frac{h}{4}$$

Neutral Axis Location

$$c_e := \text{root}\left(T_c(c) + \sum T_s(c) + \sum T_{ps}(c) - C_c(c), c\right) = 1.697 \text{ in}$$

Nominal Flexural Strength

$$M_n(c) := C_c(c) \cdot Z(c) + T_c(c) \cdot X(c) + T_{ps}(c) \cdot (d_p - c) + T_s(c) \cdot (d - c)$$

$$\varepsilon_t := \psi(c_e) \cdot (d_t - c_e) = 0.0017$$

$$\varepsilon_c := \psi(c_e) \cdot c_e = 0.0006$$

$$\Phi_2 := \phi(\varepsilon_t) = 0.75$$

$$\Psi_2 := \psi(c_e) = 0.00033 \frac{1}{\text{in}}$$

$$M_2 := M_n(c_e) = 38.1 \text{ kip} \cdot \text{ft}$$

$$\Phi_{\mu_2} := 0.75$$

1st Peak Point (Crack Localization)

Curvature

$$\psi(c) := \frac{\varepsilon_{t,loc}}{h - c}$$

UHPC Compression Force

$$C_c(c) := \int_{0 \text{ in}}^c b(c - y) \cdot f_c(\psi(c) \cdot y) \, dy$$

Compression Force C.G. from N.A.

$$Z(c) := \frac{1}{C_c(c)} \cdot \int_{0 \text{ in}}^c b(c - y) \cdot f_c(\psi(c) \cdot y) \cdot y \, dy$$

UHPC Tension Force

$$T_c(c) := \int_{0 \text{ in}}^{h-c} b(c + x) \cdot f_t(\psi(c) \cdot x) \, dx$$

Tension Force C.G. from N.A.

$$X(c) := \frac{1}{T_c(c)} \cdot \int_{0 \text{ in}}^{h-c} b(c + x) \cdot f_t(\psi(c) \cdot x) \cdot x \, dx$$

Strain in Non-Pre-stressing Steel

$$\varepsilon_s(c) := (d - c) \cdot \psi(c)$$

Stress in Non-Pre-stressing Steel

$$f_{ss}(c) := \begin{array}{l} \text{for } i \in 0 \dots \text{last}(d) \\ \left\| \begin{array}{l} R_i \leftarrow \text{if } d_i > c \\ \left\| \begin{array}{l} f_s(\varepsilon_s(c)_i) - f_t(\varepsilon_s(c)_i) \\ \text{else} \\ f_s(\varepsilon_s(c)_i) + f_c(\varepsilon_s(c)_i) \end{array} \right\| \end{array} \right\| \\ R \end{array}$$

Force in Non-Pre-stressing Steel

$$T_s(c) := \overline{A_s \cdot f_{ss}(c)}$$

Strain in Pre-stressing Strands

$$\varepsilon_{ps}(c) := \psi(c) \cdot (d_p - c) + \varepsilon_{se}$$

Stress in Pre-stressing Strands

$$f_{ps}(c) := \begin{array}{l} \text{for } i \in 0 \dots \text{last}(d_p) \\ \left\| \begin{array}{l} R_i \leftarrow \text{if } d_{pi} > c \\ \left\| \begin{array}{l} f_p(\varepsilon_{ps}(c)_i) - f_t(\varepsilon_{ps}(c)_i - \varepsilon_{se}) \\ \text{else} \\ f_p(\varepsilon_{ps}(c)_i) + f_c(\varepsilon_{ps}(c)_i - \varepsilon_{se}) \end{array} \right\| \end{array} \right\| \\ R \end{array}$$

Force in Pre-stressing Strands

$$T_{ps}(c) := \overline{A_{ps} \cdot f_{ps}(c)}$$

Initial Guess of c

$$c := \frac{h}{8}$$

Neutral Axis Location

$$c_e := \text{root}\left(T_c(c) + \sum T_s(c) + \sum T_{ps}(c) - C_c(c), c\right) = 1.317 \text{ in}$$

Nominal Flexural Strength

$$M_n(c) := C_c(c) \cdot Z(c) + T_c(c) \cdot X(c) + T_{ps}(c) \cdot (d_p - c) + T_s(c) \cdot (d - c)$$

$$\varepsilon_t := \psi(c_e) \cdot (d_t - c_e) = 0.004$$

$$\varepsilon_c := \psi(c_e) \cdot c_e = 0.00092$$

$$\Phi_3 := \phi(\varepsilon_t) = 0.839$$

$$\Psi_3 := \psi(c_e) = 0.0007 \frac{1}{\text{in}}$$

$$M_3 := M_n(c_e) = 46.3 \text{ kip} \cdot \text{ft}$$

Curvature Ductility Ratio

$$\mu := \frac{\Psi_3}{\Psi_2} = 2.125$$

Curvature Ductility
Resistance Factor

$$\Phi_{\mu_3} := \text{if}\left(\mu < 1, 0.75, \text{if}\left(\mu > \mu_t, 0.9, 0.75 + 0.15 \cdot \frac{(\mu - 1)}{(\mu_t - 1)}\right)\right) = 0.834$$

2nd Peak Point (Ultimate)

Curvature $\psi(c) := \min\left(\frac{\epsilon_{su}}{d_t - c}, \frac{\epsilon_{cu}}{c}\right)$ Use $\epsilon_{pu} - \epsilon_{se}$ for prestressed, ϵ_{su} otherwise

UHPC Compression Force $C_c(c) := \int_{0 \text{ in}}^c b(c-y) \cdot f_c(\psi(c) \cdot y) dy$

Compression Force C.G. from N.A. $Z(c) := \frac{1}{C_c(c)} \cdot \int_{0 \text{ in}}^c b(c-y) \cdot f_c(\psi(c) \cdot y) \cdot y dy$

UHPC Tension Force $T_c(c) := \int_{0 \text{ in}}^{h-c} b(c+x) \cdot f_t(\psi(c) \cdot x) dx$

Tension Force C.G. from N.A. $X(c) := \frac{1}{T_c(c)} \cdot \int_{0 \text{ in}}^{h-c} b(c+x) \cdot f_t(\psi(c) \cdot x) \cdot x dx$

Strain in Non-Pre-stressing Steel $\epsilon_s(c) := (d-c) \cdot \psi(c)$

Stress in Non-Pre-stressing Steel $f_{ss}(c) := \left\| \begin{array}{l} \text{for } i \in 0 \dots \text{last}(d) \\ \left\| \begin{array}{l} R_i \leftarrow \text{if } d_i > c \\ \left\| \begin{array}{l} f_s(\epsilon_s(c)_i) - f_t(\epsilon_s(c)_i) \\ \text{else} \\ f_s(\epsilon_s(c)_i) + f_c(\epsilon_s(c)_i) \end{array} \right\| \end{array} \right\| \\ R \end{array} \right\|$

Force in Non-Pre-stressing Steel $T_s(c) := \overrightarrow{A_s \cdot f_{ss}(c)}$

Strain in Pre-stressing Strands $\epsilon_{ps}(c) := \psi(c) \cdot (d_p - c) + \epsilon_{se}$

Stress in Pre-stressing Strands $f_{ps}(c) := \left\| \begin{array}{l} \text{for } i \in 0 \dots \text{last}(d_p) \\ \left\| \begin{array}{l} R_i \leftarrow \text{if } d_{p_i} > c \\ \left\| \begin{array}{l} f_p(\epsilon_{ps}(c)_i) - f_t(\epsilon_{ps}(c)_i - \epsilon_{se}) \\ \text{else} \\ f_p(\epsilon_{ps}(c)_i) + f_c(\epsilon_{ps}(c)_i - \epsilon_{se}) \end{array} \right\| \end{array} \right\| \\ R \end{array} \right\|$

Force in Pre-stressing Strands $T_{ps}(c) := \overrightarrow{A_{ps} \cdot f_{ps}(c)}$

Initial Guess of c

$$c := \frac{h}{16}$$

Neutral Axis Location

$$c_e := \text{root} \left(T_c(c) + \sum T_s(c) + \sum T_{ps}(c) - C_c(c), c \right) = 0.378 \text{ in}$$

Nominal Flexural Strength

$$M_n(c) := C_c(c) \cdot Z(c) + T_c(c) \cdot X(c) + T_{ps}(c) \cdot (d_p - c) + T_s(c) \cdot (d - c)$$

$$\varepsilon_t := \psi(c_e) \cdot (d_t - c_e) = 0.051$$

$$\varepsilon_c := \psi(c_e) \cdot c_e = 0.003$$

$$\Phi_4 := \phi(\varepsilon_t) = 0.9$$

$$\Psi_4 := \psi(c_e) = 0.00795 \frac{1}{\text{in}}$$

$$M_4 := M_n(c_e) = 34.8 \text{ kip}\cdot\text{ft}$$

Curvature Ductility Ratio

$$\mu := \frac{\Psi_4}{\Psi_2} = 24.261$$

Curvature Ductility Resistance Factor

$$\Phi_{\mu_4} := \text{if} \left(\mu < 1, 0.75, \text{if} \left(\mu > \mu_l, 0.9, 0.75 + 0.15 \cdot \frac{(\mu - 1)}{(\mu_l - 1)} \right) \right) = 0.9$$

PCI Design Flexural Strength

$$M_r := \max(\Phi_3 \cdot M_3, \Phi_4 \cdot M_4) = 38.8 \text{ kip}\cdot\text{ft}$$

FHWA Design Flexural Strength

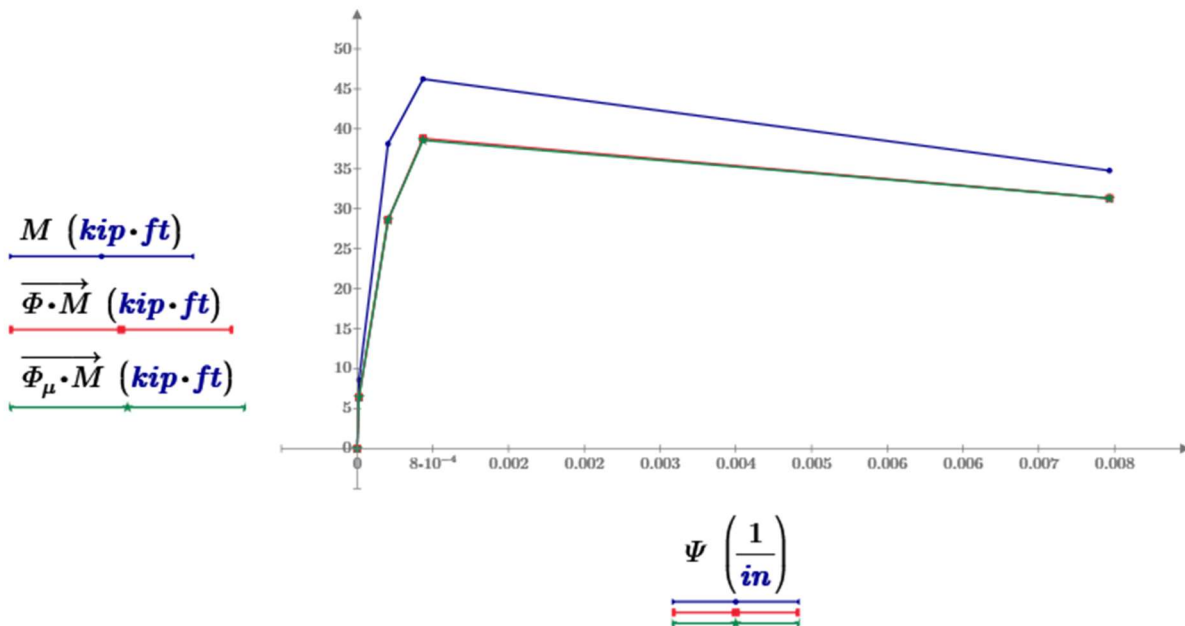
$$M_r := \Phi_{\mu_3} \cdot M_3 = 38.6 \text{ kip}\cdot\text{ft}$$

$$\Psi = \begin{bmatrix} 0 \\ 2.087 \cdot 10^{-5} \\ 3.275 \cdot 10^{-4} \\ 6.961 \cdot 10^{-4} \\ 0.008 \end{bmatrix} \frac{1}{\text{in}}$$

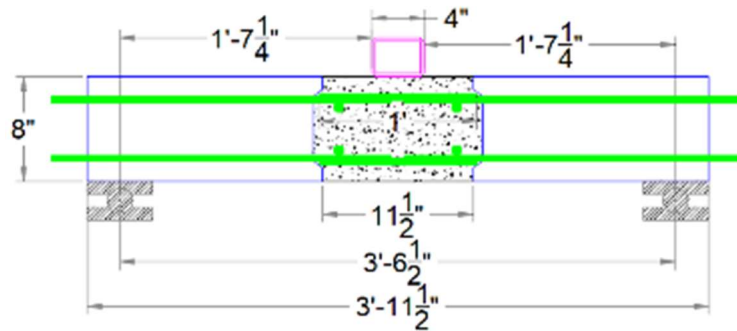
$$M = \begin{bmatrix} 0 \\ 8.6 \\ 38.1 \\ 46.3 \\ 34.8 \end{bmatrix} \text{ kip}\cdot\text{ft}$$

$$\Phi = \begin{bmatrix} 0 \\ 0.75 \\ 0.75 \\ 0.839 \\ 0.9 \end{bmatrix}$$

$$\Phi_{\mu} = \begin{bmatrix} 0 \\ 0.75 \\ 0.75 \\ 0.834 \\ 0.9 \end{bmatrix}$$



Flexural Testing of Longitudinal Joint



Loading Calculation

Specimen Span

$$L := 42.5 \text{ in}$$

Test Load

$$P_{test} := 33.1 \text{ kip}$$

Distance to Critical Section

$$a := \frac{L - 12.5 \text{ in}}{2} - 2 \text{ in} = 13 \text{ in}$$

Test Moment

$$M_{test} := \frac{P_{test}}{2} \cdot a = 17.93 \text{ kip} \cdot \text{ft}$$

Capacity Prediction

Section Height

$$h := 8 \text{ in}$$

Section Width

$$b := 18 \text{ in}$$

Tension Steel

$$A_s := 0.31 \text{ in}^2$$

Tension Steel Depth

$$d := h - 1.75 \text{ in} = 6.25 \text{ in}$$

Compression Steel

$$A_s' := 0.31 \text{ in}^2$$

Compression Steel Depth

$$d' := 1.75 \text{ in}$$

Yield Strength

$$f_y := 60 \text{ ksi}$$

Compressive Strength

$$f_c' := 17.4 \text{ ksi}$$

Compression Block

$$a := \frac{A_s \cdot f_y + A_s' \cdot f_y}{0.65 f_c' \cdot b} = 0.183 \text{ in} \quad c := \frac{a}{0.65} = 0.281 \text{ in}$$

Steel Strain

$$\epsilon_s := 0.003 \cdot \frac{d - c}{c} = 0.064 \quad \epsilon_s' := 0.003 \cdot \frac{d' - c}{c} = 0.016$$

Nominal Flexural Capacity

$$M_n := A_s \cdot f_y \cdot \left(d - \frac{a}{2} \right) + A_s' \cdot f_y \cdot \left(d' - \frac{a}{2} \right) = 12.12 \text{ kip} \cdot \text{ft}$$

Solid and Ribbed Slab Section Properties

SOLID SLAB

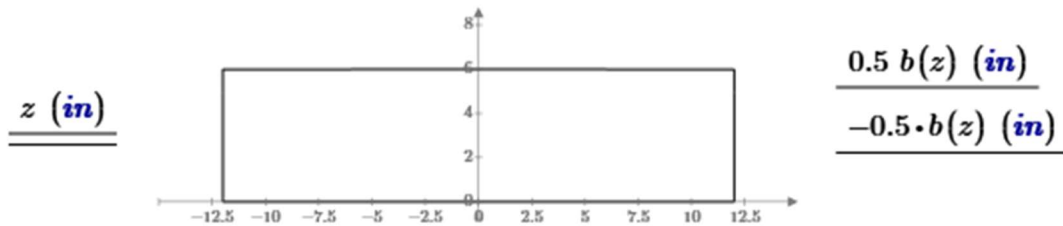
Section Height

$$h := 6 \text{ in}$$

Section Width (function of distance from bottom fibers z)

$$b(z) := \begin{cases} 24 \text{ in} & \text{if } 0 < z \leq h \\ 0 \text{ in} & \text{else} \end{cases}$$

$$z := 0, 0.01 \text{ in} .. h + 0.01 \text{ in}$$



Section Area

$$A := \int_{0 \text{ in}}^h b(z) dz = 144 \text{ in}^2$$

Section C.G. from bottom

$$y_b := \frac{\int_{0 \text{ in}}^h b(z) \cdot z dz}{A} = 3 \text{ in}$$

Section C.G. from top

$$y_t := h - y_b = 3 \text{ in}$$

Section Inertia

$$I := \int_{0 \text{ in}}^h b(z) \cdot (z - y_b)^2 dz = 432 \text{ in}^4$$

Bottom Section Modulus

$$S_b := \frac{I}{y_b} = 144 \text{ in}^3$$

Top Section Modulus

$$S_t := \frac{I}{y_t} = 144 \text{ in}^3$$

RIBBED SLAB

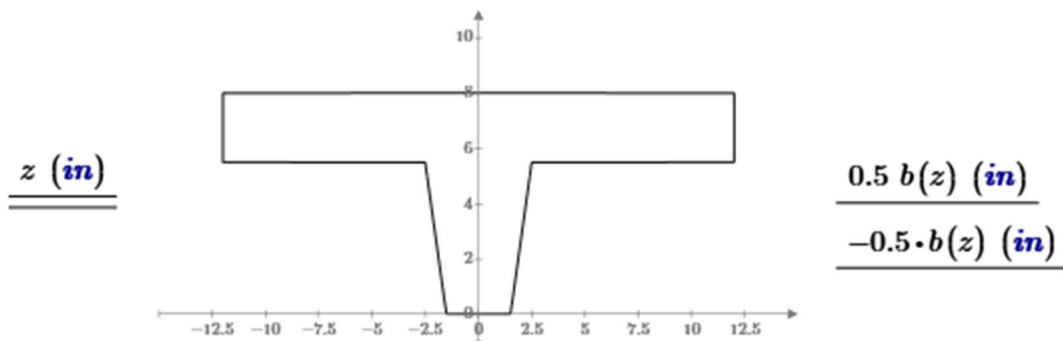
Section Height

$$h := 8 \text{ in}$$

Section Width (function of distance from bottom fibers z)

$$b(z) := \begin{cases} \text{if } 0 < z \leq 5.5 \text{ in} \\ \quad \left\| \begin{array}{l} 3 \text{ in} + 2 \text{ in} \cdot \frac{z}{5.5 \text{ in}} \\ \text{else if } 5.5 \text{ in} < z \leq h \\ \quad \left\| \begin{array}{l} 24 \text{ in} \\ \text{else} \\ \quad \left\| \begin{array}{l} 0 \text{ in} \end{array} \right. \end{array} \right. \end{array} \right. \end{cases}$$

$$z := 0, 0.01 \text{ in} \dots h + 0.01 \text{ in}$$



Section Area

$$A := \int_{0 \text{ in}}^h b(z) dz = 82 \text{ in}^2$$

Section C.G. from bottom

$$y_b := \frac{\int_{0 \text{ in}}^h b(z) \cdot z dz}{A} = 5.74 \text{ in}$$

Section C.G. from top

$$y_t := h - y_b = 2.26 \text{ in}$$

Section Inertia

$$I := \int_{0 \text{ in}}^h b(z) \cdot (z - y_b)^2 dz = 314 \text{ in}^4$$

Bottom Section Modulus

$$S_b := \frac{I}{y_b} = 54.78 \text{ in}^3$$

Top Section Modulus

$$S_t := \frac{I}{y_t} = 138.99 \text{ in}^3$$

Equivalent Solid Slab Thickness

$$h_{eq} := \sqrt[3]{\frac{12 I}{24 \text{ in}}} = 5.4 \text{ in}$$

APPENDIX C: DESIGN EXAMPLES

Example #1: Pretensioned UHPC DIB with Ribbed Slab

Example #2: Pretensioned UHPC DIB with Solid Slab

Will be provided as pdf and Mathcad sheets Only. (Not in print)